Boussinesq modelling with higher-order dispersion; derivation and numerical modelling

Lucas Merckelbach

M.Sc. Thesis, September 1995

Delft University of Technology
Faculty of Civil Engineering
Hydraulic and Geotechnical Engineering Division
Hydraulic Engineering Group

Supervision:

Prof. dr ir J.A. Battjes
Prof. dr ir G.S. Stelling
Dr ir M.W. Dingemans

Abstract

In this thesis the modelling of water wave propagation over uneven bottoms using Boussinesq-like models with higher-order frequency dispersion is studied. Boussinesq-like equations describe the propagation of weakly non-linear shallow water waves. As for long waves the depth-dependence of the velocity field is almost absent, the vertical coordinate z has been removed in deriving Boussinesq-like models.
A problem with Boussinesq-like models which were in use some time ago, is that they do not have particularly good frequency dispersion characteristics, especially not at depths where practical problems had to be solved. Therefore, many efforts have been spent to improve the dispersion characteristics.

Dingemans (1994b) has started with a higher-order dispersion relation written in the form of a rational polynomial as obtained by Schäffer and Madsen (1994). Using operator correspondence four different Boussinesq-like models with only third and lower derivatives can be derived for horizontal bottom. Uneven bottom terms can be obtained by splitting $(kh)^2$ in hk^2h and h^2k^2 whereupon operator correspondence is applied by replacing k by $i\partial_x$. In this manner a total number of 48 different models is obtained each with four degrees of freedom, denoted by γ_i. By comparing the linear shoaling coefficient with the exact linear shoaling coefficient the γ's are optimized. It turned out that 24 models have exactly the same linear shoaling coefficient, which is very accurate up to $kh=5$. However, the models (may) differ in higher-order shoaling behaviour.

The higher-order shoaling is invesitigated by solving the models numerically using the Keller's Box compact difference scheme. This scheme is implicit and therefore unconditionally stable and it has a second-order accuracy. The procedure is to rewrite the set of two third-order partial differential equations to a set of six first-order partial differential equations by introducing four more variables. The system of linear finite difference equations has block-diagonal structure, which fits in a 17 diagonal matrix and is solved by a Thomas algorithm. Subsequently, a weakly reflecting boundary condition is formulated by the Sommerfeld radiation condition for the classical shallow water equations together with a sponge layer resulting in a reflection coefficient of $O(10^{-3})$.

The numerical models are validated against the measurements used in the intercomparison study of Dingemans (1994a). It turned out that the best correspondence with measurements is obtained by four models with essentially the same accuracy.

It is concluded that the new Boussinesq-like equations with higher-order dispersion has increased the applicability of Boussinesq modelling for wave propagation over uneven bottoms and that Keller's Box method is a very suitable method for integrating Boussinesq-like equations.

Contents

Abstract

Contents

1 Introduction

In engineering practice a need exists for wave propagation models which predict the wave properties in space. The basic problem in water wave propagation is that the waves have a propagation space and a cross space. The propagation space is in horizontal directions and has a distinct wave character. But in vertical direction, i.e. the cross space, the solution is altogether different and is not wave-like. This is in contrast with for example sound waves; these waves have a propagation space in three dimensions.
The implication is that two different solutions should be found. These solutions have a different character, but are interrelated. This makes a description of water waves complicated. Therefore, many approaches are based on separation of the propagation space and cross space.

The waves in a coastal zone are fairly long waves. It is known that the velocity field is almost depth-independent. A perturbation approach can be used assuming that the intrinsic scale of wave motion, the wave length L, is very much larger than the characteristic depth, see for example Boussinesq (1872) or Peregrine (1967). This also limits the possible bottom slopes. At least one wave should fit in a region in which no appreciable changes in water depth occur. Boussinesq-like models are derived within these restrictions and are therefore only valid for fairly long waves. We speak of Boussinesq-*like* equations, since many different forms exist, but all of them are asymptotically equivalent. Yet the Boussinesq-like equations may behave totally different for engineering purposes. Although Boussinesq-like models are only valid for long waves, for applications an extension to deeper water is desired.

For a long time efforts have been spent in deriving Boussinesq-like models with properties which are as good as possible. Most models did not have particularly good frequency dispersion behaviour, especially not for deeper water where practical problems had to be solved. Consequently, the correct wave profile is computed at a wrong place.
Witting (1984) suggested to use a [1/1] Padé expansion of the exact linear dispersion relation in $(kh)^2$. The remaining problem was finding the corresponding equations. This matter has been taken up by Madsen et al. (1991) who devised the most accurate Boussinesq-like model by perturbation techniques at that time. Later, Schäffer and Madsen (1994) devised a Boussinesq-like model based on a [2/2] Padé expansion of the dispersion relation, but needing only the usual third derivatives. Dingemans (1994b) started with the [2/2] Padé expansion of the dispersion relation and constructed a Boussinesq-like model with several degrees of freedom with respect to the depth-dependent terms.

The first aim of the present study is to optimize the shoaling characteristics of the Boussinesq-like models which are derived by Dingemans on the basis of [2/2] Padé expansion of the dispersion relation. To achieve this, all possibilities have to be considered and evaluated. The model with the best shoaling characteristics is selected.

Boussinesq-like equations are difficult to treat numerically, since they contain third-order derivatives. In practice a variety of methods is used and many of them are *ad hoc* methods. Here, a more general method for solving Boussinesq-like equations is used. The idea is as

follows. Neglecting the typical Boussinesq terms, the Boussinesq-like equations reduce to the classical shallow water equations. In practice, the shallow water equations are mostly integrated by means of Keller's Box method or (similar) Preissman method, at least in one-dimensional cases.

The second aim of this study is to develop a method based on the Keller's Box method for integrating Boussinesq-like equations. The advantage of such a method is that 1D shallow water models are easily modified to Boussinesq-like models without a drastical change in the numerical formulation.

Finally, the selected Boussinesq-like equations are implemented into a numerical model, which is validated by comparison with measurements. The findings will lead to a conclusion on practical applicability of the new optimized Boussinesq-like model.

The outline of the report

In Chapter 2 one specific Boussinesq-like model will be discussed briefly and some characteristics will be given. This model is used as reference. Chapter 3 describes the derivation of a new set Boussinesq-like equations which corresponds to a higher order dispersion relation. Subsequently, the shoaling properties of the various models, which arise due to many degrees of freedom, are investigated. This finally results in a set of equations optimized with respect to the shoaling characteristics. In Chapter 4 the discretization of these new Boussinesq-like equations is discussed. This will result in a numerical code, which is verified on the basis of measurements in Chapter 5. At last, in Chapter 6 the conclusions of this study are drawn.

2 A Boussinesq-like equation with improved dispersion

In this chapter one specific Boussinesq-like model is briefly discussed. It is not the intention to give an overview of the different types of Boussinesq models, since this has recently been done in for example Dingemans (1994a). The characteristics of this model are used as reference in Chapter 3. In Chapter 5 some numerical results of this model are used for validating the numerical method. The reason why only this model is used is because of availability of numerical data on disk, which enables a more accurate comparison than only by means of figures.

Madsen and Sørensen (1992) derived a Boussinesq-like model which is valid for small bottom slopes and written in fluxes. This model can be considered as a reduction of a model valid for larger bottom slopes given by Dingemans (1994b). The model derived by Dingemans is rewritten in the depth-averaged velocity u and has been used in the study of Boussinesq modelling of wave-induced particle velocities (Bosboom, 1995). This model, which in that study is called DUT2, reads

$$\frac{\partial \zeta}{\partial t} + \frac{\partial}{\partial x}\left[(h+\zeta)u\right] = 0 \tag{2.1a}$$

$$\frac{\partial u}{\partial t} + u\frac{\partial u}{\partial x} + g\frac{\partial \zeta}{\partial x} = \left(\frac{1}{2}+b\right)h\frac{\partial^3 hu}{\partial x^2 \partial t} - \frac{1}{6}h^2\frac{\partial^3 u}{\partial x^2 \partial t} + bgh\frac{\partial^2}{\partial x^2}\left(h\frac{\partial \zeta}{\partial x}\right) \tag{2.1b}$$

where $b=1/15$.

Dispersion relation

As argued before the main concern with Boussinesq-like equations is the poor representation of the dispersion characteristics. The linear dispersion relation according to the linear Stokes theory is used as reference, which reads

$$\frac{\omega^2}{gh} = k^2\frac{\tanh(kh)}{kh} \tag{2.2}$$

Madsen et al. (1991) showed that the dispersion relation pertaining to equations (2.1) can be written as

$$\frac{c^2}{gh} = \frac{1+b(kh)^2}{1+\left[\frac{1}{3}+b\right](kh)^2} \tag{2.3}$$

The value $b=1/15$ is obtained by matching with the [1/1] Padé expansion of equation (2.2) in the parameter $(kh)^2$. In figure (2.1) the exact linear dispersion relation and the Padé approximation are presented.

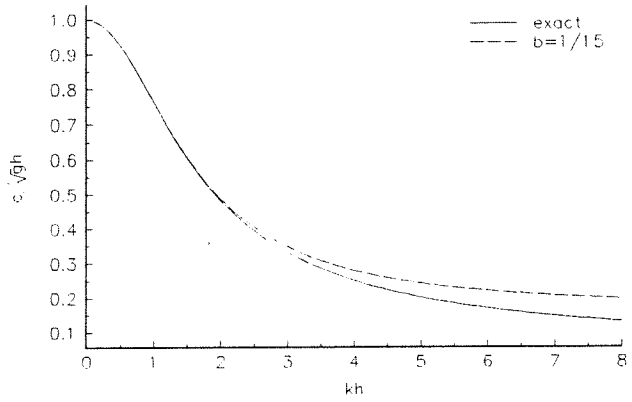

Figure (2.1) Dispersion relation normalized with $(gh)^{1/2}$

As can be seen, the approximation is quite good for values up to $kh=3$. For higher values of kh the deviation increases. For applications both the basic waves and the significant higher harmonics, which are due to non-linearities, should have a value of kh less than three, so that the phase velocity is represented correctly. In many cases it turns out that the dispersion is not good enough for higher harmonics.

Shoaling

In the context of this study the linear shoaling coefficient is defined as

$$\alpha_s = \frac{a_x/a}{h_x/h} \tag{2.4}$$

Equation (2.4) can be written as

$$\frac{a_x}{a} = -\alpha_s \frac{h_x}{h} \tag{2.5}$$

The subscripts x denote derivatives with respect to x. The shoaling coefficient α_s according to the linear Stokes theory reads

$$\alpha_s^L = -khT\frac{(1-khT)(1-T^2)}{\left[T+kh(1-T^2)\right]^2} \tag{2.6}$$

where
T = tanh(kh)

A procedure for determining the shoaling coefficient of equations (2.1) is described in detail by Bosboom (1995). The procedure is similar to the one used by Madsen et al. (1991).

The exact shoaling coefficient according to the linear Stokes theory and the shoaling coefficient pertaining to equations (2.1) are presented in figure (2.2).

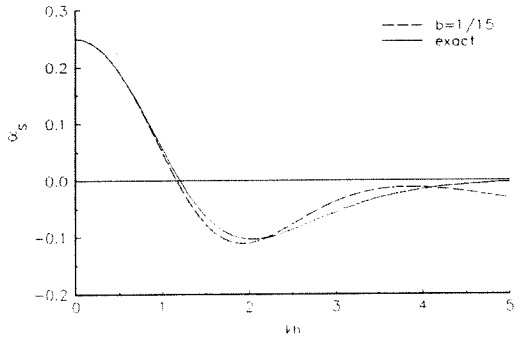

Figure (2.2) Shoaling coefficient

As can be seen, the shoaling coefficient is represented quite acceptably even for values of *kh* up to 5. In general the dispersion relation is much more important, therefore higher deviations in α_s are acceptable.

3 Boussinesq-like equations with higher order dispersion

In this chapter the derivation of a new set of Boussinesq-like equations based on a [2/2] Padé expansion of the exact linear dispersion relation in the parameter $(kh)^2$ will be given. In order to achieve this, use is made of systems in Fourier space and operator correspondence. These subjects will be discussed first.

3.1 Systems in Fourier space and operator correspondence

A system of linear partial differential equations can be written in Fourier space. Here only systems of two partial differential equations in $u(x,t)$ and $\zeta(x,t)$ are considered. The solutions for $u(x,t)$ and $\zeta(x,t)$ are written in complex notation as

$$\begin{aligned} u(x,t) &= Re\left\{U e^{i(kx-\omega t)}\right\} \\ \zeta(x,t) &= Re\left\{Z e^{i(kx-\omega t)}\right\} \end{aligned} \tag{3.1}$$

where U and Z are constant complex amplitudes.

By differentiating $u(x,t)$ with respect to x, we get

$$\partial_x\{u(x,t)\} = \frac{\partial}{\partial x}u(x,t) = Re\left\{U\frac{\partial e^{i(kx-\omega t)}}{\partial x}\right\} = Re\left\{ikU e^{i(kx-\omega t)}\right\} = Re\{ik\,u(x,t)\} \tag{3.2}$$

which shows that the differential operator ∂_x corresponds to a multiplication ik. By differentiating $\zeta(x,t)$ with respect to t, we get

$$\partial_t\{\zeta(x,t)\} = \frac{\partial}{\partial t}\zeta(x,t) = Re\left\{Z\frac{\partial e^{i(kx-\omega t)}}{\partial t}\right\} = Re\left\{-i\omega Z e^{i(kx-\omega t)}\right\} = Re\{-i\omega\,\zeta(x,t)\} \tag{3.3}$$

where the operator ∂_t is substituted by $-i\omega$. By analogy, it can be proved that ∂^2_x corresponds to $-k^2$. These substitutions are usually referred to as operator correspondence.

By using operator correspondence a set of linear partial differential equations is transformed into a system in Fourier space.

In order to illustrate this, a set of linear partial differential equations is written in a Fourier space. For this purpose, the linearized equations (2.1), written in averaged velocities, are used:

$$\frac{\partial \zeta}{\partial t} + \frac{\partial}{\partial x}[hu] = 0 \tag{3.4a}$$

$$\frac{\partial u}{\partial t} + g\frac{\partial \zeta}{\partial x} = \left[\frac{1}{2}+b\right] h\frac{\partial^3 hu}{\partial x^2 \partial t} - \frac{1}{6}h^2\frac{\partial^3 u}{\partial x^2 \partial t} + bgh\frac{\partial^2}{\partial x^2}\left[h\frac{\partial \zeta}{\partial x}\right] \tag{3.4b}$$

where $b=1/15$.

Substituting the differential operators yields after dividing by $i\, e^{i(kx-\omega t)}$ and writing in a matrix form

$$\begin{bmatrix} gk+bghk^2hk & -\omega\left[1+\left[\frac{1}{2}+b\right]hk^2h-\frac{1}{6}h^2k^2\right] \\ -\omega & hk \end{bmatrix} \begin{bmatrix} Z \\ U \end{bmatrix} = 0 \tag{3.5}$$

Equations (3.5) are written in Fourier space.

In order for a system in Fourier space to have non-trivial solutions for U and Z, it is needed that equations (3.5) are consistent. Therefore, the determinant of the matrix should be equal to zero. Computing the determinant of the matrix in equation (3.5) yields

$$gk^2h+bgk^4h^3-\omega^2\left[1+\left[\frac{1}{3}+b\right]k^2h^2\right] = 0 \tag{3.6}$$

which can be written as

$$\omega^2 = ghk^2\frac{1+bk^2h^2}{1+\left[b+\frac{1}{3}\right]k^2h^2} \tag{3.7}$$

Equation (3.7) is the linear frequency dispersion relation pertaining to equations (3.4) and is equal to equation (2.3).

In the next section, a system in Fourier space is formulated of which the determinant corresponds to a (higher order) Padé expansion of the dispersion relation. Using operator correspondence, this system is transformed into a set of partial differential equations, valid

for horizontal bottoms. Subsequently, this set of equations is extended for small bottom slopes and optimized for shoaling characteristics.

3.2 Boussinesq-like equations with higher order dispersion for horizontal bottom

Schäffer en Madsen (1994) derived a model with a dispersion relation which corresponds to a [2/2] Padé expansion in $(kh)^2$ by addition of higher order terms. This dispersion relation is in the form

$$\omega^2 = ghk^2 \frac{(1 + \alpha_1(kh)^2)\ (1 + \alpha_2(kh)^2)}{(1 + \beta_1(kh)^2)\ (1 + \beta_2(kh)^2)} \tag{3.8}$$

which can also be written as

$$\omega^2(1+\beta_1(kh)^2)(1+\beta_2(kh)^2) - kh(1+\alpha_1(kh)^2)(1+\alpha_2(kh)^2)gk = 0 \tag{3.9}$$

In order to determine the parameters α_i and β_i, a comparison with the [2/2] Padé expansion of the exact linear dispersion relation in the parameter $(kh)^2$ should be made. To that end equation (3.8) is written as

$$\frac{\omega^2}{gh} = k^2 \frac{1 + (\alpha_1+\alpha_2)(kh)^2 + (\alpha_1\alpha_2)(kh)^4}{1 + (\beta_1+\beta_2)(kh)^2 + (\beta_1\beta_2)(kh)^4} \tag{3.10}$$

The exact linear dispersion relation, known from the linear wave theory, reads

$$\frac{\omega^2}{gh} = k^2 \frac{\tanh(kh)}{kh} \tag{3.11}$$

The [2/2] Padé expansion of the exact linear dispersion in the parameter $(kh)^2$ reads

$$\frac{\omega^2}{gh} = k^2 \frac{1 + \frac{1}{9}(kh)^2 + \frac{1}{945}(kh)^4}{1 + \frac{4}{9}(kh)^2 + \frac{1}{63}(kh)^4} + O(k^{10}h^{10}) \tag{3.12}$$

In figure (3.1) the exact dispersion relation, the [1/1] and the [2/2] Padé expansion of the exact relation are plotted. The dispersion relation of the DUT2 model corresponds to the [1/1] Padé expansion, see Chapter 2.

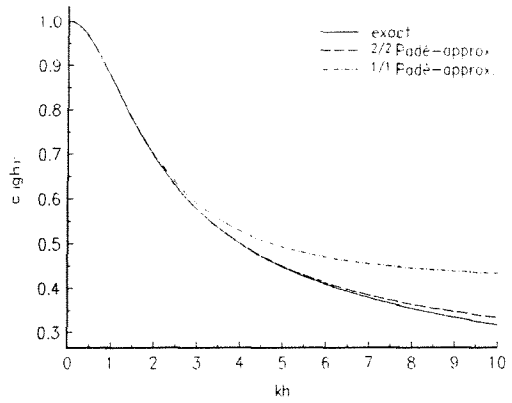

Figure (3.1) Phase velocity versus kh normalized with $(gh)^{1/2}$

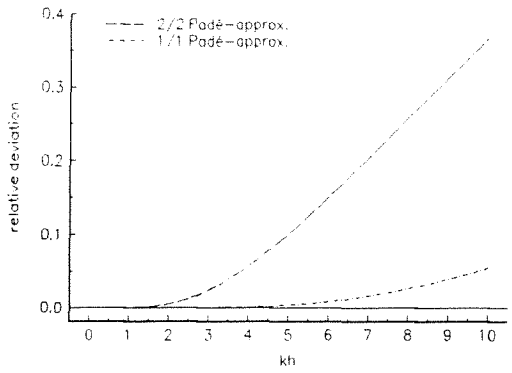

Figure (3.2) Relative deviations

It can be seen that the [2/2] Padé approximation performs much better than the [1/1] Padé approximation. The correspondence of the [2/2] Padé approximation is almost exact up to $kh=5$. The deviation at $kh=10$ has not even reached the 10%.

Equating the corresponding coefficients in equations (3.11) and (3.13) yields the four equations

$$\alpha_1 + \alpha_2 = \frac{1}{9} \qquad \alpha_1\alpha_2 = \frac{1}{945}$$
$$\beta_1 + \beta_2 = \frac{4}{9} \qquad \beta_1\beta_2 + = \frac{1}{63} \tag{3.13}$$

This set of equations has four solutions. One solution is

$$\alpha_1 = \frac{1}{18} + \frac{\sqrt{23}\sqrt{35}}{630} \qquad \alpha_2 = \frac{1}{18} - \frac{\sqrt{23}\sqrt{35}}{630}$$
$$\beta_1 = \frac{2}{9} + \frac{\sqrt{19}\sqrt{7}}{63} \qquad \beta_2 = \frac{2}{9} - \frac{\sqrt{19}\sqrt{7}}{63} \tag{3.14}$$

The other three solutions can be obtained by interchanging
- α_1 and α_2 or
- β_1 and β_2 or
- α_1 and α_2 and β_1 and β_2.

Dingemans (1994b) has started with the dispersion relation in the form of equation (3.8) and has derived the corresponding equations by using operator correspondence. This procedure is followed here as well.
The right-hand side of equation (3.9) can be interpretated as the determinant of the matrix in the Fourier system, which pertains to the partial differential equations we are looking for. In order to find the elements of the matrix, equation (3.9) should be split. One of the possible forms is

$$\begin{bmatrix} -\omega(1+\beta_2(kh)^2) & hk(1+\alpha_1(kh)^2) \\ gk(1+\alpha_2(kh)^2) & -\omega(1+\beta_1(kh)^2) \end{bmatrix} \begin{bmatrix} Z \\ U \end{bmatrix} = 0 \qquad (3.15)$$

Notice that the dimensions match. Checking the dimensions yields $L\ T^{-1}$ for the continuity equation (first row) and yields $L\ T^{-2}$ for the momentum equation (second row).

Since four solutions are obtained for equation (3.14), the following four different sets of equations in Fourier space can be discerned:

model 1
$$\begin{bmatrix} -\omega(1+\beta_1(kh)^2) & hk(1+\alpha_1(kh)^2) \\ gk(1+\alpha_2(kh)^2) & -\omega(1+\beta_2(kh)^2) \end{bmatrix} \begin{bmatrix} Z \\ U \end{bmatrix} = 0 \qquad (3.16a)$$

model 2
$$\begin{bmatrix} -\omega(1+\beta_1(kh)^2) & hk(1+\alpha_2(kh)^2) \\ gk(1+\alpha_1(kh)^2) & -\omega(1+\beta_2(kh)^2) \end{bmatrix} \begin{bmatrix} Z \\ U \end{bmatrix} = 0 \qquad (3.16b)$$

model 3
$$\begin{bmatrix} -\omega(1+\beta_2(kh)^2) & hk(1+\alpha_1(kh)^2) \\ gk(1+\alpha_2(kh)^2) & -\omega(1+\beta_1(kh)^2) \end{bmatrix} \begin{bmatrix} Z \\ U \end{bmatrix} = 0 \qquad (3.16c)$$

model 4
$$\begin{bmatrix} -\omega(1+\beta_2(kh)^2) & hk(1+\alpha_2(kh)^2) \\ gk(1+\alpha_1(kh)^2) & -\omega(1+\beta_1(kh)^2) \end{bmatrix} \begin{bmatrix} Z \\ U \end{bmatrix} = 0 \qquad (3.16d)$$

Each of the factors within parenthesis, like $(1+\beta_2(kh)^2)$, is dimensionless, since the factor kh has no dimension. Therefore the distribution of ω, hk and gk follows from dimensional arguments. This means that every factor containing $(kh)^2$ is preceded by either ω or k. By using operator correspondence, always derivatives of the third order occur. Thus, a factor $(kh)^3$ or even $(kh)^4$ yields a fourth or fifth derivative. These derivatives make the numerical integration more complicated and are not desired. Thus, equations (3.16a) through (3.16d) are the only possibilities which contain no higher derivatives than the third.
Eventually, we have to determine the shoaling behaviour of each of the four models. But first

equations (3.16a) will be considered. By using operator correspondence, the linear equations (3.16a) in case of a horizontal bottom are transformed into

$$\begin{aligned} \frac{\partial \zeta}{\partial t} + h\frac{\partial u}{\partial x} &= \beta_1 h^2 \frac{\partial^3 \zeta}{\partial x^2 \partial t} + \alpha_1 h^3 \frac{\partial^3 u}{\partial x^3} \\ \frac{\partial u}{\partial t} + g\frac{\partial \zeta}{\partial x} &= \beta_2 h^2 \frac{\partial^3 u}{\partial x^2 \partial t} + \alpha_2 g h^2 \frac{\partial^3 \zeta}{\partial x^3} \end{aligned} \qquad (3.17)$$

3.3 Boussinesq-like equations for uneven bottoms

In equations (3.17), no derivatives of h with respect to x occur. Thus, the effect of the bottom slope is not included. A way to introduce h_x-terms is by changing the sequence of k and h. In the case of kh a derivative h_x arises after using operator correspondence, whereas hk gives no h_x-terms. To avoid that one possibility rules out the other, kh can be split into kh and hk. The most common combination of kh is in $(kh)^2$, which occurs in every element in the matrices of equations (3.16). Considering equations (3.16a), splitting the factor $(kh)^2$ can be done at four different locations. We only do not know how to split $(kh)^2$. In view of this the factor $(kh)^2$ is written as

$$(kh)^2 = (1 + \gamma_i) hk^2 h - \gamma_i h^2 k^2 \qquad \forall \qquad i = 1,2,3,4 \qquad (3.18)$$

where γ_i is the splitting coefficient. However, the splitting need not to be the same in all the four cases. Therefore, the suffix i is added.

Other splitting possibilities exist, for example k^2h^2. By using the operator correspondence for this case the term $\partial_x^2(h^2u)$ is obtained. In the usual Boussinesq-like equations this term does not occur. Thus, it seems permissible to disregard this possibility. The same reasoning holds for the possibility kh^2k, because the term $\partial_x(h^2\partial_x u)$ does not occur in the usual equations either.

It is important to notice that different values of γ do not affect the dispersion relation and the Boussinesq-like equations in case of a horizontal bottom. They only affect the equations in case of an uneven bottom. In general, a variation in depth causes a variation in wave amplitude. This effect is called shoaling. Consequently, the γ_i have to be determined in such a way that the model has the best possible shoaling properties.

3.3.1 Working out the elements in the matrix separately

In the previous subsection it was made clear that the sequence of expressions containing k result after use of operator correspondence, in different Boussinesq-like equations. In this

section, the first element is worked out in detail in order to show the application of operator correspondence on terms like $(1+\beta_1(kh)^2)$, which is similar for all elements. In the second and third element an additional degree of freedom occurs, which gives several possibilities. The fourth term is similar to the first and is not considered. Subsequently, from the alternative formulations of the second and the third element one possibility is selected, so that one model remains, of which the linear shoaling behaviour is investigated. Later, the other possibilities will be considered.

The first element

The complete first element in the matrix (equation (3.16a)) reads

$$[-\omega(1 + \beta_1(kh)^2)]Z \tag{3.19}$$

For simplicity the term $(kh)^2$ is taken apart. Multiplying this term by Z and splitting yields

$$(kh)^2Z = (1 + \gamma)hk^2(hZ) - \gamma h^2k^2Z \tag{3.20}$$

Using the operator correspondence $k \rightarrow i\partial_x$ yields

$$\begin{aligned}
&-(1 + \gamma_1)h\partial_x^2(h\zeta) + \gamma_1 h^2\partial_x^2\zeta = \\
&-h^2\zeta_{xx} - 2hh_x\zeta_x - hh_{xx}\zeta - 2\gamma_1 hh_x\zeta_x - \gamma_1 hh_{xx}\zeta = \\
&-h^2\zeta_{xx} - 2(1 + \gamma_1)hh_x\zeta_x + O(h_{xx}) = \\
&-[h^2\partial_x^2 + 2(1 + \gamma_1)hh_x\partial_x]\zeta + O(h_{xx})
\end{aligned} \tag{3.21}$$

Since we are only interested in contributions to linear shoaling, the terms containing h_{xx} are omitted. The term $(1+\beta_1(kh)^2)$ results in

$$(1 - \beta_1 h^2\partial_x^2 - 2\beta_1(1 + \gamma_1)hh_x\partial_x) \tag{3.22}$$

Finally, the whole element becomes

$$i\partial_t(1 - \beta_1 h^2\partial_x^2 - 2\beta_1(1 + \gamma_1)hh_x\partial_x) \tag{3.23}$$

The second element

The factor $(1+\alpha_1(kh)^2)$ in the second element is treated in the same way as in the first element. However, the factor kh gives an additional degree of freedom, and can be written as $kh=(1+\theta)hk-\theta kh$. To limit the number of possibilities, only the cases $\theta=0$ and $\theta=-1$ are considered.

With $\theta=0$, the following three possibilities can be formed:

$$hk(1 + \alpha_1(kh)^2) = hk(1 + \alpha_1(kh)^2) \quad (3.24a)$$

$$= h(1 + \alpha_1(kh)^2)k \quad (3.24b)$$

$$= (1 + \alpha_1(kh)^2)hk \quad (3.24c)$$

With $\theta=-1$, three possibilities can be formed as well, which read:

$$= k(1 + \alpha_1(kh)^2)h \quad (3.24d)$$

$$= (1 + \alpha_1(kh)^2)kh \quad (3.24e)$$

$$= kh(1 + \alpha_1(kh)^2) \quad (3.24f)$$

In the first instance option (3.24f) is selected. The other possibilities will be considered later.

The third element

The factor $(1+\alpha_2(kh)^2)$ is also treated in the same way as in the first element. The additional degree of freedom is obtained by the position of k. The third element reads

$$gk(1+\alpha_2(kh)^2) \quad (3.25a)$$

Another form that can be discerned is:

$$g(1+\alpha_2(kh)^2)k \quad (3.25b)$$

In the first instance (3.25b) is selected. Option (3.25a) will be considered later.

The provisional model

So far, in equations (3.16a), the degrees of freedom, provided by the splitting of $(kh)^2$, are represented by four γ_i. Furthermore, alternative formulations of the second and third element are concerned. For both elements one alternative is selected in advance, resulting in a model with four indefinite γ_i. Of this model the shoaling behaviour is determined. Subsequently, models formulated with the other alternatives are considered. In this manner, 2 x 6 models

can be made from equations (3.16a). The same holds for equations (3.16b) through (3.16d), we have 48 different models.

The provisional model is given by equations (3.16a), where equations (3.24f) and (3.25b) represent the second and the third element respectively and $(kh)^2$ is written as equation (3.22). Using operator correspondence, this model is transformed into a system valid for small bottom slopes, since the higher order terms of h are neglected in equation (3.21). This system reads

$$\begin{bmatrix} \partial_t(1-\beta_1 h^2\partial_x^2-\beta_1\delta_1 h h_x\partial_x) & \partial_x[h(1-\alpha_1 h^2\partial_x^2-\alpha_1\delta_2 h h_x\partial_x)] \\ g(1-\alpha_2 h^2\partial_x^2-\alpha_2\delta_3 h h_x\partial_x)\partial_x & \partial_t(1-\beta_2 h^2\partial_x^2-\beta_2\delta_4 h h_x\partial_x) \end{bmatrix} \begin{bmatrix} \zeta \\ u \end{bmatrix} = 0 \qquad (3.26)$$

where $\delta_i = 2(1+\gamma_i)$.

The linear system (3.26) can be written as

$$\frac{\partial\zeta}{\partial t} + \frac{\partial(hu)}{\partial x} = \alpha_1\frac{\partial}{\partial x}\left[h^3\frac{\partial^2 u}{\partial x^2} + \delta_2 h^2 h_x\frac{\partial u}{\partial x}\right] + \beta_1 h\left[h\frac{\partial^3\zeta}{\partial t\partial x^2} + \delta_1 h_x\frac{\partial^2\zeta}{\partial t\partial x}\right] \qquad (3.27a)$$

$$\frac{\partial u}{\partial t} + g\frac{\partial\zeta}{\partial x} = \beta_2 h\left[h\frac{\partial^3 u}{\partial x^2\partial t} + \delta_4 h_x\frac{\partial^2 u}{\partial t\partial x}\right] + \alpha_2 g h\left[h\frac{\partial^3\zeta}{\partial x^3} + \delta_3 h_x\frac{\partial^2\zeta}{\partial x^2}\right] \qquad (3.27b)$$

In the next section the δ_i for this and other models will be optimized for good shoaling behaviour. The model with the best shoaling properties will be written with γ_i and the usual non-linear terms will be inserted, yielding a non-linear Boussinesq-like model valid for larger bottom slopes.

3.4 Shoaling

In the previous section it is shown that several models can be formulated, which obey to the [2/2] Padé approximation of the exact dispersion relation. From these models one provisional model is selected, which still has four degrees of freedom represented by the factors δ_i. The factors δ_i are determined in such a way that the shoaling coeffient of this model matches as good as possible to the exact linear shoaling coefficient.

First, a method for the derivation of the shoaling coefficient is given. Subsequently, the procedure followed to optimize the shoaling coefficient is described. Here after, the other models are considered.
In this section use is made of the mathematical symbolic software package *MAPLE*. Many computations are extremely extensive. Therefore, only where necessary results are given.

3.4.1 Derivation of the shoaling coefficient α_s

As argued before, a condition for Boussinesq-like equations is that the bottom slope is at most so large that at least one primary wave length fits in a region in which no appreciable changes in water depth occur. This implies that amplitudes and wave lengths vary much more slowly than phases. To that end a slowly varying parameter $X=\beta x$, with $\beta \ll 1$, is introduced.

To investigate the shoaling properties we put:

$$\zeta(x,t) = [a(\beta x)+i\beta c(\beta x)]\exp\left[-i\omega t + \frac{i}{\beta}S(\beta x)\right] \tag{3.28}$$

$$u(x,t) = [b(\beta x)+i\beta d(\beta x)]\exp\left[-i\omega t + \frac{i}{\beta}S(\beta x)\right] \tag{3.29}$$

where

$a(\beta x)+i\beta c(\beta x)$ denotes a slowly varying in space complex elevation amplitude,
$b(\beta x)+i\beta d(\beta x)$ denotes a slowly varying in space complex velocity amplitude and
$\int k(\beta x)\,dx = \beta^{-1}S(\beta x)$

The complex contributions $ic(\beta x)$ and $id(\beta x)$ represent a phase-shift in the surface elevation function and the velocity function respectively. These terms will be needed later in this section in order to provide a solvability condition. Notice that the complex contribution $id(\beta x)$ has also been used by Schäffer and Madsen (1994).

Substituting equations (3.28) and (3.29) in the set of linear equations (3.27) yields two equations in which terms of $O(\beta^2)$ can be ignored. Consequently, we have two equations containing β^0-terms and β^1-terms.

The zeroth-order approximation of these two equations reads

$$\begin{bmatrix} -\omega(1+\beta_2(kh)^2) & hk(1+\alpha_1(kh)^2) \\ gk(1+\alpha_2(kh)^2) & -\omega(1+\beta_1(kh)^2) \end{bmatrix} \begin{bmatrix} a \\ b \end{bmatrix} = 0 \tag{3.30}$$

Equation (3.30) can be written symbolically as

$$A \begin{bmatrix} a \\ b \end{bmatrix} = 0 \tag{3.31}$$

Since equations (3.30) are homogenous, a nontrivial solution is found if and only if $\mathrm{Det}(A)=0$. From $\mathrm{Det}(A)=0$ follows the dispersion relation, see section (3.1).
A homogeneous system with a determinant being zero is a system with consistent equations.

Therefore, both the first and the second equation in the system (3.30) can be used to expres $b(\beta x)$ in terms of $a(\beta x)$:

$$b = \frac{\omega a}{kh}\frac{\left(1+\beta_1 kh^2\right)}{\left(1+\alpha_1 kh^2\right)} \tag{3.32}$$

For the β^1-terms an inhomogeneous system is obtained, which reads symbolically

$$A \begin{bmatrix} c \\ d \end{bmatrix} = \begin{bmatrix} r_1 \\ r_2 \end{bmatrix} \tag{3.33}$$

where

$$r_1 = -(2\omega\beta_1 h^2 k)a_x + (3\alpha_1 h^3 kb - \omega\beta_1 h^2 a)k_x + (3\alpha_1 h^2 k^2 b - \omega\beta_1\delta_1 hka + b + \alpha_1\delta_2 h^2 k^2 b)h_x + (h + 3\alpha_1 h^3 k^2)b_x$$

$$r_2 = (g + 3g\alpha_2 h^2 k^2)a_x + (3g\alpha_2 h^2 ka - \beta_2 h^2\omega b)k_x + (g\alpha_2\delta_3 hk^2 a - \beta_2\delta_4 hk\omega b)h_x - (2\beta_2 h^2 k\omega)b_x$$

The subscripts x denote derivatives with respect to x.

As Det(A)=0, solutions for c and d from equation (3.33) only follow under certain conditions on the right-hand side. These solvability conditioins demand the right-hand side of equation (3.33) to be orthogonal to every solution of the adjoint homogeneous system, e.g, see Nayfeh (1981), section 15.1.
The homogeneous adjoint system reads

$$A^* \begin{bmatrix} v_1 \\ v_2 \end{bmatrix} = 0 \tag{3.34}$$

where $A^*=A^T$ because A is real.

Solving v_2 for v_1 yields

$$\boldsymbol{v} = \mu \begin{bmatrix} 1 \\ \dfrac{\omega\left(1+\beta_1(kh)^2\right)}{gk\left(1+\alpha_2(kh)^2\right)} \end{bmatrix} \tag{3.35}$$

where μ is any constant.
Orthogonality demands that the innerproduct $\boldsymbol{v}\cdot\boldsymbol{r}=0$.
Thus,

$$r_1 + \frac{\omega\left(1+\beta_1(kh)^2\right)}{gk\left(1+\alpha_2(kh)^2\right)} r_2 = 0 \tag{3.36}$$

This lengthy expression is a relation between the quantities a, b, k, h and their first derivatives. Notice that $c(\beta x)$ and $d(\beta x)$ need not be solved, but are only used to formulate solvability conditions. By differentiation of equation (3.32) with respect to x and substituting this expression together with equation (3.32) in equation (3.36), both b and b_x can be eliminated, which leads to the expression

$$\alpha_1 \frac{a_x}{a} + \alpha_2 \frac{h_x}{h} + \alpha_3 \frac{k_x}{k} = 0 \tag{3.37}$$

By differentiating equation (3.8) with respect to x yields

$$0 = \alpha_4 \frac{k_x}{k} + \alpha_5 \frac{h_x}{h} \tag{3.38}$$

Substituting equation (3.38) in equation (3.37) gives

$$\frac{a_x}{a} = -\alpha_s^B \frac{h_x}{h} \tag{3.39}$$

where

$$\alpha_s^B = -\frac{\alpha_2\alpha_4 - \alpha_3\alpha_5}{\alpha_1\alpha_4}$$

After substitution of the dispersion relation, i.e. equation (3.8), for ω^2 the shoaling coefficient α_s^B only contains the arguments δ_i and kh. Because of the lengthy expression of α_s^B, it will not be presented here. In the next section, δ_i are optimized in such a way that the shoaling coefficient α_s^B compares well to the exact linear shoaling coefficient α_s^L.

3.4.2 Determination of δ_i

It is known that the exact linear shoaling coefficient reads

$$\alpha_s^L = \frac{kh\tanh(kh)(1 - kh\tanh(kh))(1-\tanh^2(kh))}{[\tanh(kh) + kh(1 - \tanh^2(kh))]^2} \tag{3.40}$$

For optimizing the δ_i, the least-squares method is used, i.e. minimizing

$$Integrated\ Error = \int_{kh=0}^{kh=kh_0} (\alpha_s^B - \alpha_s^L)^2 d(kh) \tag{3.41a}$$

First $(\alpha_s^B-\alpha_s^L)^2$ is computed. Because of the complexity of this expression *MAPLE* is not able to integrate this analytically. Numerical integration is not possible either, as the δ_i are still unknown. Therefore, the right-hand side of equation (3.40) is expanded in a power series by a Padé [8/8] expansion in (kh). The advantage is that α_s^L and α_s^B are of the same type: a polynomial in kh, so they can easily be subtracted. It turns out that the denominator of the normalized expression $(\alpha_s^B-\alpha_s^L)^2$ does not contain any δ_i. By collecting all terms with kh raised to the same power, the integration of $(\alpha_s^B-\alpha_s^L)^2$ can be split in a summation of subintegrations:

$$\begin{aligned}\int \frac{c_0+c_1q^2 + c_2q^4 + c_3q^6 + \ldots}{1 + d_1q^2 + d_2q^4 + \ldots}\, dq = {} & c_0 \int \frac{1}{1 + d_1q^2 + d_2q^4 + \ldots}\, dq + \\ & c_1 \int \frac{q^2}{1 + d_1q^2 + d_2q^4 + \ldots}\, dq + \\ & c_2 \int \frac{q^4}{1 + d_1q^2 + d_2q^4 + \ldots}\, dq + \ldots\end{aligned} \tag{3.41b}$$

where q = kh.
MAPLE is capable to perform the subintegrations in the right-hand side of equation (3.41b) numerically, as no δ_i occur in d_i.

The integration range in kh has not yet been discussed. It is obvious that the lower value for kh is equal to zero. On the other hand the upper value for kh is the problem. As α_s^B is a polynomial the approximation is only accurate for low values of kh ($kh<O(1)$) and will diverge for increasing kh. For engineering practice an upper limit for kh of three suffices. To achieve a reliable model the δ_i are determined by an integration from $kh=0$ to $kh=5$. On the other hand, the dispersion relation is used to derive the shoaling coefficient. Therefore it is expected that the range, on which the shoaling behaviour is reliable, is a little bit smaller than the range on which the dispersion relations is reliable. From figure (3.1), it follows that the dispersion relation is reliable for kh up to 6 or 7, consequently the upper value $kh_0=5$ is found.

Integrating equation (3.41b) from $kh=0$ to $kh=5$ yields an expression for the integrated error in δ_1, δ_2, δ_3 and δ_4. The integrated error is minimized by partially differentiation of the integrated error with respect to δ_i and equating the four expressions to zero. In this manner four linear equations are obtained from which δ_i are easily solved. The results obtained for the provisional model are tabulated below.

i	δ_i	γ_i
1	3.00	0.500
2	2.79	0.394
3	0.354	-0.823
4	1.77	-0.111

The shoaling coefficient α_s^B, in which the δ_i tabulated above are substituted, is given in Appendix J.
In figure (3.3) α_s^B, α_s^{DUT2} and α_s^L are plotted as function of kh. This plot shows that the shoaling coefficient α_s^B is almost exact up to $kh=5$. It can also be seen that the shoaling coefficient pertaining to model DUT2 performs worse.

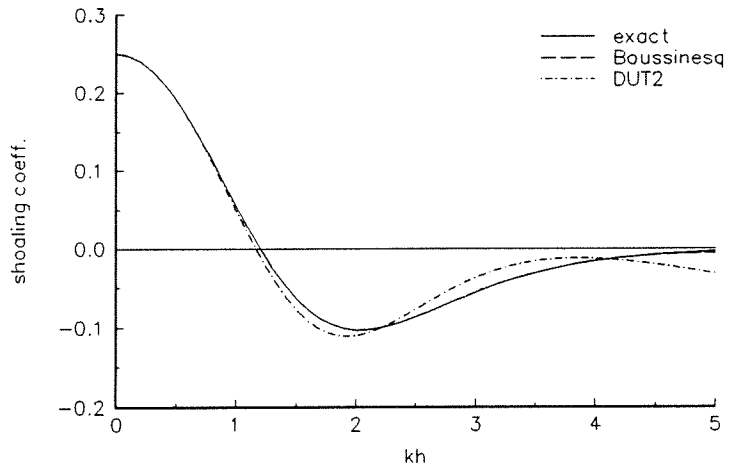

Figure (3.3) Shoaling coefficient

In order to quantify the accuracy, the computed δ_i are substituted in the integrated error, yielding a numerical value. This quantity is a measure for the squared area enclosed by the curve of the exact shoaling coefficient and the curve of the Boussinesq shoaling coefficient. The integrated error in the case of the provisional model equals $0.36 \cdot 10^{-7}$. The integrated error pertaining to the DUT2 model can be obtained directly by (numerical) integration of $(\alpha_s^B - \alpha_s^L)^2$ with respect to kh from 0 to 5 yielding $0.72 \cdot 10^{-3}$, which is much larger the integrated error of the provisional model.

Until now only the provisional model has been considered. In the next section the remaining models are investigated.

3.4.3 Investigation of the remaining models

In Section 3.2, four models have been derived with higher order dispersion, which contain only third-order derivatives. These four basic models are denoted here as model 1, model 2, model 3 and model 4. In Section 3.3 the model 1, i.e. set (3.16a), is considered in the case of uneven bottoms. The second element in the matrix of (3.16a) gives 6 different models, which are denoted here by the letters (a..f), see equations (3.24). The third element gives 2 different models, which are denoted here by an A or B, see equations (3.25). Thus, 12 different models based on set (3.16a) can be formed. Of these models one provisional model, here after called as model 1fB, has been investigated. In this section both the other 11 models and the 3x12 models that can be formed similarly from sets (3.16b) through (3.16d) are considered. First the basic models 1fB, 2fB, 3fB and 4fB are compared. Subsequently, the variants a through f and A and B are considered.

Comparing of the four basic models

Equations (3.16a) through (3.16d) look similar. The only difference is found in the coefficients α_i and β_i, which can be interchanged, see section 3.2. The shoaling coefficients corresponding to equations (3.16b, 3.16c and 3.16d) are computed by *MAPLE* as well. It is found that, if all δ_i are taken equal to some value Δ, all four models (1fB, 2fB, 3fB and 4fB) have the same expression for shoaling coefficient. But, if no assumptions are made for the δ_i, different expressions in kh and δ_i are found. Below the optimized δ_i in the models 1fB, 2fB, 3fB and 4fB are tabulated.

	Model 1fB	Model 2fB	Model 3fB	Model 4fB
δ_1	3.00	3.00	1.77	1.77
δ_2	2.79	0.354	2.79	0.354
δ_3	0.354	2.79	0.354	2.79
δ_4	1.77	1.77	3.00	3.00
Integrated error	$0.36 \cdot 10^{-7}$	$0.30 \cdot 10^{-7}$	$0.31 \cdot 10^{-7}$	$0.33 \cdot 10^{-7}$

It can be seen that all models have the same optimized values, but spread over the δ_i differently. The integrated error is almost the same. The differences are due to the numerical integration. From these results it can be concluded that apart from the values for δ_i, the models have equivalent linear shoaling coefficients. Therefore, we will continue investigating model 1fB and models 2, 3 and 4 will be left out of consideration.

Comparison of the alternative formulations of the third element of the matrix

The third element of the matrix in equation (3.27) is written as

$$g(1 + \alpha_2(kh)^2)k \tag{3.42}$$

Multiplying (3.42) by Z and using operator correspondence as usual, an expression is obtained in which Z is replaced by ζ. Substituting equation (3.28) and neglecting the terms with β^2, β^3 and β^4 yields

$$g\alpha_2 hh_x\beta ak^2\delta_b + g(a_x\beta + iak + 3\alpha_2 h^2 a_x\beta k^2 + 3\alpha_2 h^2 ak_x\beta k + i\alpha_2 h^2 ak^3) \tag{3.43}$$

The third element of the matrix in equation (3.27) can also be written as

$$gk(1 + \alpha_2(kh)^2) \tag{3.44}$$

Repeating the same procedure as used for equation (3.42), a different expression is obtained. Substituting equation (3.28) and neglecting the terms with β^2, β^3 and β^4 yields

$$g\alpha_2 hh_x\beta ak^2\delta_a + g(a_x\beta + iak + 2\alpha_2 hh_x\beta ak^2 + 3\alpha_2 h^2 a_x\beta k^2 + 3\alpha_2 h^2 ak_x\beta k + i\alpha_2 h^2 ak^3) \tag{3.45}$$

Equating equation (3.43) and (3.45) yields

$$g\alpha_2 hh_x\beta ak^2\delta_a + 2g\alpha_2 hh_x\beta ak^2 - g\alpha_2 hh_x\beta ak^2\delta_b = 0 \tag{3.46}$$

Solving for δ_a yields

$$\delta_a = \delta_b - 2 \tag{3.47}$$

Apparently, if equation (3.47) is satisfied, equations (3.25a) and (3.25b) are identical, at least to order (β^1). For higher powers of β the two equations may differ, but it is not possible to make a choice for these orders based on linear shoaling behaviour.
Comparing *MAPLE's* results for optimized δ_i in the following table, it can be concluded that equations (3.25a) and (3.25b) affect only δ_3. And indeed, δ_{3a} equals δ_{3b}-2.

	model 1fA	model 1fB
δ_1	3.00	3.00
δ_2	2.79	2.79
δ_3	-1.646	0.354
δ_4	1.77	1.77
Integrated error	$0.32\cdot10^{-7}$	$0.36\cdot10^{-7}$

Computing γ_{3a} resp. γ_{3b} from δ_{3a} resp. δ_{3b} by

$$\gamma_i = \frac{\delta_i - 2}{2} \tag{3.48}$$

gives γ_{3a}=-1.823 and γ_{3b}=-0.823.

Although the models 1fA and 1fB have the same linear shoaling behaviour, the model 1fB, based on equation (3.25b), is preferred, since γ_{3b} has a more logical value. A logical value for γ would be between -1 and 1, see equation (3.17). Apparently, the extra derivatives introduced by k in equation (3.25a) do not contribute to a better (linear) shoaling behaviour and therefore they are eliminated by taking $\gamma_{3a}=\gamma_{3b}-1$. Since the formulation according to equation (3.25b) is preferred above equation (3.25a), the addition B in the name-giving will be dropped hereafter.

The limit behaviour of the shoaling coefficient for $kh \to 0$

Before we continue with the discussion of equations (3.24), the limit behaviour of the shoaling coefficient for $kh \to 0$ should be discussed first. Because dissipation is left out of consideration in Boussinesq-like equations in general, no wave energy is produced or dissipated. Therefore, energy is conserved, i.e. the energy flux remains constant. This can be written as

$$\nabla \cdot (c_g E) = 0 \tag{3.49}$$

where in the case of uni-directional propagation and very shallow water, equation (3.49) reduces to

$$\frac{\partial}{\partial x}\left(\sqrt{h}\, a^2\right) = 0$$

$$\sqrt{h} \cdot 2a \frac{\partial a}{\partial x} + a^2 \cdot \frac{1}{2} \frac{1}{\sqrt{h}} \frac{\partial h}{\partial x} = 0 \tag{3.50}$$

$$\frac{a_x}{a} = -\frac{1}{4} \frac{h_x}{h}$$

Thus, the shoaling coefficient approaches to $^1/_4$ for $kh \to 0$. This is known as Green's law. The reader should notice the minus sign in front of the shoaling coefficient.

Comparison of the alternative formulations for the second element of the matrix

The second element of the matrix in equations (3.16) can be formulated at six different ways, leading to six different models, see equation (3.24). In this section the models 1a through 1f are considered.
The models 1a through 1f can be divided into two groups. The first group, derived with $\theta=0$, contains models 1a, 1b and 1c. The second group, derived with $\theta=-1$, contains models 1d, 1e and 1f.
First, model 1a is considered. Although *MAPLE* is able to compute the optimized δ_i, the resulting graph does not make any sense. Even the limit value for $kh\rightarrow 0$ is wrong. The coefficient $\alpha_s^B(kh=0)$ equals $-1/4$ in stead of $+1/4$, see figure (3.4). This error cannot be corrected by choosing δ_i, since if $kh=0$ no δ_i are involved. This model is disapproved immediately, as it violates Green's law. Exactly the same problems arises for model 1b and 1c. Obviously, all equations derived with $\theta=0$ are useless.

The second group, containing the models 1d, 1e and 1f is investigated. These models satisfy the condition $\alpha_s^B(kh=0)=-1/4$. The second element of the matrix is worked out in terms of $O(\beta^1)$. For model 1d we get

$$(h_x b+\alpha_1\delta_{2d}h^2h_x k^2 b+hbp+5h_x\alpha_1 h^2k^2b-hkd+3\alpha_1 h^3k_x kb-\alpha_1 h^3k^3d+3\alpha_1 h^3k^2bp)\beta \tag{3.51}$$

and for both model 1e and model 1f we get

$$(h_x b+3h_x\alpha_1 h^2k^2b+hb_x-hkd+3\alpha_1 h^3k^2b_x+3\alpha_1 h^3k_x kb-\alpha_1 h^3k^3d+\alpha_1\delta_{2e/f}h^2h_x k^2b)\beta \tag{3.52}$$

Obviously, the linear shoaling coefficient of model 1e is equivalent to the linear shoaling coefficient of model 1f. Equating expression (3.51) to (3.52) and solving for δ_{2e} or δ_{2f} yields

$$\delta_{2f}=\frac{(2\alpha_1 h^2h_x\beta k^2b+\beta\alpha_1\delta_{2d}h^2h_x k^2b)}{\alpha_1 h^2h_x\beta k^2b} \quad \Rightarrow$$

$$\delta_{2f}=2+\delta_{2d} \tag{3.53}$$

Thus, if equation (3.53) is satisfied, the models 1d and 1f have exactly the same linear shoaling behaviour. The δ_i for the models 1d, 1e and 1f, optimized by the least-squares method, are tabulated below.

	Model 1d	Model 1e	Model 1f
δ_1	3.00	3.00	3.00
δ_2	0.792	2.792	2.792
δ_3	0.354	0.354	0.354
δ_4	1.77	1.77	1.77
Integrated error	$0.19 \cdot 10^{-7}$	$0.30 \cdot 10^{-7}$	$0.36 \cdot 10^{-7}$

From the table above it can be seen that the models 1e and 1f have the same optimized δ_i, This was expected, since the expression for the $O(\beta^1)$-terms of model 1e and 1f is identical. From this tabel it can also be seen that $\delta_{2f}=\delta_{2d}+2$, which is in accordance with equation (3.53).

As mentioned earlier, the models 1a, 1b and 1c do not satisfy because $\alpha_s^B(kh=0) \neq {}^1/_4$. This does not necessarily mean that terms with hk are not allowed. Therefore θ is taken equal to $-{}^1/_2$. This model will be called model 1t. The second element now becomes

$$\frac{1}{2}\left(1+\alpha_1(kh)^2\right)hk + \frac{1}{2}\left(1+\alpha_1(kh)^2\right)kh \tag{3.54}$$

The model 1t also turns out to have a wrong limit behaviour. The shoaling coefficient of model 1t for $kh=0$ equals 0. In figure (3.4) the corresponding $\alpha_s B$ for $\theta=0$, $\theta=-½$ and $\theta=-1$ and α_s^L are plotted as function of kh. From this figure it may be assumed that θ affects $\alpha_s^B(kh=0)$ linearly, so that the limit behaviour is only correct when $\theta=-1$.

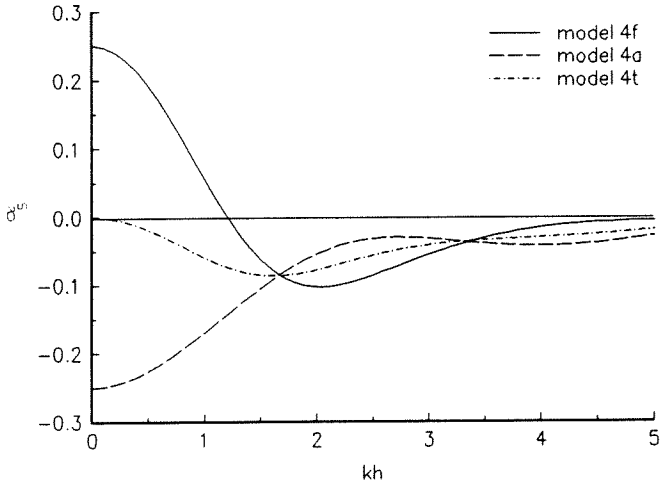

Figure (3.4) Shoaling coefficient

3.4.4 The remaining models with the same linear shoaling characteristics

The models 1d, 1e and 1f turn out to have the same linear dispersion relation and the same linear shoaling behaviour (with optimized δ_i). Yet, different sets of equations are obtained. The system in Fourier space corresponding to model 1d (using equations (3.17), (3.24d) and (3.26)) reads

$$\begin{bmatrix} -\omega\left\{1+\beta_1\left[(1+\gamma_1)hk^2h-\gamma_1h^2k^2\right]\right\} & k\left\{1+\alpha_1\left[(1+\gamma_2)hk^2h-\gamma_2h^2k^2\right]\right\}h \\ g\left\{1+\alpha_2\left[(1+\gamma_3)hk^2h-\gamma_3h^2k^2\right]\right\}k & -\omega\left\{1+\beta_2\left[(1+\gamma_4)hk^2h-\gamma_4h^2k^2\right]\right\} \end{bmatrix} \begin{bmatrix} Z \\ U \end{bmatrix} = 0 \tag{3.55a}$$

The system in Fourier space corresponding to model 1e (using equations (3.17), (3.24e) and (3.26)) reads

$$\begin{bmatrix} -\omega\left\{1+\beta_1\left[(1+\gamma_1)hk^2h-\gamma_1h^2k^2\right]\right\} & \left\{1+\alpha_1\left[(1+\gamma_2)hk^2h-\gamma_2h^2k^2\right]\right\}kh \\ g\left\{1+\alpha_2\left[(1+\gamma_3)hk^2h-\gamma_3h^2k^2\right]\right\}k & -\omega\left\{1+\beta_2\left[(1+\gamma_4)hk^2h-\gamma_4h^2k^2\right]\right\} \end{bmatrix} \begin{bmatrix} Z \\ U \end{bmatrix} = 0 \tag{3.55b}$$

The system in Fourier space corresponding to model 1f (using equations (3.17), (3.24f) and (3.26)) reads

$$\begin{bmatrix} -\omega\left\{1+\beta_1\left[(1+\gamma_1)hk^2h-\gamma_1h^2k^2\right]\right\} & kh\left\{1+\alpha_1\left[(1+\gamma_2)hk^2h-\gamma_2h^2k^2\right]\right\} \\ g\left\{1+\alpha_2\left[(1+\gamma_3)hk^2h-\gamma_3h^2k^2\right]\right\}k & -\omega\left\{1+\beta_2\left[(1+\gamma_4)hk^2h-\gamma_4h^2k^2\right]\right\} \end{bmatrix} \begin{bmatrix} Z \\ U \end{bmatrix} = 0 \tag{3.55c}$$

Using the operator correspondence and inserting the non-linear terms yields

$$\frac{\partial\zeta}{\partial t} + \frac{\partial}{\partial x}\left[(h+\zeta)u\right] = \beta_1 h\left[(1+\gamma_1)\frac{\partial^3 h\zeta}{\partial x^2\partial t} - \gamma_1 h\frac{\partial^3\zeta}{\partial x^2\partial t}\right] + \boldsymbol{R} \tag{3.56a}$$

$$\frac{\partial u}{\partial t} + u\frac{\partial u}{\partial x} + g\frac{\partial\zeta}{\partial x} = \beta_2 h\left[(1+\gamma_4)\frac{\partial^3 hu}{\partial x^2\partial t} - \gamma_4 h\frac{\partial^3 u}{\partial x^2\partial t}\right] + \alpha_2 gh\left[(1+\gamma_3)\frac{\partial^2}{\partial x^2}\left[h\frac{\partial\zeta}{\partial x}\right] - \gamma_3 h\frac{\partial^3\zeta}{\partial x^3}\right] \tag{3.56b}$$

The models 1d, 1e, 1f have each a different expression for **R** in equation (3.56a).

$$\boldsymbol{R}_d = \alpha_1 \frac{\partial}{\partial x}\left[h\left\{(1+\gamma_2)\frac{\partial^2 hu}{\partial x^2} - \gamma_2 h\frac{\partial^2 hu}{\partial x^2}\right\}\right] \tag{3.57a}$$

$$\boldsymbol{R}_e = \alpha_1\left[(1+\gamma_2)h\frac{\partial^2}{\partial x^2}\left[h\frac{\partial hu}{\partial x}\right] - \gamma_2 h^2\frac{\partial^3 hu}{\partial x^3}\right] \tag{3.57b}$$

$$\boldsymbol{R}_f = \alpha_1 \frac{\partial}{\partial x}\left[h^2\left\{(1+\gamma_2)\frac{\partial^2 hu}{\partial x^2} - \gamma_2 h\frac{\partial^2 u}{\partial x^2}\right\}\right] \tag{3.57c}$$

The δ_i and γ_i pertaining to model 1d, 1e and 1f are summarized in the next table.

	δ_1	γ_1	δ_2	γ_2	δ_3	γ_3	δ_4	γ_4
model 1d	3.00	0.500	0.792	-0.606	0.354	-0.823	1.77	-0.111
model 1e	3.00	0.500	2.792	0.394	0.354	-0.823	1.77	-0.111
model 1f	3.00	0.500	2.792	0.394	0.354	-0.823	1.77	-0.111

Since no discrimininating analytical criterion is found, comparisons with measurements has to give the decisive answer to which model is to be proposed.

3.4.5 Extension to deeper water

The δ_i, which are determined by minimizing the integration of $(\alpha_s^B-\alpha_s^L)^2$ from $kh=0$ to $kh=5$, give a shoaling behaviour with excellent results for $kh\in[0,5]$, but beyond this range α_s^B diverges. For $kh\to\infty$ the limit value of α_s^B equals -½. Although the limit value of α_s^L equals 0, this is not a bad result. Most polynomials have no asymptotes. In figure (3.5) α_s^B is plotted for $kh\in[0,10]$.

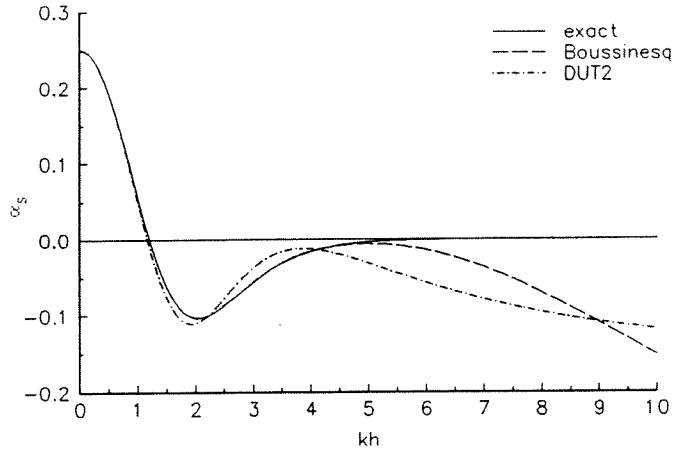

Figure (3.5) Shoaling coefficient

Instead of optimizing the δ_i by integration of $(\alpha_s^B-\alpha_s^L)^2$ from $kh=0$ to $kh=5$, the δ_i can also be optimized by integration from $kh=0$ to $kh=8$. Other coefficients are found, which are tabulated below.

	model 1f integrated to $kh=8$	model 1f integrated to $kh=5$
δ_1	3.08	3.00
δ_2	3.36	2.79
δ_3	1.62	0.354
δ_4	2.99	1.77
Integrated error	$0.52\cdot10^{-4}$	$0.36\cdot10^{-7}$

As argued before the quality of the shoaling depends on the quality of the dispersion relation. In figure (3.1) it can be seen that the dispersion relation is not very accurate any more for values of kh larger than 7 or 8. The advantage of integrating from $kh=0$ to $kh=8$ is that the shoaling behaviour performs relatively well up to $kh=9$. But, over the whole range small deviations occur. In figure (3.6) $\alpha_s^{B}{}_{int.\ to\ 8}$ and α_s^L are plotted as function of kh. The integrated error of $\alpha_s^{B}{}_{int.\ to\ 8}$ is expected to be larger than the integrated error of $\alpha_s^{B}{}_{int.\ to\ 5}$, since the integration is carried out over a larger range. However, the difference is about a factor 1000 and that is significantly less accurate. In figure (3.7) $(\alpha_s^L-\alpha_s^{B}{}_{int.\ to\ 5})$ and $(\alpha_s^L-\alpha_s^{B}{}_{int.\ to\ 8})$ are plotted. Absolute errors are preferred against relative error, as α_s^L has one zero and a limit value equal to zero.

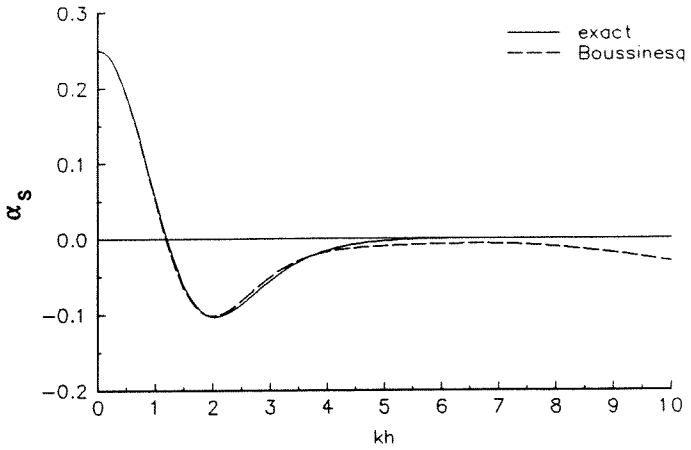

Figure (3.6) Shoaling coefficient by integration of from kh=0 to kh=8

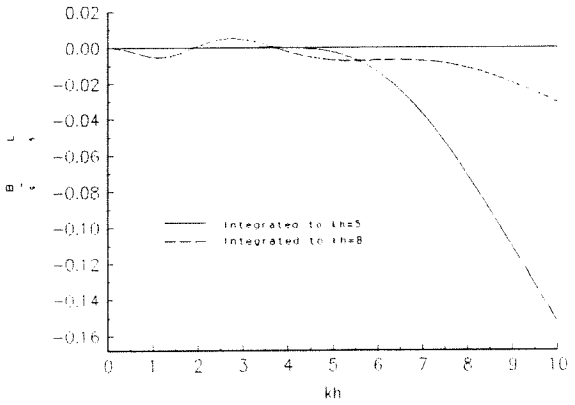

Figure (3.7) Absolute deviation

Usually, a maximum value of kh of 3 suffices. Therefore, δ_i corresponding to a integration from $kh=0$ to $kh=5$ is recommended. But in the special case that higher values of kh of 5 are wanted, the δ_i corresponding to an integration from $kh=0$ to $kh=8$ can be useful. The values for δ_i and γ_i are tabulated for the case in which they are optimized by integration of $kh=0$ to $kh=8$.

i	δ_i	γ_i
1	3.08	0.539
2	3.36	0.681
3	1.62	-0.191
4	2.99	0.497

These values only hold for model 1f. To obtain values for other models, the γ_i have to be interchanged like usual, see section 3.4.3.

4 Numerical computation of Boussinesq-like equations

4.1 Introduction

In Chapter 3, three sets of Boussinesq-like equations were derived. In almost all cases, no analytical solution can be obtained. Therefore, we have to solve these equations numerically. In this chapter, the application of Keller's Box method will be described. In the case of solving the classical shallow water equations, the use of the Preissman method, which is similar to Keller's Box method, is quite common. The question is how far existing shallow water models can be extended with Boussinesq-like terms without changing the numerical method drastically. Therefore, no other methods for solving Boussinesq-like equations are considered.
Since most problems will consist in a given surface elevation at a certain point and the question how this wave will behave over a given bathymetry, no inconvenient reflections of any border are wanted. In order to keep the computational domain as small as possible and with that, the computation time as small as possible, special attention will be paid to weakly reflecting boundaries.

4.2 Keller's Box method

Keller's Box method is a simple, second-order accurate and efficient method for solving the laminar and turbulent boundary-layer equations (Cebeci and Smith,1974). The method was developed by Keller (1970) and turned out to be easier to program, much faster and more flexible than most other numerical methods that have been employed for such problems. Because of its box structure the method allows varying mesh-sizes.
These boundary-layer equations contain both non-linear terms and third derivatives, like the Boussinesq-like equations do. In the next sections, we will formulate the method for the case of one dimensional Boussinesq-like equations.

One of the basic features of the procedure is to write the system of third-order partial differential equations in the form of a first-order system. Thus, some derivatives of u and ζ must be introduced as new unknown functions. The first-order partial differential equations are approximated on an arbitrary rectangular grid, using simple centred-difference quotients and averages at the midpoints of grid rectangles to get $O(\Delta x^2,\Delta t^2)$ accurate finite-difference equations.
The scheme is implicit and unconditionally stable, but the equations are non-linear as well. In general, solving non-linear equations has to be done by means of iteration. As will be shown, it is possible to discretize the non-linear terms in such a way that linear finite-difference equations occur.

4.2.1 Keller's Box method for Boussinesq-like equations

For the sake of convenience, the set Boussinesq-like equations pertaining to model 1f are repeated here

$$\frac{\partial \zeta}{\partial t} + \frac{\partial}{\partial x}[(h+\zeta)u] = \beta_1 h\left[(1+\gamma_1)\frac{\partial^3 h\zeta}{\partial x^2 \partial t} - \gamma_1 h\frac{\partial^3 \zeta}{\partial x^2 \partial t}\right] + \alpha_1 \frac{\partial}{\partial x}\left[h^2\left\{(1+\gamma_2)\frac{\partial^2 hu}{\partial x^2} - \gamma_2 h\frac{\partial^2 u}{\partial x^2}\right\}\right] \tag{4.1a}$$

$$\frac{\partial u}{\partial t} + u\frac{\partial u}{\partial x} + g\frac{\partial \zeta}{\partial x} = \beta_2 h\left[(1+\gamma_4)\frac{\partial^3 hu}{\partial x^2 \partial t} - \gamma_4 h\frac{\partial^3 u}{\partial x^2 \partial t}\right] + \alpha_2 gh\left[(1+\gamma_3)\frac{\partial^2}{\partial x^2}\left(h\frac{\partial \zeta}{\partial x}\right) - \gamma_3 h\frac{\partial^3 \zeta}{\partial x^3}\right] \tag{4.1b}$$

For later use, equations (4.1a and 4.1b) are expanded. Due to this operation the equations are not written in conservative form any more. If no discontinuities occur, the solution is sufficiently smooth and if both Δx and Δt are small enough, the non-conservative equations will converge as well. The Boussinesq-like equations are solved within these restrictions.

The expanded equations read for the continuity equation

$$A_1\zeta_t + A_2\zeta_{xt} + A_3\zeta_{xxt} + A_4 u + A_5 u_{xx} + A_6 u_{xxx} + A_7 u_x + \zeta u_x + \zeta_x u = 0 \tag{4.2a}$$

where

$$\begin{aligned} A_1 &= 1-\beta_1 h_{xx} h(1+\gamma_1) \\ A_2 &= -2\beta_1 h_x h(1+\gamma_1) \\ A_3 &= -\beta_1 h^2 \\ A_4 &= h_x - 2\alpha_1 h_{xx} h_x h(1+\gamma_2) - \alpha_1 h^2 h_{xxx} \end{aligned} \qquad \begin{aligned} A_5 &= -\alpha_1 h_x h^2(5+2\gamma_2) \\ A_6 &= -\alpha_1 h^3 \\ A_7 &= h - 3\alpha_1 h_{xx} h^2(1+\gamma_2) - 4\alpha_1 h_x^2 h(1+\gamma_2) \end{aligned}$$

and for the momentum equation

$$B_1\zeta_x + B_2\zeta_{xx} + B_3\zeta_{xxx} + B_4 u_{xt} + B_5 u_{xxt} + B_6 u_t + u u_x = 0 \tag{4.2b}$$

where

$$\begin{aligned} B_1 &= g - \alpha_2 g h_{xx} h(1+\gamma_3) \\ B_2 &= -2\alpha_2 g h_x h(1+\gamma_3) \\ B_3 &= -\alpha_2 g h^2 \end{aligned} \qquad \begin{aligned} B_4 &= -2\beta_2 h_x h(1+\gamma_4) \\ B_5 &= -\beta_2 h^2 \\ B_6 &= 1-\beta_2 h_{xx} h(1+\gamma_4) \end{aligned}$$

First the (expanded) continuity equation (4.2a) and the (expanded) momentum equation (4.2b) have to be written as a system of first-order partial differential equations. For that purpose, we introduce four new dependent variables *ux(u)*, *uxx(ux)*, *ζx(ζ)* and *ζxx(ζx)* such that the equations (4.2a and 4.2b) can be written as

$$A_1\frac{\partial \zeta}{\partial t}+A_2\frac{\partial(\zeta x)}{\partial t}+A_3\frac{\partial(\zeta xx)}{\partial t}+A_4 u+A_5(uxx)+A_6\frac{\partial(uxx)}{\partial x}+A_7(ux)+\zeta(ux)+u(\zeta x) = 0 \tag{4.3a}$$

$$B_1(\zeta x)+B_2(\zeta xx)+B_3\frac{\partial(\zeta xx)}{\partial x}+B_4\frac{\partial(ux)}{\partial t}+B_5\frac{\partial(uxx)}{\partial t}+B_6\frac{\partial(u)}{\partial t}+u(ux) = 0 \tag{4.3b}$$

$$ux = \frac{\partial u}{\partial x}, \qquad uxx = \frac{\partial ux}{\partial x}, \qquad \zeta x = \frac{\partial \zeta}{\partial x}, \qquad \zeta xx = \frac{\partial \zeta x}{\partial x} \tag{4.3c}$$

We now consider a rectangular grid shown in figure (4.1). We denote the grid points by

$$\begin{array}{llll} t_0 = 0 & t_n = t_{n-1} + \Delta t_n & n & = 1,2,\ldots,N \\ x_0 = 0 & x_j = x_{j-1} + \Delta x_j & j & = 1,2,\ldots,J \end{array}$$

The quantities (ζ, u, ζx, ux, ζxx, uxx) at the grid points (x_{j+1},t_{n+1}) are approximated by grid functions denoted by (ζ_{j+1}^{n+1}, u_{j+1}^{n+1}, ζx_{j+1}^{n+1}, ux_{j+1}^{n+1}, ζxx_{j+1}^{n+1}, uxx_{j+1}^{n+1}). Quantities midway between grid points are defined for any grid function $q_{j+\frac{1}{2}}^{n+1}$ by

$$q_{j+\frac{1}{2}}^{n+1} = \tfrac{1}{2}(q_j^{n+1} + q_{j+1}^{n+1}) \tag{4.4}$$

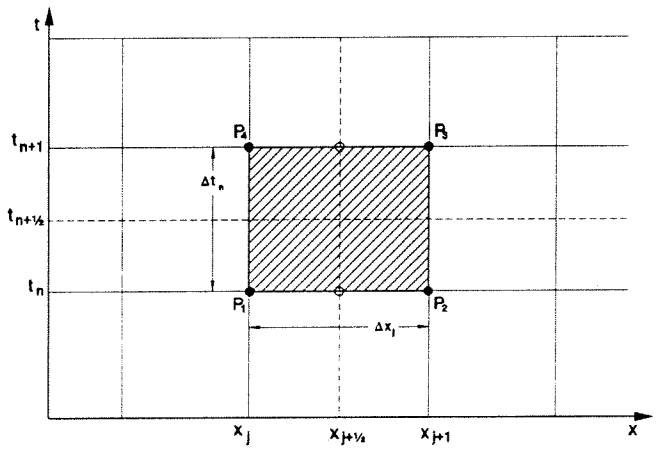

Figure 4.1 Grid definition

Thus, equation (4.3c) is approximated by a finite difference equation as follows:

$$ux_{j+\frac{1}{2}}^{n+1} = \frac{u_{j+1}^{n+1} - u_j^{n+1}}{\Delta x}$$

$$\Rightarrow \quad \frac{u_{j+1}^{n+1} - u_j^{n+1}}{\Delta x} = \frac{ux_{j+1}^{n+1} + ux_j^{n+1}}{2} \tag{4.5}$$

$$ux_{j+\frac{1}{2}}^{n+1} = \frac{ux_{j+1}^{n+1} + ux_j^{n+1}}{2}$$

Similarly, the approximating equations of (4.3d), (4.3e) and (4.3f) read

$$\frac{ux_{j+1}^{n+1} - ux_j^{n+1}}{\Delta x} = \frac{uxx_{j+1}^{n+1} + uxx_j^{n+1}}{2} \tag{4.6}$$

$$\frac{\zeta_{j+1}^{n+1} - \zeta_j^{n+1}}{\Delta x} = \frac{\zeta x_{j+1}^{n+1} + \zeta x_j^{n+1}}{2} \tag{4.7}$$

$$\frac{\zeta x_{j+1}^{n+1} - \zeta x_j^{n+1}}{\Delta x} = \frac{\zeta xx_{j+1}^{n+1} + \zeta xx_j^{n+1}}{2} \tag{4.8}$$

Although equations (4.3a) and (4.3b) are more complicated, the procedure of formulation is quite similar, except for the non-linear terms, which may result in non-linear difference equations. As illustration, the non-linear term $u_x\zeta$ is considered. The difference equation may be defined as

$$\zeta\frac{\partial u}{\partial x} \Rightarrow \tfrac{1}{2}\zeta_{j+\frac{1}{2}}^{n+1}ux_{j+\frac{1}{2}}^{n+1} + \tfrac{1}{2}\zeta_{j+\frac{1}{2}}^{n}ux_{j+\frac{1}{2}}^{n} \Rightarrow$$

$$\frac{\left(\zeta_{j+1}^{n+1} + \zeta_j^{n+1}\right)\left(ux_{j+1}^{n+1} + ux_j^{n+1}\right)}{8} + \frac{\left(\zeta_{j+1}^{n} + \zeta_j^{n}\right)\left(ux_{j+1}^{n} + ux_j^{n}\right)}{8} \tag{4.9}$$

In equation (4.9) products containing two quantities at a new time level occur. Because of that the resulting difference equation is non-linear. In order to solve a non-linear system of equations, an iteration method has to be used, which is not attractive.

A slightly different approximating equation is

$$\zeta\frac{\partial u}{\partial x} \Rightarrow \tfrac{1}{2}\zeta_{j+\frac{1}{2}}^{n+1}ux_{j+\frac{1}{2}}^{n} + \tfrac{1}{2}\zeta_{j+\frac{1}{2}}^{n}ux_{j+\frac{1}{2}}^{n+1} \Rightarrow$$
$$\frac{\left(\zeta_{j+1}^{n+1}+\zeta_{j}^{n+1}\right)\left(ux_{j+1}^{n}+ux_{j}^{n}\right)}{8} + \frac{\left(\zeta_{j+1}^{n}+\zeta_{j}^{n}\right)\left(ux_{j+1}^{n+1}+ux_{j}^{n+1}\right)}{8} \tag{4.10}$$

Expansion of equation (4.10) will result in quite a few products, however, none of them produce non-linear equations. Therefore, the resulting system of equations is relatively easy to solve without iteration.

Equation (4.10) is not the only possibility resulting in linear equations. Another form is

$$\zeta\frac{\partial u}{\partial x} \Rightarrow \frac{\zeta_{j+1}^{n}ux_{j+1}^{n+1}+\zeta_{j}^{n}ux_{j}^{n+1}}{4} + \frac{\zeta_{j+1}^{n+1}ux_{j+1}^{n}+\zeta_{j}^{n+1}ux_{j}^{n}}{4} \tag{4.11}$$

Both equation (4.10) as (4.11) have a truncation error of $O(\Delta x^2,\Delta t^2,\Delta x\Delta t)$. Formulation (4.11) corresponds to the representation of A_i and B_i, in which h and its derivatives occur. In every A_i and B_i the quantities h, h_x, h_{xx} and h_{xxx} are averaged over x_j and x_{j+1}. In equation (4.10), the known quantities u and ζ are averaged as well. Only for this reason equation (4.10) is chosen instead of equation (4.11).

Working out very carefully all terms of equation (4.3a), its approximating equation yields after some manipulation

$$\left(\frac{A_1}{\Delta t}+\frac{ux_{j+\frac{1}{2}}^{n}}{2}\right)\zeta_{j}^{n+1}+\left(\frac{A_2}{\Delta t}+\frac{u_{j+\frac{1}{2}}^{n}}{2}\right)\zeta x_{j}^{n+1}+\frac{A_3}{\Delta t}\zeta xx_{j}^{n+1}+\left(\frac{A_4}{2}+\frac{\zeta x_{j+\frac{1}{2}}^{n}}{2}\right)u_{j}^{n+1}+\left(\frac{A_7}{2}+\frac{\zeta_{j+\frac{1}{2}}^{n}}{2}\right)ux_{j}^{n+1}+\left(\frac{A_5}{2}-\frac{A_6}{\Delta x}\right)uxx_{j}^{n+1}+$$
$$\left(\frac{A_1}{\Delta t}+\frac{ux_{j+\frac{1}{2}}^{n}}{2}\right)\zeta_{j+1}^{n+1}+\left(\frac{A_2}{\Delta t}+\frac{u_{j+\frac{1}{2}}^{n}}{2}\right)\zeta x_{j+1}^{n+1}+\frac{A_3}{\Delta t}\zeta xx_{j+1}^{n+1}+\left(\frac{A_4}{2}+\frac{\zeta x_{j+\frac{1}{2}}^{n}}{2}\right)u_{j+1}^{n+1}+\left(\frac{A_7}{2}+\frac{\zeta_{j+\frac{1}{2}}^{n}}{2}\right)ux_{j+1}^{n+1}+\left(\frac{A_5}{2}+\frac{A_6}{\Delta x}\right)uxx_{j+1}^{n+1} =$$

$$\frac{A_1}{\Delta t}\left(\zeta_{j+1}^{n}+\zeta_{j}^{n}\right)\frac{A_2}{\Delta t}\left(\zeta x_{j+1}^{n}+\zeta x_{j}^{n}\right)\frac{A_3}{\Delta t}\left(\zeta xx_{j+1}^{n}+\zeta xx_{j}^{n}\right)$$
$$-\frac{A_4}{2}\left(u_{j+1}^{n}+u_{j}^{n}\right)-\frac{A_5}{2}\left(uxx_{j+1}^{n}+uxx_{j}^{n}\right)-\frac{A_6}{\Delta x}\left(uxx_{j+1}^{n}+uxx_{j}^{n}\right)-\frac{A_7}{2}\left(ux_{j+1}^{n}+ux_{j}^{n}\right) \tag{4.12}$$

Notice that the right-hand-side contains only known quantities at time level n.

Finally, the approximating equation of (4.3b) reads

$$\frac{B_1}{2}\zeta x_j^{n+1}+(\frac{B_2}{2}-\frac{B_3}{\Delta x})\zeta xx_j^{n+1}+(\frac{B_6}{\Delta t}+\frac{ux_{j+\frac{1}{2}}^{n}}{2})u_j^{n+1}+(\frac{B_4}{\Delta t}+\frac{u_{j+\frac{1}{2}}^{n}}{2})ux_j^{n+1}+\frac{B_5}{\Delta t}uxx_j^{n+1}+$$

$$\frac{B_1}{2}\zeta x_{j+1}^{n+1}+(\frac{B_2}{2}-\frac{B_3}{\Delta x})\zeta xx_{j+1}^{n+1}+(\frac{B_6}{\Delta t}+\frac{ux_{j+\frac{1}{2}}^{n}}{2})u_{j+1}^{n+1}+(\frac{B_4}{\Delta t}+\frac{u_{j+\frac{1}{2}}^{n}}{2})ux_{j+1}^{n+1}+\frac{B_5}{\Delta t}uxx_{j+1}^{n+1}= \tag{4.13}$$

$$-\frac{B_1}{2}(\zeta x_{j+1}^{n}+\zeta x_j^{n})-\frac{B_2}{2}(\zeta xx_{j+1}^{n}+\zeta xx_j^{n})-\frac{B_3}{\Delta x}(\zeta xx_{j+1}^{n}+\zeta xx_j^{n})$$
$$+\frac{B_4}{\Delta t}(ux_{j+1}^{n}+ux_j^{n})+\frac{B_5}{\Delta t}(uxx_{j+1}^{n}+uxx_j^{n})+\frac{B_6}{\Delta t}(u_{j+1}^{n}+u_j^{n})$$

The equations (4.5), (4.6), (4.7), (4.8), (4.10), (4.12) and (4.13) can be written in matrix notation as

$$\begin{bmatrix} Cl_j & Cr_{j+1} \end{bmatrix} \begin{bmatrix} Q_j \\ Q_{j+1} \end{bmatrix} = \begin{bmatrix} r_1 & r_2 & 0 & 0 & 0 & 0 \end{bmatrix}^T \tag{4.14}$$

where

$$Q_j = \begin{bmatrix} \zeta_j^{n+1} & ux_j^{n+1} & \zeta xx_j^{n+1} & u_j^{n+1} & \zeta x_j^{n+1} & uxx_j^{n+1} \end{bmatrix}^T$$

$$r_1 = \frac{A_1}{\Delta t}(\zeta_{j+1}^{n}+\zeta_j^{n})\frac{A_2}{\Delta t}(\zeta x_{j+1}^{n}+\zeta x_j^{n})\frac{A_3}{\Delta t}(\zeta xx_{j+1}^{n}+\zeta xx_j^{n})$$
$$-\frac{A_4}{2}(u_{j+1}^{n}+u_j^{n})-\frac{A_5}{2}(uxx_{j+1}^{n}+uxx_j^{n})-\frac{A_6}{\Delta x}(uxx_{j+1}^{n}+uxx_j^{n})-\frac{A_7}{2}(ux_{j+1}^{n}+ux_j^{n})$$

$$r_2 = -\frac{B_1}{2}(\zeta x_{j+1}^{n}+\zeta x_j^{n})-\frac{B_2}{2}(\zeta xx_{j+1}^{n}+\zeta xx_j^{n})-\frac{B_3}{\Delta x}(\zeta xx_{j+1}^{n}+\zeta xx_j^{n})$$
$$+\frac{B_4}{\Delta t}(ux_{j+1}^{n}+ux_j^{n})+\frac{B_5}{\Delta t}(uxx_{j+1}^{n}+uxx_j^{n})+\frac{B_6}{\Delta t}(u_{j+1}^{n}+u_j^{n})$$

The (6 x 6) matrices Cl_j and Cr_{j+1} are inserted in Appendix B.

In fact, the sequence of the quantities in Q_j is arbitrary. However, the sequence as suggested in equation (4.14) will later be more convenient. The system (4.14) holds only for any single grid point. A system encompassing all grid points reads

$$MQ = R \tag{4.15}$$

where

$$M = \begin{bmatrix} Cl_1 & Cr_2 & & & & \\ & Cl_2 & Cr_3 & & & \\ & & . & & 0 & \\ & & & . & & \\ & & & & . & \\ & 0 & & & Cl_{J-2} & Cr_{J-1} \\ & & & & & Cl_{J-1} \quad Cr_J \end{bmatrix}$$

$$R = \begin{bmatrix} r_1 & r_2 & r_3 & r_4 & r_5 & r_6 & . & . & . & r_{6J-4} & r_{6J-3} & r_{6J-2} & r_{6J-1} & r_{6J} \end{bmatrix}^T$$

$$Q = \begin{bmatrix} Q_0 & Q_1 & . & . & . & Q_{J-1} & Q_J \end{bmatrix}^T$$

The matrix M appears to be a block diagonal matrix. Many techniques are available solving systems of linear equations. Because its simplicity and speed a direct solver is preferable. However, direct solvers may suffer from severe matrix conditions.

4.2.2 Solving the system of linear equations

In section (4.3) the boundary conditions are discussed in detail. First, we will confine ourselves to state that six boundary conditions are needed to solve equations (4.3). Besides prescribing u and ζ, their first and second spatial derivatives have to be prescribed as well. In most cases, the boundary values will be spread over the boundaries in equal numbers, i.e. three at both sides. Other combinations are possible and the same procedure can be followed.

Let us consider the case that we prescribe ζ, ux, ζxx at the left boundary and u, ζx, uxx at the right boundary. This is in agreement with the sequence of quantities in Q_j.

For each left boundary quantity, a relation can be formulated. The most simple form for any function q is $q=q_{bnd}(t)$, but other relations may be formulated as well, such as a relation between two quantities. For the left boundary we get

$$BND\ Q_0 = \begin{bmatrix} \zeta_{bnd}(t) \\ ux_{bnd}(t) \\ \zeta xx_{bnd}(t) \end{bmatrix} \tag{4.16}$$

After some manipulations, the (3x6) BND matrix can be written as

$$BND = \begin{bmatrix} 1 & 0 & 0 & bnd_{14} & bnd_{15} & bnd_{16} \\ 0 & 1 & 0 & bnd_{24} & bnd_{25} & bnd_{26} \\ 0 & 0 & 1 & bnd_{34} & bnd_{35} & bnd_{36} \end{bmatrix} \tag{4.17}$$

In the simple case that $q=q_{bnd}(t)$, all $bnd_{ij}=0$. When one or more relations between two quantities are specified, some coefficients $bnd_{ij}\neq 0$.

By subtracting the rows of equation (4.17) from the matrix Cl_0, the matrix Cl_0 can be reduced to

$$Cl_0 = \begin{bmatrix} 0 & 0 & 0 & c_1 & d_1 & e_1 \\ 0 & 0 & 0 & c_2 & d_2 & e_2 \\ 0 & 0 & 0 & c_3 & d_3 & e_3 \\ 0 & 0 & 0 & c_4 & d_4 & e_4 \\ 0 & 0 & 0 & c_5 & d_5 & e_5 \\ 0 & 0 & 0 & c_6 & d_6 & e_6 \end{bmatrix} \tag{4.18}$$

Similar procedure can be applied for the right boundary. But instead of vanishing of the first three columns, the last three columns vanish. Consequently, the matrix M reduces to a ($6J$ x $6J$) block diagonal matrix, which can be solved with a Thomas-like algorithm. The Thomas algorithm is a very efficient method for solving tridiagonal matrices, see Golub and Van Loan (1983). The matrix we are considering, may be conceived as a kind of a diagonal matrix. To solve this matrix, the Thomas algorithm is extended.

4.2.3 Solving the blockdiagonal matrix with an extended Thomas algorithm

The matrix M can be written as a diagonal matrix. With the band-width of 17 elements all elements of Cl_i and Cr_i are encompassed, see figure (4.2).

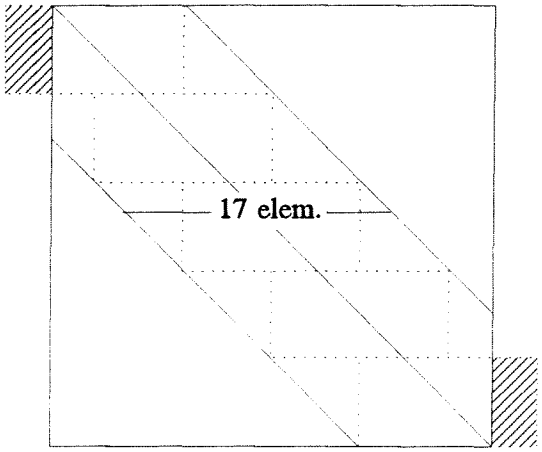

Figure 4.2 Matrix M

The hatched areas are the eliminated boundary conditions, which fall outside the actual square matrix M.

Diagonalizing M yields

$$M = \begin{bmatrix}
\underline{\boldsymbol{d_1}} & e_1 & f_1 & g_1 & h_1 & i_1 & j_1 & k_1 & l_1 & & & & & & & & & \\
d_2 & \underline{\boldsymbol{e_2}} & f_2 & g_2 & h_2 & i_2 & j_2 & k_2 & l_2 & & & & & & & & & \\
d_3 & e_3 & \underline{\boldsymbol{f_3}} & g_3 & h_3 & i_3 & j_3 & k_3 & l_3 & & & & 0 & & & & & \\
d_4 & e_4 & f_4 & \underline{\boldsymbol{g_4}} & h_4 & i_4 & j_4 & k_4 & l_4 & & & & & & & & & \\
d_5 & e_5 & f_5 & g_5 & \underline{\boldsymbol{h_5}} & i_5 & j_5 & k_5 & l_5 & & & & & & & & & \\
 & & & g_6 & h_6 & \underline{\boldsymbol{i_6}} & j_6 & k_6 & l_6 & m_6 & n_6 & o_6 & p_6 & q_6 & r_6 & & & \\
 & & & g_7 & h_7 & i_7 & \underline{\boldsymbol{j_7}} & k_7 & l_7 & m_7 & n_7 & o_7 & p_7 & q_7 & r_7 & & & \\
 & & & g_8 & h_8 & i_8 & j_8 & \underline{\boldsymbol{k_8}} & l_8 & m_8 & n_8 & o_8 & p_8 & q_8 & r_8 & & & \\
 & & & g_9 & h_9 & i_9 & j_9 & k_9 & \underline{\boldsymbol{l_9}} & m_9 & n_9 & o_9 & p_9 & q_9 & r_9 & & & \\
 & & & g_{10} & h_{10} & i_{10} & j_{10} & k_{10} & l_{10} & \underline{\boldsymbol{m_{10}}} & n_{10} & o_{10} & p_{10} & q_{10} & r_{10} & & & \\
 & & & g_{11} & h_{11} & i_{11} & j_{11} & k_{11} & l_{11} & m_{11} & \underline{\boldsymbol{n_{11}}} & o_{11} & p_{11} & q_{11} & r_{11} & & & \\
 & & & & & & & & & & & & & & & & & \\
 & & & & & & & & & . & . & . & . & . & . & . & . & \\
 & & & & & & & & & . & . & . & . & . & . & . & . & \\
 & & & & & & & & & . & . & . & . & . & . & . & . &
\end{bmatrix} \tag{4.19}$$

To solve the matrix M, the matrix is swept once from top to bottom, followed by a back substitution. The sweeping procedure will be discussed briefly.
The element d_2 is made zero by subtracting the first row multiplied by d_2/d_1 from the second. The second row now reads

$$\begin{bmatrix} 0 & e_2 - \frac{d_2}{d_1} e_1 & f_2 - \frac{d_2}{d_1} f_1 & g_2 - \frac{d_2}{d_1} g_1 & \cdots \end{bmatrix} \tag{4.20}$$

Similarly, all d_i, $(i>1)$, can be made zero. This procedure is repeated for all e_i $(i>2)$ and so on until all elements below the main diagonal, the bold and underlined elements, are eliminated. For this procedure it is important that the main diagonal is dominant, i.e. larger than all other elements in the row. If this is the case, it is a sufficient condition for limited round-off errors, see Golub and Van Loan (1983). The diagonal dominance can be enhanced by re-ordering the equations (4.3a through 4.3f) and/or by changing the sequence of quantities in equation (4.14), but all quantities specified at the left border should be ordered left from all quantities specified at the right boundary.

Subsequently, we continue with the back substitution, beginning from the bottom. Equation (4.21) represents a detail of the bottom of matrix M.

$$\begin{bmatrix} \cdot & \cdot & \cdot & w_{J-5} & x_{J-5} & y_{J-5} & z_{J-5} \\ & \cdot & \cdot & w_{J-4} & x_{J-4} & y_{J-4} & z_{J-4} \\ & & \cdot & w_{J-3} & x_{J-3} & y_{J-3} & z_{J-3} \\ & & & & x_{J-2} & y_{J-2} & z_{J-2} \\ & & & & & y_{J-1} & z_{J-1} \\ & & & & & & z_J \end{bmatrix} \begin{bmatrix} q_{J-5} \\ q_{J-4} \\ q_{J-3} \\ q_{J-2} \\ q_{J-1} \\ q_J \end{bmatrix} = \begin{bmatrix} r_{J-5} \\ r_{J-4} \\ r_{J-3} \\ r_{J-2} \\ r_{J-1} \\ r_J \end{bmatrix} \tag{4.21}$$

The unknown q_J can be solved directly as r_J/z_J. The equation for J-1 is containing only unknown q_{J-1}, since q_J is just computed. Thus, q_{J-1} can be computed by substitution of q_J. This procedure is repeated until all q_i are solved.
Now that the quantities at the new time level are computed, they are used in the repeated computation of the quantities at the next time level.

However, the diagonal matrix used here still contains quite a number of permanent zero elements. In a computer program only the diagonal elements have to be stored, which is in this case 6Jx17 elements, where J equals the number of nodes. In Appendix A, a different solving technique is described where the matrix M reduces to a hepta-diagonal matrix. This method has the advantage that it reduces the size of the allocated memory with about 40%. But it turned out that it was impossible to solve reduced Boussinesq-like equations in this manner.

4.3 Boundary conditions

A set of differential equations has no definite solution unless appropriate boundary conditions are specified. Boundaries are used to enclose the region of interest. Here, only one-dimensional problems are considered, like waves in a flume. In practice, a boundary can be a physical boundary, like a shore or a wall. Another possibility is an *open* boundary. This is an imaginary line in the flume. At an open boundary mostly ζ is prescribed, as these data can be obtained quite easily and accurately.
It should be emphasized that the boundary conditions have to be specified with care, since they are fully responsible for the behaviour of the solution in the flume. In other words, specifying wrong boundary conditions can mean that a different problem is solved and, as will be shown later, even instabilities may occur.

Prescribing boundary conditions cannot be done before knowing which and how many boundary conditions are needed. First this question can be answered from the perspective of solvability of the system of linear equations.
Although every node has 12 unknowns, i.e. six at grid point x_j and six at grid point x_{j+1}, six

of them are shared with a preceding node, which results in six unknowns per node. Only the first node does not have a preceding node. Therefore the total number of unknowns equals $6J+6$, where J equals the number of nodes. On the other hand, every node has six equations, which makes the number of equations equal to $6J$. Thus, from this point of view, six boundary values are needed to close the problem.

From a mathematical point of view also six boundary conditions have to be speciefied. This is explained as follows. Considering set (4.3), all quantities u, ux, uxx, ζ, ζx and ζxx are differentiated with respect to x. Therefore, when set (4.3) is integrated with respect to x, six integration constants occur. Consequently, six boundary conditions have to be specified.

From a physical point of view, the boundary conditions are determined by the behaviour of characteristics, i.e. lines that carry information in the x-t plane. This is explained in the next section.

4.3.1 Determination of characteristic directions

As argued before, the behaviour of the characteristics is essential for the boundary choices. Information is carried along the characteristic lines. Thus, the number of information *carriers* has to be equal to the number of information *providers*, i.e. boundary conditions.
To analyze the characteristics, equations (4.3) are written in the form

$$A\frac{\partial f}{\partial t} + B\frac{\partial f}{\partial x} + Cf = 0 \ , \qquad f = \begin{bmatrix} \zeta \\ u \end{bmatrix} \tag{4.22}$$

We find for A and B the matrices

$$A = \begin{bmatrix} A_1 & A_2 & A_3 & 0 & 0 & 0 \\ 0 & 0 & 0 & B_6 & B_4 & B_5 \\ 0 & 0 & 0 & 0 & 0 & 0 \\ 0 & 0 & 0 & 0 & 0 & 0 \\ 0 & 0 & 0 & 0 & 0 & 0 \\ 0 & 0 & 0 & 0 & 0 & 0 \end{bmatrix} , \qquad B = \begin{bmatrix} 0 & 0 & 0 & 0 & 0 & A_6 \\ 0 & 0 & B_3 & 0 & 0 & 0 \\ 1 & 0 & 0 & 0 & 0 & 0 \\ 0 & 1 & 0 & 0 & 0 & 0 \\ 0 & 0 & 0 & 1 & 0 & 0 \\ 0 & 0 & 0 & 0 & 1 & 0 \end{bmatrix} \tag{4.23}$$

The characteristic directions $\rho = dt/dx$ follow from $\mathrm{Det}(\rho B\text{-}A)=0$, yielding the condition

$$-A_6B_3\rho^6+A_3B_5\rho^4 = 0 \tag{4.24}$$

The solutions of equation (4.24) are

$$\rho_{1,2} = \pm \frac{\sqrt{\alpha_1 \alpha_2 \beta_1 \beta_2 gh}}{\alpha_1 \alpha_2 gh} \qquad (4.25)$$
$$\rho_{3,4,5,6} = 0$$

Obviously, the characteristic directions are independent of the solution of either ζ or u. This is rather remarkable, since the usual Boussinesq-like equations have characteristics depending on u, see Otta and Dingemans (1994).
According to equation (4.25), ρ_1 and ρ_2 have an opposite direction. Consequently, ζ and u must be specified at different boundaries.

4.3.2 Initial conditions

Formally, the line at time $t=0$ is also a boundary of region in the x-t space. The rule on the number of boundary conditions (here initial conditions) applies just as well. As all characteristics are entering the region across this line, we need six initial conditions in any case. This is in agreement with what we found in section 4.3.

A problem which can arise in practice is that we do not know precise initial data. Some assumptions have to be made. The simplest one is taking all initial quantities equal to zero, i.e. the fluid is in rest and the water level is horizontal. This situation can be considered as a disturbance on the real situation. This disturbance will travel through the computational domain. Fortunately, the influence of wrong initial data gradually fades out due to damping. (Bottom friction is not accounted in Boussinesq-like equations.) The fading can be increased by using weakly reflecting boundaries, see the next section. When the disturbance hits a weakly reflecting boundary, it will be reflected scarcely and after some time, approximately two times the travel time from boundary to boundary, the disturbance will have vanished. In the meantime, the solution gets more and more influenced by the incoming waves.

4.4 Weakly reflecting boundaries

In practice, it is not desirable to have boundaries that reflect waves. For example, if we are investigating the case of figure (4.3), waves generated at location A are propagating to location B. If the waves arriving at B are reflected, they cause disturbances in the domain of interest. Thus, waves should be absorbed totally at location B or the right boundary should be put far away, in order that the reflected waves do not reach the domain of interest before the end of the computation. The latter option is very time consuming and is not preferred. Therefore, efforts are made in deriving weakly reflecting boundaries.

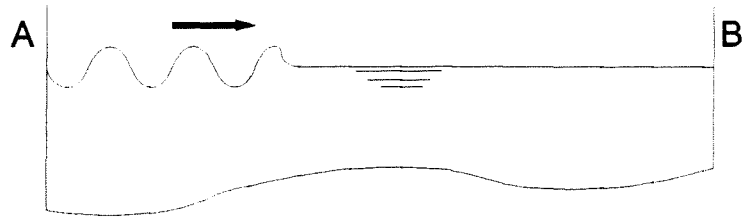

Figure 4.3 Situation sketch

To achieve this, a weakly reflecting shallow water boundary condition or Sommerfeld condition is used. Though for the classical shallow water equations this condition is 100% absorbing, for Boussinesq-like equations some partial reflection will occur. To enhance the boundary performances, the computational domain is extended by a sponge layer, see figure (4.4). It works similar to its physical variant: the sponge layer reduces the waveheight by means of damping and is most effective for higher harmonics. The Sommerfeld condition can be applied accurately on the basic wave. The combination of these two methods leads to a boundary causing very weakly reflections.

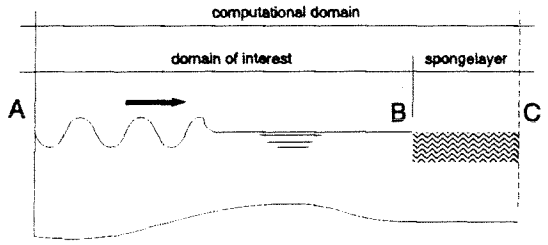

Figure 4.4 Situation sketch with weakly reflecting boundaries

Next, we first will discuss the weakly reflecting shallow water condition and the sponge layer separately. Subsequently, the combination of the two conditions will be evaluated.

4.4.1 The weakly reflecting shallow water condition

By taking α_i and β_i equal to zero and leaving out the non-linear terms, the equations (4.1) are reduced to

$$\begin{aligned} \frac{\partial \zeta}{\partial t} + h\frac{\partial u}{\partial x} &= 0 \\ \frac{\partial u}{\partial t} + g\frac{\partial \zeta}{\partial x} &= 0 \end{aligned} \tag{4.26}$$

which are often referred to as the linearized classical shallow water equations. Assuming that the solution is in the form of

$$\begin{bmatrix} \zeta \\ u \end{bmatrix} = \begin{bmatrix} Z \\ U \end{bmatrix} e^{i(kx-\omega t)} \tag{4.27}$$

the equations (4.26) can be written in Fourier space

$$\begin{bmatrix} -\omega & hk \\ gk & -\omega \end{bmatrix} \begin{bmatrix} Z \\ U \end{bmatrix} = 0 \tag{4.28}$$

Computing the eigenvectors yields

$$\begin{bmatrix} v_\zeta \\ v_u \end{bmatrix}_1 = \begin{bmatrix} 1 \\ \sqrt{\frac{g}{h}} \end{bmatrix} \quad , \quad \begin{bmatrix} v_\zeta \\ v_u \end{bmatrix}_2 = \begin{bmatrix} 1 \\ -\sqrt{\frac{g}{h}} \end{bmatrix} \tag{4.29}$$

For simplicity, we assume that the computational domain holds for $x \leq 0$. A general boundary condition at $x=0$ can be formulated as follows

$$\alpha u + \beta \zeta = f(t) \tag{4.30}$$

The functions ζ and u can be considered as a summation of an outgoing wave with amplitude a_1 and an incoming wave with amplitude a_2. At $x=0$, the functions ζ and u read

$$\begin{aligned} \zeta &= (a_1 + a_2)e^{-i\omega t} \\ u &= \left[a_1\sqrt{\frac{g}{h}} + a_2\left(-\sqrt{\frac{g}{h}}\right)\right] e^{-i\omega t} \end{aligned} \tag{4.31}$$

The function $f(t)$ must have the same phase function $e^{-i\omega t}$, otherwise different waves are generated. The function f can be written as

$$f(t) = Fe^{-i\omega t} \tag{4.32}$$

Substituting equations (4.31) and (4.32) into equation (4.30) yields after some manipulation

$$R = \frac{\alpha\sqrt{g} + \beta\sqrt{h}}{\alpha\sqrt{g} - \beta\sqrt{h}} - \frac{F\sqrt{h}}{a_1} \tag{4.33}$$

where

$$R = \frac{a_2}{a_1} \tag{4.34}$$

R is called the reflection coefficient.
Apparently, the reflection coefficient R is dependent on the amplitude a_1 of the outgoing wave. This dependency can be avoided by taking F equal to zero. Then we have no reflection if R is equal to zero, which can be achieved by taking $\alpha=1$ and $\beta=-\sqrt{g/h}$.
With this, the boundary condition finally reads

$$u - \sqrt{\frac{g}{h}}\,\zeta = 0 \tag{4.35}$$

The boundary condition (4.35) absorbs every wave when it is applied to the classical shallow water equations. When applying condition (3.35) on Boussinesq-like equations, the reflection coefficient R increases for increasing values of kh, as the difference between the Boussinesq phase velocity and the shallow water phase velocity, $c = \sqrt{gh}$, increases for increasing values of kh.

Analytical determination of $R_{Boussinesq}$

In the previous section a boundary condition is determined which gives no reflection when it is applied to the linearized shallow water equations. In this section the reflection coeffient is determined in the case that condition (4.35) is applied to Boussinesq-like equations.

Instead of the shallow water equations in Fourier space, we start with the Boussinesq-like equations in Fourier space, e.g. equation (3.16a). This system has two different eigenvectors $\begin{bmatrix}1\\ v_1\end{bmatrix}$ and $\begin{bmatrix}1\\ v_2\end{bmatrix}$. The equations (4.31) can be written more general as

$$\begin{aligned}\zeta &= (a_1 + a_2)e^{-i\omega t}\\ u &= \left[a_1 v_1 + a_2 v_2\right]e^{-i\omega t}\end{aligned} \tag{4.36}$$

Substituting equation (4.36) into equation (4.35) and some manipulations yields

$$R = f(\omega,k,h,g,\alpha_1,\alpha_2,\beta_1,\beta_2) \tag{4.37}$$

The factor kh is considered to be a single parameter. By substitution equation (3.12), ω, g and the remaining single parameters h vanish. With this, equation (4.37) becomes

$$R = -\frac{2kh^2\alpha_2+2+kh^{\frac{3}{2}}\sqrt{T}(\beta_1-\beta_2)-\sqrt{kh^3T(\beta_1-\beta_2)^2+4kh^2(\alpha_1+\alpha_2)+4(1+kh^4\alpha_1\alpha_2)}}{2kh^2\alpha_2+2+kh^{\frac{3}{2}}\sqrt{T}(\beta_1-\beta_2)+\sqrt{kh^3T(\beta_1-\beta_2)^2+4kh^2(\alpha_1+\alpha_2)+4(1+kh^4\alpha_1\alpha_2)}} \tag{4.38}$$

where

$T = \tanh(kh)$

$$\alpha_1 = \frac{1}{18} + \frac{\sqrt{23}\sqrt{35}}{630} \qquad \alpha_2 = \frac{1}{18} - \frac{\sqrt{23}\sqrt{35}}{630}$$

$$\beta_1 = \frac{2}{9} + \frac{\sqrt{19}\sqrt{7}}{63} \qquad \beta_2 = \frac{2}{9} - \frac{\sqrt{19}\sqrt{7}}{63}$$

As can be seen from equation (4.38) the reflection coefficient is dependent on kh. In the next section, the reflection coefficient, determined by numerical experiments is determined and the reflection coefficient according to equation (4.38) is compared with the numerical reflection coefficient.

Numerical determination of $R_{Boussinesq}$

Above, an expression for R is derived. In this section, results of numerical experiments are given. The reflection coefficient is determined for the two cases:

- linear waves : $H = 0.0002$ m, $3.10^{-3} < \frac{H}{h} < 5.10^{-5}$
- non-linear waves : $\frac{H}{h} = 0.20$

In both cases the bottom is horizontal and the wave signal is sinusoidal with an amplitude of $H/2$ and a period $T=2.02$ s. For various values of kh the depths are computed by solving the linear dispersion relation (3.12) with $T=2.02$ s resulting in the following table:

kh (-)	L (m)	h (m)	k (m^{-1})
0.25	1.56	$6.21 \cdot 10^{-2}$	4.03
0.50	2.94	$2.34 \cdot 10^{-1}$	2.13
0.6725	3.74	$4.00 \cdot 10^{-1}$	1.68
1.0	4.85	$7.72 \cdot 10^{-1}$	1.30
2.0	6.14	1.96	1.02
3.0	6.34	3.03	$9.91 \cdot 10^{-1}$
4.5	6.37	4.56	$9.87 \cdot 10^{-1}$

In order to estimate the reflection, for every value of kh two runs are made with $\Delta t=0.0125$ s and $\Delta x=0.025$ m. In the first run, the computational domain is 80 m long. In the second run, the right boundary condition is specified at 30 m from the left boundary condition. Output is given at X=10 and X=29 m. After some time, the signal of the second run is getting influenced by reflections. Subtracting the two signals yields the reflected signal. The amplitude of the reflected signal can be estimated. The reflection coefficient can be calculated by dividing the amplitude of the reflected wave by the amplitude of the signal of the 80 m run.

It has to be said that this procedure is not very accurate, it is just an indication. Within the range of accuracy, the locations $X=10$ m and $X=29$ m give the same results. The results are plotted in figure (4.5). It appears that non-linear waves have a higher reflection coefficient, as expected, but the influence is rather small.

In figure (4.5), the analytical reflection coefficient is compared with numerical results. In this figure two analytic reflection coefficients are plotted: *Analytical I*, pertaining to equations (3.16a) and *Analytical II*, pertaining to equations (3.16b). Both lines are according to equation (4.38).

It is quite remarkable that the analytic reflection coefficient of model (3.16b) predicts numerical reflection coefficient better than the analytic reflection coefficient of model (3.16a), while the numerical results are obtained by model (3.16a).

However, the comparison of the analytical and numerical reflection coefficient is not completely fair, since two different systems are compared. In the analytical approach, the two third order partial differential equations are the basis. But in the numerical model, these two equations are written as six first order partial differential equations, see section 4.2.1 As argued before, this implies specifying three boundary quantities at the weakly reflecting boundary. In section 4.4.1, a relation for the first quantity, u, is formulated, see equation (4.35). The remaining quantities ζx and uxx are taken equal to zero, which means they cause 100% reflections. Apparently, the numerical reflection coefficient is some weighted mean of the three separate reflection coefficients.
However, by differentiating equation (4.35), conditions for ζ_x and uxx similar to condition (4.35) can be formulated, which read

$$\begin{aligned} ux - \sqrt{\frac{g}{h}}\,\zeta x &= 0 \\ uxx - \sqrt{\frac{g}{h}}\,\zeta xx &= 0 \end{aligned} \qquad (4.39)$$

It is found that the use of one or both equations (4.39) in combination with equation (4.35) leads to instabilities. This may be explained by the fact that no new information is provided by equations (4.39), so the problem is not well posed.

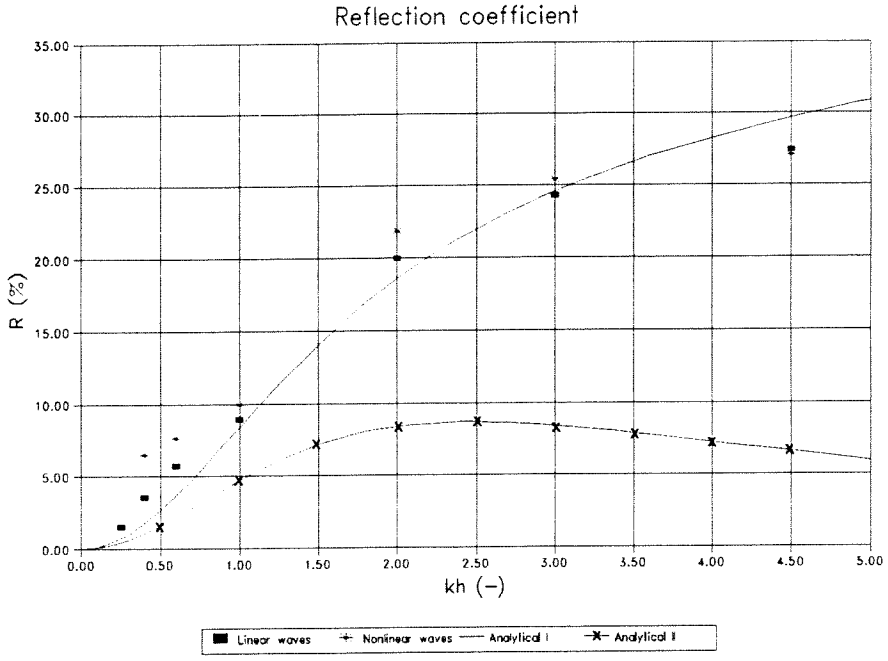

Figure 4.5 Reflection coefficients analytical and numerical

4.4.2 The sponge layer

As shown in section 4.4.1, the shallow water condition still has reflections up to about 30%. For practice, this is not good enough. Applying a sponge layer as suggested in section 4.4, most of energy of the outgoing waves is damped. Subsequently, the shallow water boundary condition absorbs a large amount of the remaining waves. The energy of the reflected waves is damped again, since the reflected waves have to pass the sponge layer again. In this section, the use of a sponge layer is discussed separately.

The damping is introduced by a term $\nu_c\zeta$ in the continuity equation (4.1a) and by a term $\nu_m u$ in the momentum equation:

$$\frac{\partial\zeta}{\partial t} + \frac{\partial}{\partial x}[(h+\zeta)u] = \beta_1 h\left[(1+\gamma_1)\frac{\partial^3 h\zeta}{\partial x^2\partial t} - \gamma_1 h\frac{\partial^3\zeta}{\partial x^2\partial t}\right] + \alpha_1\frac{\partial}{\partial x}\left[h^2\left\{(1+\gamma_2)\frac{\partial^2 hu}{\partial x^2} - \gamma_2 h\frac{\partial^2 u}{\partial x^2}\right\}\right] - \nu_c\zeta \tag{4.40a}$$

$$\frac{\partial u}{\partial t} + u\frac{\partial u}{\partial x} + g\frac{\partial\zeta}{\partial x} = \beta_2 h\left[(1+\gamma_4)\frac{\partial^3 hu}{\partial x^2\partial t} - \gamma_4 h\frac{\partial^3 u}{\partial x^2\partial t}\right] + \alpha_2 gh\left[(1+\gamma_3)\frac{\partial^2}{\partial x^2}\left[h\frac{\partial\zeta}{\partial x}\right] - \gamma_3 h\frac{\partial^3\zeta}{\partial x^3}\right] - \nu_m u \tag{4.40b}$$

The dimension of the damping coefficients ν_c and ν_m equals T^{-1}. For sake of convenience, ν_c and ν_m are taken equal to ν. In order to let the differential equations be valid for the whole domain the coefficient ν is made dependent on x, such that, within the domain of interest (see figure 4.4), $\nu(x)=0$ and within the sponge layer $\nu(x)\neq 0$.

It is very likely that a sponge layer itself causes some reflections, especially if the transition to the sponge layer is quite abrupt. Therefore, the transition should be smooth and reaches its maximum damping capacity gradually. In order to avoid inconsistency, the damping capacity of the sponge layer should be zero at the boundary. This can be accomplished by using the smoothing formula suggested by Hill (1995).

$$\nu(x) = \nu\, f_s\left[\frac{x-L_0}{L}\right] \tag{4.41}$$

where

$$f_s(x) = \tfrac{1}{2}\tanh\left[\frac{\sin\left[\frac{\pi(4x-1)}{2}\right]}{1-(4x-1)^2}\right] + \tfrac{1}{2}, \quad 0 \le x < \tfrac{1}{2}$$

$$f_s(x) = \tfrac{1}{2}\tanh\left[\frac{\sin\left[\frac{\pi(-4x+3)}{2}\right]}{1-(-4x+3)^2}\right] + \tfrac{1}{2}, \quad \tfrac{1}{2} \le x \le 1 \tag{4.42}$$

L and L_0 are scaling parameters. L denotes the length of the sponge layer which starts at $x=L_0$.
In figure (4.6), equation (4.42) is plotted.

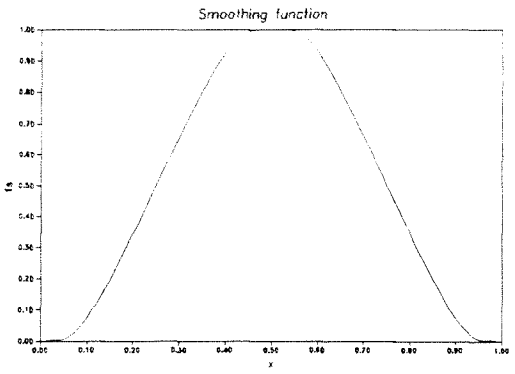

Figure 4.6 Smoothing function

It is clear that the length of the sponge is essential for its functioning. A short sponge layer demands strong damping, which result in relatively large reflections. A long sponge layer, however, suffices with a weakly damping sponge with weak reflections, but needs a larger computational domain. Therefore, the length of the sponge layer is limited to approximately five times the characteristic wavelength. In order to find an optimized value for ν, some numerical experiments are performed.

The determination of the damping coefficient ν

The damping coefficient ν is determined for the case

h = 0.4 m
T = 2.02 s
H/h = 0.2
L_{sponge} = 20 m $\approx$ 5 $L_{characteristic\ wave}$

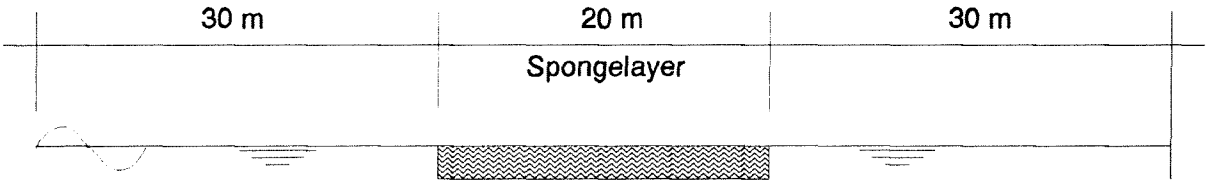

Figure 4.7 Situation sketch

Six runs are performed with various values for ν, which are tabulated below.

run	ν (s^{-1})
1	0.001
2	0.01
3	0.1
4	1
5	10
6	100

The waveheight at several stations in the sponge layer is determined. In figure (4.8), the reduced waveheight divided by the incident waveheight is plotted. The x-axis denotes the sponge layer, which is from X = 30 m through X = 50 m.

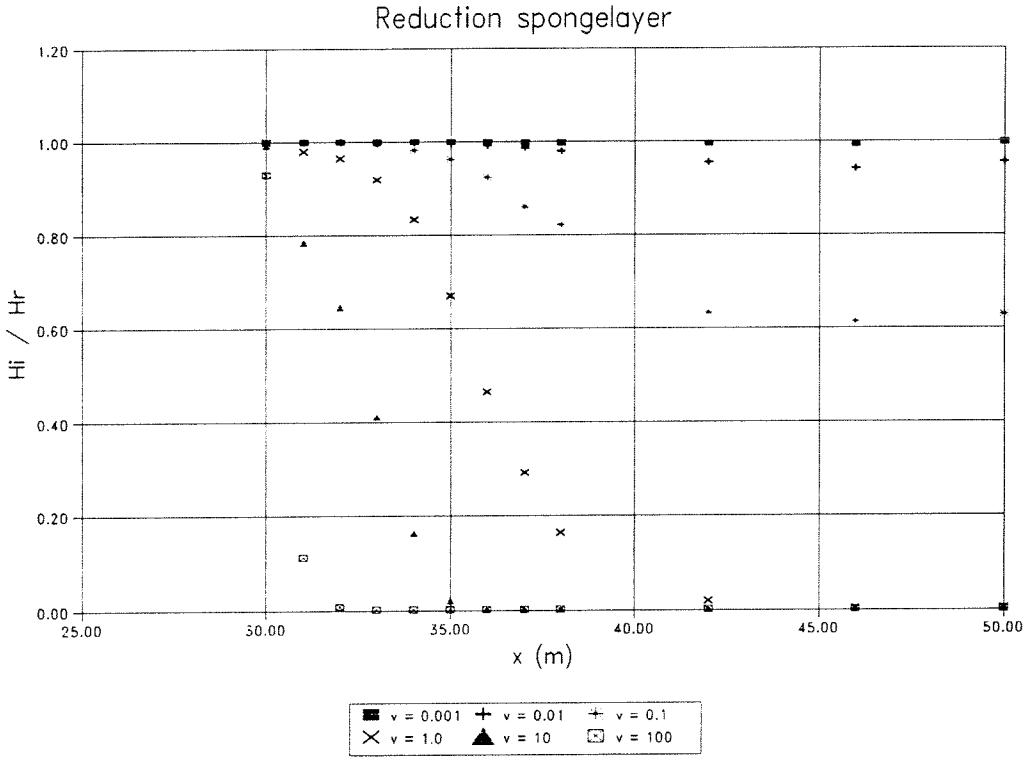

It can be concluded from figure (4.8) that efficient values for ν are between 1 s^{-1} and 10 s^{-1}. Smaller values need a longer sponge layer and higher values damp too strong, which leads to higher reflections. In the next section, the combination of the shallow water condition and the sponge layer with various values of ν is evaluated.

4.4.3 Resulting reflections of the sponge layer and the shallow water condition together.

As seen in the previous section, the sponge layer damping features are satisfactory. On the reflections, however, nothing has been said. The reflection of waves is assumed to be proportional to the gradient of $\nu(x)$. Thus, the reflection coefficient is not constant and reaches its maximum at about 1/3 and 2/3 of the sponge layer. This results in a highly complex pattern of reflected waves, since some reflections stay within the sponge layer, but are strongly reduced then.
The main question stays how much is the total reflection of the combination of both types. To answer this question, a procedure is used similar to the procedure followed in order to estimate the reflection coefficient of the shallow water boundary condition alone.

The same conditions as in the former section are used, except for the sponge layer length, which is reduced to 12 m, i.e. approximately 3 $L_{\text{characteristic wave}}$, and the shallow water condition is applied just behind the sponge layer.

Very roughly, the reflection coefficient can be estimated from the results of the two conditions separately. Say, a wave with amplitude a_1 enters the sponge layer. The reduction because of the sponge layer is to about 10%, see figure (4.8). The reflection of the shallow water condition for kh=0.6725 is about 8%. These reflected waves are reduced to 10 % again yielding a total reflection coefficient of $O(10^{-3})$.

In figure (4.9) a detail of the reflected waves for the ν=0.5 s^{-1}, ν=2 s^{-1}, ν=4 s^{-1} and ν=6 s^{-1} is presented. It appears that the amplitude of the reflected waves decreases with decreasing values for ν. Lower values of ν result in waves that are lagging in phase. This phenomenon can be explained as follows. The lower the values of ν, the lower is the damping. Thus, waves can penetrate deeper into the sponge layer before they are reflected, which causes the phase difference.
However, the reflections in the case of ν=0.5 s^{-1} and ν=2 s^{-1} do not differ very much in amplitude any more, but only in phase. The behaviour of the reflections is a little bit different. The reflections in the case ν=2 s^{-1} seems to be slightly less. Thus, the proposed value of ν equals 2 s^{-1}.

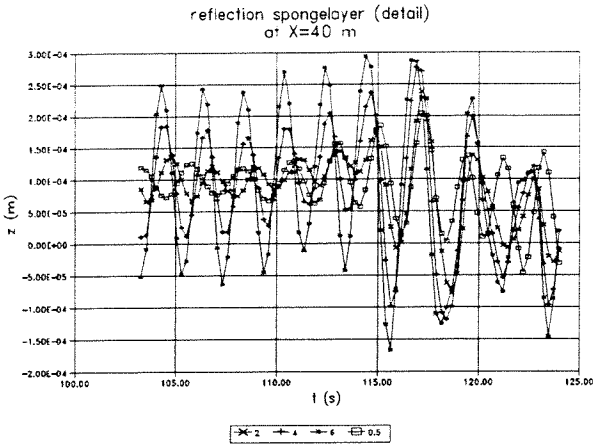

Figure 4.9 Detail of the reflected wave

From figure (4.9) the amplitude of the reflected wave is estimated as $2 \cdot 10^{-4}$ m, although most reflected waves have smaller amplitudes. The incident wave amplitude is equal to $6 \cdot 10^{-2}$. The reflection coefficient R equals approximately $3 \cdot 10^{-3}$, which is in agreement with the estimated value. The conclusion that can be drawn is that the combination of the shallow water boundary condition and a sponge layer results in a boundary condition with a reflection coefficient of $O(10^{-3})$ or even smaller.

However, when cases are considered with different scale magnitudes, different values of ν may be found.

5 Validation and verification

In Chapter 4 Keller's Box method applied to Boussinesq-like equations is described resulting in a numerical model. Before accepting the numerical model, it is subjected to tests. In section 5.1, some qualitative tests have been performed. Subsequently, the representation of the dispersion relation and the shoaling behaviour is investigated and compared with the analytical characteristics. In section 5.2 the best model is selected on the basis of comparisons with measurements, since in Chapter 3 it has turned out that 24 models, namely 4 basic models, 3 options in equation (3.24) and 2 options in equation 3.25, have the same linear shoaling coefficient. Finally, in section (5.3) Keller's Box method is applied to set (2.1). In this manner the equations integrated by the DUT2 model are also integrated by Box method. Since the same problem is solved with the same equations, the results have to correspond. This provides an additional test for Box method.

5.1 Testing the programme code

5.1.1 General test procedures

Before accepting a numerical model, we have to be convinced that no mistakes are made in the formulations of the difference equations or in the programme code. Only by passing all tests it can be made *likely* that the numerical model is correct, but it may contain not detected errors.

Qualitative tests

In this subsection three qualitative tests are described:

1) The first test is the so called zero test. The functions $u(x,t)=0$ and $\zeta(x,t)=0$ are, although trivial, solutions of the sets equations (3.56). When the initial boundary values $u(x,0)$, $\zeta(x,0)$ and their first and second derivatives with respect to x are taken equal to zero, the still water situation is represented. When, subsequently, no signal is put at one or both boundaries, the water surface should stay at rest.

2) The zero test can be extended by raising the still water level to $z=z_1$, where $z_1 \neq 0$. In this case the water level should stay at rest at $z=z_1$.

3) The third test is a sinusoidal wave entering a region being at rest. The wave period is chosen such that the value *kh* is about 1. In this case the waves are dispersive and the group velocity is less than the phase velocity. The ratio is about 0.7. The phenomenon that should occur is that the waves disappear in the wave front.

The tests described above indicated some programme errors. After fixing the programme errors the tests are passed. However, these test are not severe enough to accept the model. In the next subsection some quantitative tests are described.

Quantitative tests

In Chapter 3 new Boussinesq-like models have been derived which obey the [2/2] Padé approximation of the linear dispersion relation. Furthermore, the corresponding linear shoaling coefficient is determined. The correspondence of these two numerical and analytical characteristics indicates the quality of the numerical model. In this subsection the numerical characteristics are determined and compared with the (linear) analytical characteristics, but first the mesh sizes have to be determined in order to make accurate computations.

By mesh refinement it can be determined whether the numerical solutions converge. If after some refinements the numerical solution does not change, the numerical solution converges and further mesh refinement is not necessary. In order to do convergence investigation the following test problem is used. The scale of the problem corresponds to the test conditions described in section 5.2. The bottom is horizontal and the water depth is 0.4 m. At the left boundary the incoming wave is sinusoidal with a wave period T=2.02 s. The amplitude of the incoming wave equals $1 \cdot 10^{-5}$ m which is much smaller than the amplitudes used in section 5.2, but in these tests only linear waves are considered which limits the amplitude.

Besides the mesh sizes, the CFL parameter is of importance as well. It reads

$$CFL = \frac{\Delta t}{\Delta x}\sqrt{gh} \tag{5.1}$$

Since Keller's Box scheme is implicit and therefore unconditionally stable, the CFL parameter is not a measure for stability like for explicit schemes. But it is an indication for the difference between the propagation velocity of the physical wave and the numerical wave. It is obvious that no difference is desired.
In (Petit, 1994) the dissipation and dispersion of various numerical schemes, amongst others Keller's Box scheme, is considered in the case of hyperbolic equations. In figure (5.1) the ratio of the numerical phase velocity c_n to the physical phase velocity c versus $L/\Delta x$ is presented.

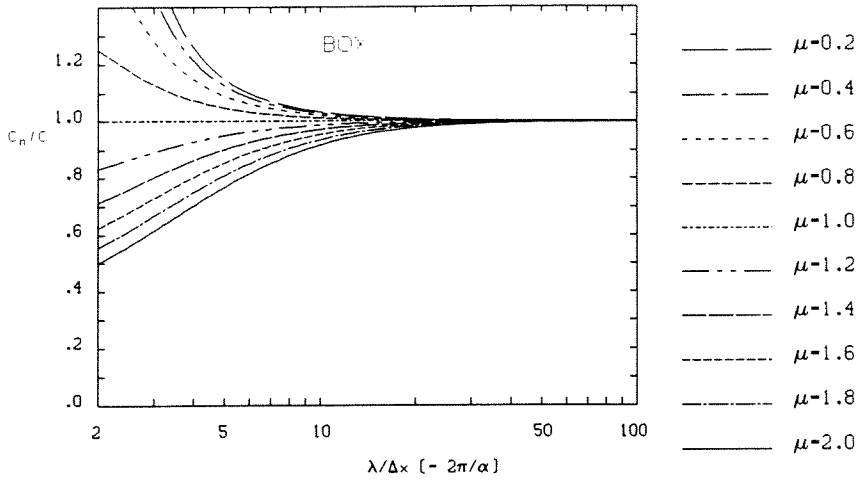

Figure 5.1 Ratio of c_n to c versus $L/\Delta x$, from Petit (1994)

From figure (5.1) it follows that μ=CFL=1 is the best choice, but for a large number of nodes per wavelength, c_n/c converges to 1 for both higher and lower CFL-values.
In practice fairly long waves are considered, which do not have a phase velocity exactly equal to $(gh)^{1/2}$. Besides, higher harmonics are generated due to non-linearities and the bathymetry affects the (local) phase velocity. Thus, for only one component it is possible to choose the ideal CFL=1 and only if the bottom is horizontal. In order to obtain sufficient accuracy, a rather high number of nodes per wavelength is needed, which allows some deviation of CFL=1.

Now, we know that the CFL parameter should be approximately 1. As a first guess for Δt, we take approximately 80 time intervals per wave period: $\Delta t = T/80 \approx 0.025$ s. According to equation (5.1) the Δx by which CFL equals 1 is equal to 0.050 m. More accuracy is obtained by mesh refinement. Halving Δt and Δx keeps CFL constant and gives the table below.

run #	Δt (s)	Δx (m)
1	0.0500	0.1000
2	0.0250	0.0500
3	0.0125	0.0250

Three runs have been carried out with the mesh sizes in the table above. In all runs ζ, ux and ζxx are specified at the left boundary, whereas u, ζx and uxx are specified at the right boundary. ζ is prescribed by a sine, the other quantities are all taken equal to zero. Output is given at X=5 m in a computational domain of 40 m. The numerical results are presented in figure (5.2).

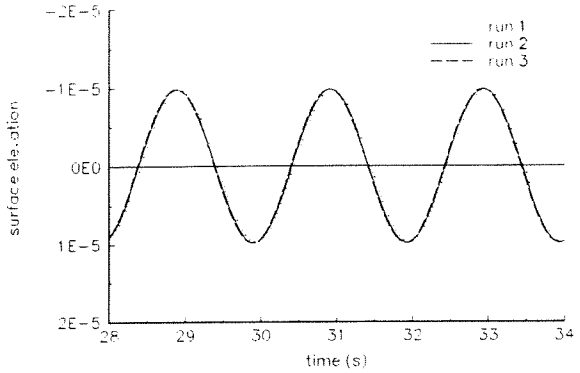

Figure 5.2 Converging solutions

From figure (5.2), it can be seen that the solution does not change if $\Delta t=0.0250$ s is halved. Therefore, for the tests in this section, $\Delta t=0.0250$ s and $\Delta x=0.0500$ m are used.

Phase velocities

The linear Boussinesq-like equations for horizontal bottom have a dispersion relation that matches a [2/2] Padé expansion in $(kh)^2$ of the exact linear dispersion relation. In case of a horizontal bottom, all remaining models are equal, so we do not have to bother about the model differences.
The phase velocity is determined as follows. For various values of kh the wave profile is computed with time intervals of Δt. From a detail plot, see figure (5.3), the covered way (i.e. Δx in the figure) is measured and divided by the Δt, which gives the phase velocity.

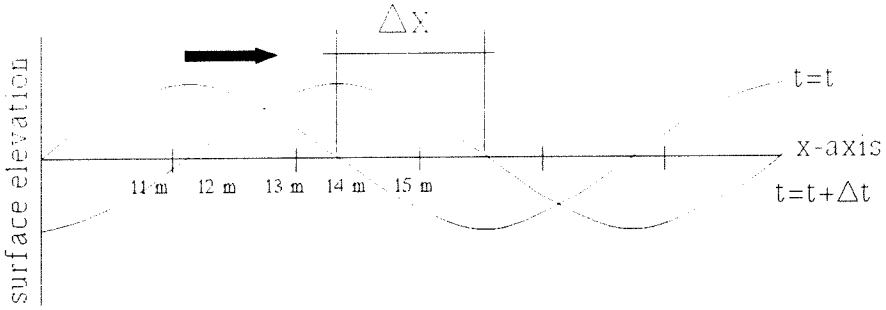

Figure 5.3 Two wave profiles at different times

The values of kh for which the phase velocity is determined are tabulated below. The corresponding depths are listed as well in the case that the wave period equals 2.02 s.

kh (-)	h (m)
0.25	0.0621
0.50	0.2343
0.6725	0.4000
1.0	0.7722
2.0	1.9550
3.0	3.0267
4.5	4.5616

The measured numerical phase velocities are plotted together with the phase velocity according to the [2/2] Padé approximation in figure (5.4).

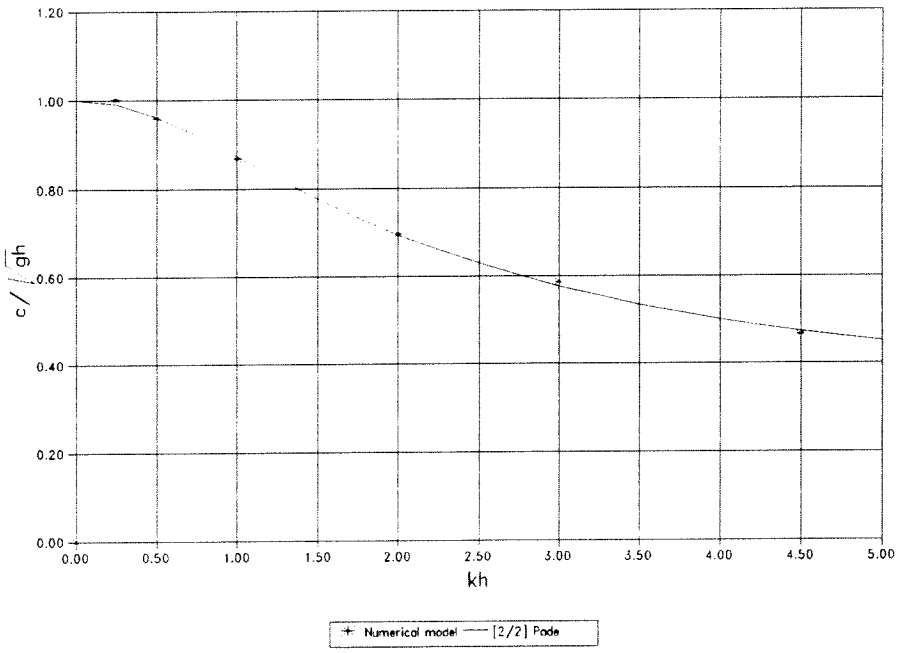

Figure 5.4 Numerical versus analytical phase velocity

From this figure it can be seen that the phase velocity is represented correctly and that the deviations are minimal. This good result indicates that the numerical method gives reliable output in the case of a horizontal bottom and linear waves.

Shoaling

In this subsection the shoaling characteristics are considered. To that end the test section is extended with a bottom with a constant slope, see figure (5.5). Near to the wavemaker, the value of *kh* equals 1.6. At the end of the flume *kh* equals approximately 0.4.
Again, the incoming wave signal is a sine with a wave period T=2.02 s and an amplitude of $1 \cdot 10^{-5}$ m.

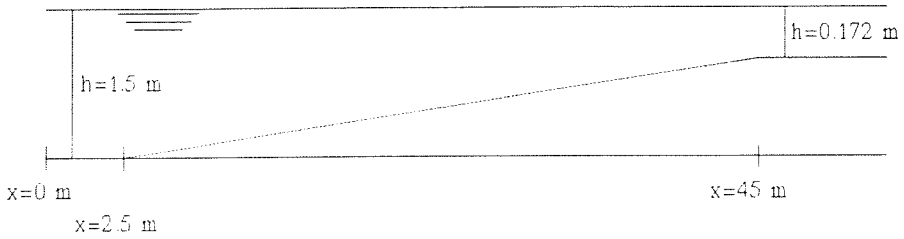

Figure 5.5 Sketch of flume for shoaling investigation

In this test the shoaling coefficient is defined differently from equation (3.39). From energy conservation it follows

$$\frac{d}{dx}F + D = 0 \tag{5.2}$$

where
F = $E c_g = \frac{1}{2} \rho g a^2 c_g$
D = Energy dissipation

Neglecting energy dissipation (by bottom friction, wave breaking) it follows that
$E c_g$ = constant.
Thus:

$$K_s = \frac{a_1}{a_0} = \sqrt{\frac{c_{g_0}}{c_{g_1}}} \tag{5.3}$$

The initial values a_0 and c_{g0} are defined at deep water. According to the linear wave theory we get

$$c_{g0} = \frac{gT^2}{4\pi} \tag{5.4}$$

The group velocity at the first station is also computed by the linear wave theory.

Consequently, the K_s at the first station can be computed from equation (5.3). The wave height at the first station can be estimated from numerical experiments, which gives an estimation for a_0.
In order to determine the K_s corresponding to the numerical model, at several locations in the flume, the amplitude is computed. Although the incoming waves have a small amplitude, the waves do show some non-linear effects, like non-constant waveheights. The amplitudes a_i are determined as the mean of the wave amplitudes which exceed the value of 90% of the peak amplitude. This is done in order to eliminate the dominance of incidentally high amplitudes.
The numerical shoaling coefficient K_s together with the shoaling coefficient pertaining to the analytical model, which is actually based on the group velocity, are presented in figure (5.6).

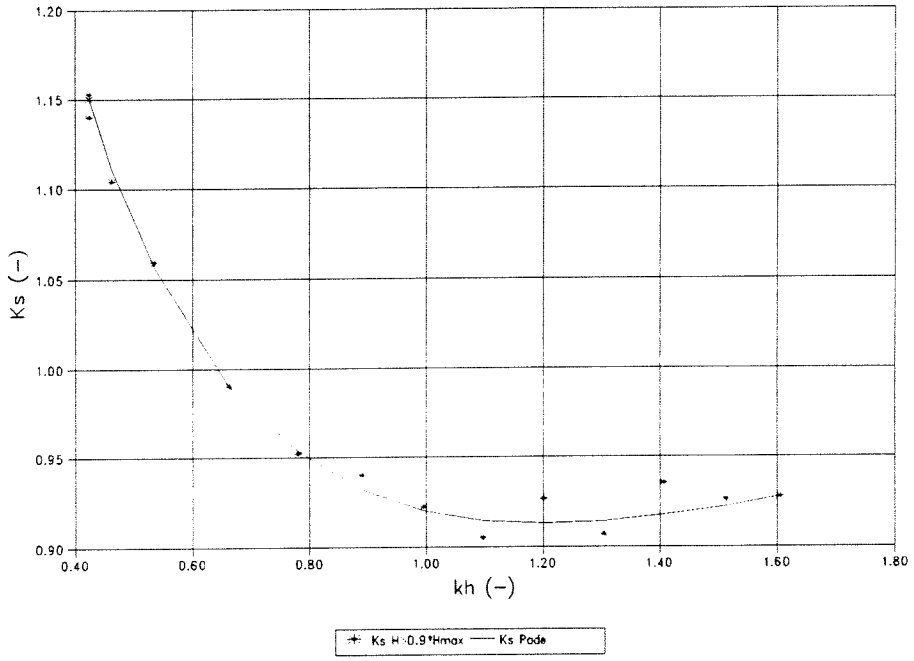

Figure 5.6 Numerical versus analytical shoaling coefficient

From this figure it can be seen that the shoaling characteristics do not appear as accurate as the phase veloctity, but are still satisfying. The deviations may be ascribed to the difficult and rather inaccurate determination of the amplitudes. The waves in the flume are not as regular as they are expected to be. This irregularity may be caused by reflections due to the bottom slope.

Group velocity

The determination of the group velocity is even more difficult than that of the shoaling characteristics. One way of determining c_g is to make a wave group by adding two sines with slightly different frequencies. For accuracy a small frequency difference is needed, which results in a long wave groups. The group velocity can be estimated by determination of the

velocity of the envelope. This procedure is extremely sensitive to errors and will not be followed here. Another way is using equation (5.3).

In the previous test shoaling both c_{g0} and a_0 are determined. In this manner the values of c_g at the locations in the flume can be computed in accordance with equation (5.3). However, c_g at the first station is estimated by the linear theory in order to determine a_0. Therefore this location is skipped. In figure (5.7) both the numerical values of c_g and c_g according to the analytical model presented dimensionless.

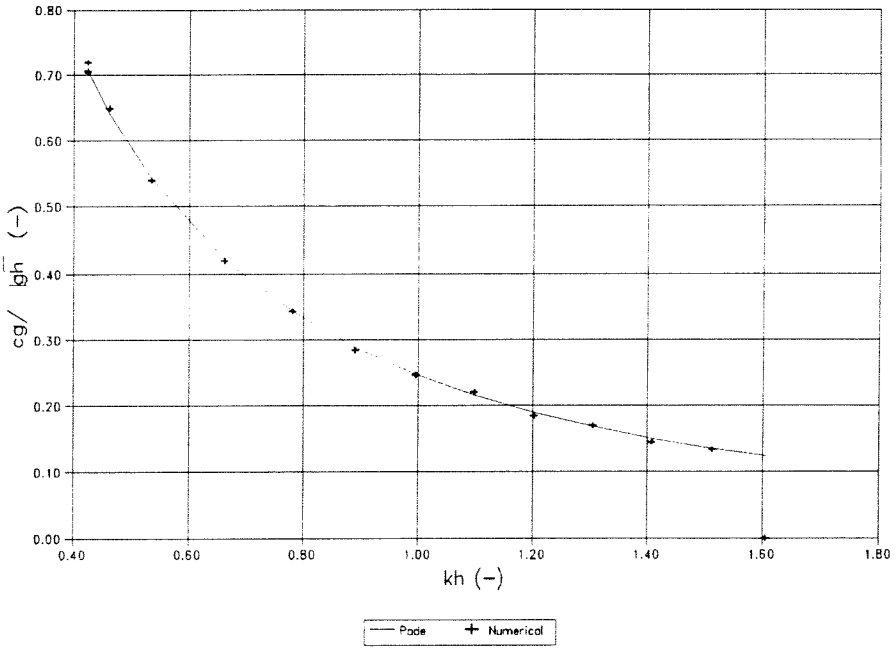

Figure 5.7 Numerical versus analytical group velocity

From this figure it can be seen that correspondence is even better than in figure (5.6) where the shoaling behaviour is presented. Because of the correspondence in derivation it is expected that the correspondence should be roughly the same. That this is not the case is ascribed to the non-dimensionalisation procedure, which reduces the absolute deviation for larger values of h. For these larger values of h and with that kh the numerical shoaling coefficient is not very accurate.

Conclusion

From the tests on the phase velocity, shoaling and group velocity which are described above, it is concluded that when linear waves are considered, the numerical model is able to represent the disperision and the shoaling characteristics correctly.

5.2 Comparison with measurements

It has already been mentioned in Chapter 1 that the major discrepancies between computations with Boussinesq-like models and measurements are due to the inaccurate representation of the linear frequency dispersion in the Boussinesq-like models. As argued before, Boussinesq-like equations are only valid for fairly long waves. However, due to non-linearity, higher harmonics are generated. Some higher harmonics are phase locked and move with the velocity of the basic wave. Other short wave components move freely in accordance with the dispersion relation. Particularly for these waves, the correct representation of the dispersion relation is of great importance.
A discriminating test for Boussinesq-like models is provided by a bar-type geometry. On the upward slope effects of non-linearity generate higher harmonics and on the backward slope the difference between the locked and free components becomes clearly visible. In case of a bad representation of the dispersion relation the free components travel with a wrong velocity, which changes the surface profile. If the depth increases fast, the difference between computation and measurement will be visible after short distances.
In 1993 a number of flume experiments on a bar-type geometry for fairly long waves had been performed by Klopman of Delft Hydraulics. These experiments are equivalent to the tests done by Beji (see Battjes and Beji, 1993), but with a linear scale of two. In order to perform the test under dynamically similar conditions, the wave period is scaled by a factor $\sqrt{2}$. The tests have been performed with an active wave absorber.
The geometry considered in this context is given in figure (5.8). This geometry is slightly different than the scaled geometry of the flume test, but these differences are estimated to be not significant, see Dingemans (1994a). The locations of the gauges are given in the table below.

station	location (m)	Station	location (m)
1	2.00	7	14.50
2	4.00	8	15.70
3	5.70	9	17.30
4	10.50	10	19.00
5	12.50	11	21.00
6	13.50		

The stations 1, 2, 10 and 11 were not included in the tests performed by Beji.

Three wave conditions have been used:

A	T=2.02	s and H = 2.0	cm	non-breaking waves
B	T=2.525	s and H = 2.9	cm	spilling breakers between 13.3 and 15.3 m
C	T=1.01	s and H = 4.1	cm	non-breaking waves

In this context only tests A and C are used for comparison.

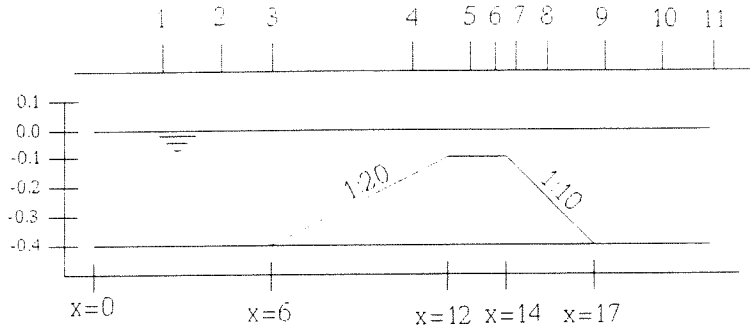

Figure 5.8 Test geometry (measures in meters)

5.2.1 Boundary specifications

In section 4.3.1 the specification of the boundary conditions has briefly been discussed. A suggestion for spreading the six variables over the boundaries is done, but many combinations are possible. However, the variables u and ζ have to be specified at different boundaries, which follows directly from the characteristic directions, see section (3.4.1). By means of numerical experiments the suggested and other spreading possibilities are investigated. The remaining problem is how to specify the boundary conditions. Mostly ζ is given as a function of time, but some derivatives of either ζ or u with respect to x have to be specified. In this section it is indicated how to deal with this problem.

The first step we have to make is to determine how many possibilities exist. As argued before, u and ζ always have to be specified at different boundaries, which reduces the number of possibilities. Thus, we have:

$$\begin{aligned} 3{:}3 &\Rightarrow 4!/(2!\cdot 2!) &&= 6 \\ 2{:}4 &\Rightarrow 2\cdot 4!/(3!\cdot 1!) &&= 8 \\ 1{:}5 &\Rightarrow 2\cdot 4!/(4!\cdot 0!) &&= 2 \\ & && \text{---} \\ & && 16 \text{ possibilities.} \end{aligned}$$

In the numerical experiments the boundary conditions are specified as follows:

$$\zeta = a\cdot\sin(\omega t), \quad \zeta x = \zeta xx = u = ux = uxx = 0.$$

The numerical tests pointed out that at both boundaries three variables have to be specified, otherwise the model is unconditionally unstable. Thus, the number of possibilities reduces to six. Notice that this instability has nothing to do with the (in)stability of the numerical method, but is obviously due to a lack of information.

Of these six remaining possibilities the following possibilities are considered:

I	Left: z ux zxx	Right: u zx uxx
II	Left: z ux zx	Right: u zxx uxx
III	Left: z zx zxx	Right: u ux uxx

From numerical experiments it appears that all three distributions give scarcely different solutions. Since in practice mostly only surface elevation records are available and the relation between the surface elevation ζ and the computational velocity u is not unambiguous, the third possibility is preferred.

For so far it is determined *where* to specify the variables. The remaining question is *how*. To answer that question two ways of prescribing ζ are considered.
The first way is prescribing ζ as a function of (x,t). For example, ζ is specified as $\zeta(x,t) = a\cdot\sin(kx-\omega t)$. Subsequently, the derivatives of ζ can be specified as $\zeta x(x,t) = ak\cdot\cos(kx-\omega t)$ and $\zeta xx(x,t) = -ak^2\cdot\sin(kx-\omega t)$, which gives no difficulties.
The second way is prescribing ζ as a function of (t) in the form of a time registration. In this case, the function cannot be differentiated with respect to x, but ζx and ζxx have to be specified. To that end the time registration is transformed into Fourier series, so that a summation of sines is obtained. Of every Fourier component the wave number k can be calculated from the linear disperision relation (3.12), since the frequency and the depth are known. Thus, the derivatives of ζ with respect to x can be specified according to the case where $\zeta(x,t)$ is prescribed.
From the above it may be clear that the specification of the boundary conditions should be done with care. However, for long waves a fair approximation may be achieved by taking the boundary conditions for ζx and ζxx equal to zero. This can be justified as follows. For long waves the wave slope, characterized by ζx, is a small quantity compared to ζ, whereas higher-order derivatives of ζ are even smaller. Thus, a wrong but simplified specification of the derivatives of ζ will affect the solution very little as long as *only* long waves are considered.

5.2.2 Convergence investigation

Before performing numerical tests, it is necessary to know what mesh-sizes should be taken for accurate results. To that end four runs are performed. The relevant parameters are tabulated below.

run	Δt (s)	Δx (m)	CFL (-)	nodes per wave period
1	$2.500\cdot10^{-2}$	$5.000\cdot10^{-2}$	1.0	80
2	$1.250\cdot10^{-2}$	$2.500\cdot10^{-2}$	1.0	160
3	$6.250\cdot10^{-3}$	$1.250\cdot10^{-2}$	1.0	320
4	$3.125\cdot10^{-3}$	$1.250\cdot10^{-2}$	0.5	640

The CFL-number is determined for h=0.4 m. For the fourth run Δx is not halved, because apparently, for $\Delta x=6.250\cdot10^{-3}$ m the limit of floating point accuracy during solving the system of linear equations is exceeded. In figure (5.9) the results of the four experiments are plotted in a time window for X=21 m. At this location which is behind the bar, see figure (5.8), higher harmonics are clearly present. These higher harmonics have to be represented accurately as well. Therefore, convergence investigation has been performed for location X=21 m.

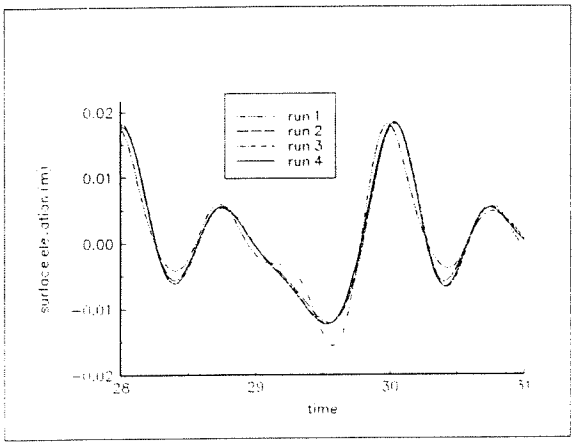

Figure 5.9 Converging solutions

From figure (5.9) it can be seen that $\Delta t=2.500\cdot10^{-2}$ s is not small enough. Further, it follows that $\Delta t=6.250\cdot10^{-3}$ s gives scarcely different results than $\Delta t=3.125\cdot10^{-3}$ s. Thus, the mesh sizes used for all condition A computations are $\Delta t=6.250\cdot10^{-3}$ s and $\Delta x=1.250\cdot10^{-2}$ m. The corresponding CFL number at a depth of 0.4 metres equals 1. The number of available grid points per harmonic is tabulated below.

harmonic	T (s)	grid points per wave period	L (m)	grid points per wave length
0	2.020	320	3.7	296
1	1.010	160	1.5	120
2	$5.050\cdot10^{-1}$	80	0.71	57
3	$2.2525\cdot10^{-1}$	40	0.40	32

From the table above it can be seen that the number of grid points available for the third harmonic is about 30 in space. The minimum number of grid points which is needed to model a wave is about 10. Thus, the number of grid points for the third harmonic is adequate.

5.2.3 Evaluation of Boussinesq-like models with the same optimized linear shoaling behaviour by comparison with measurements

Quite a number of different models with the same optimized linear shoaling behaviour can be formulated, as seen in Chapter 3. In this section the results of a number of the remaining models are compared with measurements.
First the basic models are compared. On the basis of these results it is decided which model(s) could give still better results and which models are supposed to be less good. The computations are compared at the three locations:
1 station 6 13.5 m
2 station 10 19.0 m
3 station 11 21.0 m

The basic models

First, the four basic models 1f, 2f, 3f and 4f are compared with measurements. In Appendix C the results are presented. From figures (C.1), (C.2) and (C.3) it can be seen that compared with the measurements model 3f gives too high amplitudes, whereas the amplitudes of model 2f are too small. The peaks represented by model 4f are almost equal to the peaks of the measurements. Model 1f performs less good than model 4f but better than model 2f and 3f. On the basis of these results model 4 is proposed.

The variants d, e and f

In Chapter 3, the variants d, e and f remained from equations (3.19). Since model 4f performs better than model 1f, 2f and 3f, only the models 4d, 4e and 4f are compared with measurements in order to limit the numerical experiments. The numerical results together with measurements are presented in Appendix D. From figure (D.1) it can be seen that all three numerical results are identical, but from the figures (D.2) and (D.3) it follows that model 4d performs remarkably worse. The models 4e and 4f give equivalent and better results.

For completeness it is mentioned that the use of equation (3.25a) instead of equation (3.25b) gives no different results.

The conclusion that can be drawn from the comparisons with measurement condition A is that both model 4e and 4f have the best correspondence with measurements. Since in the Chapters 3 and 4 model 1f, which can be transformed to model 4f by interchanging α_i and β_i, has been discussed, model 4f is preferred.

The Boussinesq-like equations pertaining to model 4f read

$$\frac{\partial \zeta}{\partial t} + \frac{\partial}{\partial x}\left[(h+\zeta)u\right] = \beta_2 h\left[(1+\gamma_1)\frac{\partial^3 h\zeta}{\partial x^2 \partial t} - \gamma_1 h\frac{\partial^3 \zeta}{\partial x^2 \partial t}\right] + \alpha_2 \frac{\partial}{\partial x}\left[h^2\left\{(1+\gamma_2)\frac{\partial^2 hu}{\partial x^2} - \gamma_2 h\frac{\partial^2 u}{\partial x^2}\right\}\right] \tag{4.5a}$$

$$\frac{\partial u}{\partial t} + u\frac{\partial u}{\partial x} + g\frac{\partial \zeta}{\partial x} = \beta_1 h\left[(1+\gamma_4)\frac{\partial^3 hu}{\partial x^2 \partial t} - \gamma_4 h\frac{\partial^3 u}{\partial x^2 \partial t}\right] + \alpha_1 gh\left[(1+\gamma_3)\frac{\partial^2}{\partial x^2}\left[h\frac{\partial \zeta}{\partial x}\right] - \gamma_3 h\frac{\partial^3 \zeta}{\partial x^3}\right] \tag{4.5b}$$

where

$$\alpha_1 = \frac{1}{18} + \frac{\sqrt{23}\sqrt{35}}{630} \qquad \alpha_2 = \frac{1}{18} - \frac{\sqrt{23}\sqrt{35}}{630}$$

$$\beta_1 = \frac{2}{9} + \frac{\sqrt{19}\sqrt{7}}{63} \qquad \beta_2 = \frac{2}{9} - \frac{\sqrt{19}\sqrt{7}}{63}$$

$$\gamma_1 = -0.111 \qquad \gamma_2 = -0.823$$

$$\gamma_3 = 0.394 \qquad \gamma_4 = 0.500$$

In the next two sections model 4f is compared with both measurements and the results with the DUT2 model, which is introduced in Chapter 2, for the wave conditions A and C.

5.2.4 Comparison between model 4f, DUT2 and measurements

Wave condition A

In this section model 4f and DUT2 are compared with measurements. In this manner the importance of the higher-order dispersion can be made clear.

Specifications of model 4f:

$$\begin{aligned} \Delta t &= 0.00625 \text{ s} \\ \Delta x &= 0.01250 \text{ m} \\ \zeta(t) &= a \cdot \sin(\omega \cdot t) \\ \zeta x(t) &= -ak \cdot \cos(\omega \cdot t) \\ \zeta xx(t) &= -ak^2 \cdot \sin(\omega \cdot t) \end{aligned}$$

where $a=0.01$ m
$\omega=2\pi/2.02$ rad/s
$k=1.7$ m^{-1}.

The value for k is computed from the dispersion relation (3.12) for $T=2.02$ s and $h=0.4$ m. At the right boundary the weakly reflecting boundary condition is applied as described in section (4.4).

The specification for $\zeta(t)$ in DUT2 equals that in model 4f. The other specifications of the DUT2 model are given by Bosboom (1995). Here, only the numerical results are used.

In Appendix E the results of the computations with model 4f together with the measurements are presented. In Appendix F the results of DUT2 together with the measurements are presented for comparison.

From the figures of Appendix E it can be seen that the correspondence at all locations is quite accurate. This holds especially for the wave profile, indicating that the dispersion is represented very well. The small deviations in amplitude are due to the shoaling errors.
From comparing the results of DUT2 in Appendix F with the results of model 4f and the measurements, it follows that the correspondence is improved significantly at locations X=19 m and X=21 m, whereas at the other locations both models perform equally well. This result is ascribed to the higher-order dispersion.

In section 5.2.1 it is mentioned that in case of long waves the simplification of the specification of the derivatives of ζ with respect to x by taking them equal to zero, is a fair approximation. The specification of $\zeta x=0$ and $\zeta xx=0$ gives the same results as the correct specification. This is expected since in wave condition A at the beginning of the flume fairly long waves are considered ($kh=0.67$). Thus, for wave condition A it is allowed to simplify the boundary conditions for the derivatives of ζ with respect to x.

Wave condition C

The correspondence of model 4f with measurements is very good in the case of wave condition A. Here model 4f is subjected to a comparison with measurements and DUT2 in case of wave condition C, where shorter waves are considered. In this case the dispersion characteristics become even more important. For this test the following specifications are used.

Specifications of model 4f:

Δt = 0.003125 s
Δx = 0.01250 m
$\zeta(t)$ = $a \cdot \sin(\omega \cdot t)$
$\zeta x(t)$ = $-ak \cdot \cos(\omega \cdot t)$
$\zeta xx(t)$ = $-ak^2 \cdot \sin(\omega \cdot t)$

where a=0.0205 m
$\omega = 2\pi/1.01$ rad/s
k=4.2 m^{-1}.

The value for k is computed from the dispersion relation for T=1.01 s and h=0.4 m. The time step Δt has been halved, since the wave period has been halved. The spatial step has not been changed, since smaller values for Δx than 0.01250 m give floating point errors during solving the matrix of difference equations. Therefore the CFL number equals 0.5, which is good enough since small deviations are allowed, see section 5.1.

The specifications of the DUT2 model for condition C are given by Bosboom (1995) as well.

In Appendix G the results of the computations with model 4f together with the measurements are presented. In Appendix H the results of DUT2 together with the measurements are presented for comparison.

From the figures of Appendix G it can be seen that the correspondence at all locations is still good but less accurate than the correspondence for wave condition A. However, this is expected, since shorter waves are considered. It is remarkable that the computational amplitude at location X=2 m is too small, but at farther locations the computational amplitude recovers. Perhaps the measurements are not accurate at X=2 m.

It is mentioned that the numerical warm-up time is about 6 seconds longer than the physical warm-up time. Therefore the computed signal is shifted 6 periods to the left.

From comparing the results of DUT2 in Appendix H with the results of model 4f and the measurements, it follows that the correspondence is improved significantly at locations X=17.3 m and X=19 m, whereas at the other locations both models perform equally well.

However, it is remarkable that the correspondence at location X=21 m is so good, since especially for DUT2, the correspondence at earlier stations is less good. This can be explained by the fact that not all higher harmonics have already arrived at the farthest locations.

For wave condition A the consequences of the simplification of the specification of the derivatives of ζ with respect to x have been considered. By numerical experiments it turns out that it is allowed. The simplification in the case of wave condition C is considered as well. The results of the computation with the specification of both ζ_x and ζ_{xx} equal to zero are presented in Appendix I. From these results it can be seen that at all stations the amplitude is too small. The exception is location X=19 m, where the correspondence is extremely good, but this is considered to be accidental. From the comparison of the results obtained by correct boundary specifications (Appendix F) and simplified boundary specifications (Appendix I) it is concluded that in the case of wave condition C it is not allowed to simplify the boundary condition. The value for kh in this the case of condition C equals approximately 1.7 which indicates that the waves are in intermediate depth.

5.3 An additional test by recomputing DUT2 results with Keller's Box method

In this section, the Box method is used in order to integrate the equations (2.1), on which the DUT2 model is based. The results are recomputed for wave condition A for the locations X=13.5 m and X=17.3 m. By this test it is shown that the numerical method solves indeed the problem that is desired to solve and possibility to solve models which are a reduction of the new Boussinesq-like equations.

The numerical model is based on the new Boussinesq-like equations, but set (2.1) is a reduction of set (3.58). By changing some coefficients set (3.58) together with (3.59c) turns into set (2.1). The relevant parameters are tabulated below.

α_1	0
α_2	1/15
β_1	0
β_2	2/5
γ_1	any number
γ_2	any number
γ_3	0
γ_4	5/12

The specification of the boundary conditions and the mesh-sizes is equivalent to specifications for wave condition A, see section 5.2.4. The Box method results and the DUT2 results are presented in figure (5.10) and (5.11).

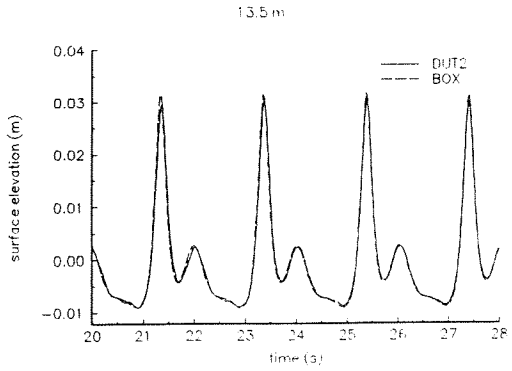

Figure 5.10 Time series at X=13.5 m

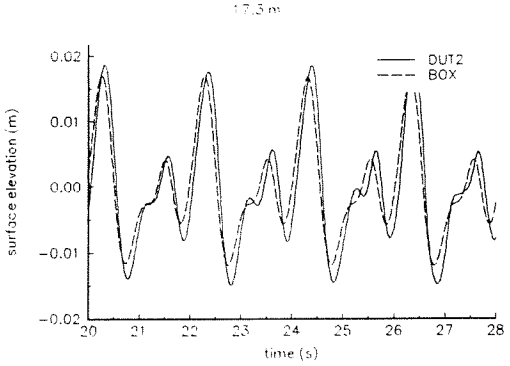

Figure 5.11 Time series at X=17.3 m

From figure (5.10) it can be seen that the results are almost equivalent. However, from figure (5.11) it can be seen that small deviations occur. Probably, the DUT2 mesh sizes are not small enough for an accurate representation of free-moving higher harmonics, since from comparison with measurements, see for example Appendix F, it seems that Keller's Box method gives better corresponding results. From this test it is concluded that the numerical method based on Keller's Box method is an appropriate method to integrate both the new Boussinesq-like equations and reductions of the new Boussinesq-like equations.

6 Conclusions and recommendations

In this thesis, a set of Boussinesq-like equations with higher order dispersion is optimized with respect to the shoaling characteristics. Subsequently, a numerical method is formulated in order to integrate Boussinesq-like equations and tested. In section 6.1 the conclusions of this study are drawn and in section 6.2 some recommendations for further investigation are presented.

6.1 Conclusions

Derivation and optimization of Boussinesq-like models

Boussinesq-like models with a linear frequency dispersion which corresponds to the [2/2] Padé expansion of the exact linear dispersion relation in the parameter $(kh)^2$, have been derived by Dingemans (1994b). The models have been optimized with respect to the shoaling characteristics. The derivation of the Boussinesq-like equations is performed by operator correspondence. Four basic models can be formulated, which contain only (mixed) third-order and lower order derivatives and which are valid for horizontal bottom.
Extending the equations for applications of uneven bottoms results in 48 different models. Of these models, 24 models turn out to have equivalent optimized linear shoaling characteristics. The optimized shoaling characteristics compared with the shoaling characteristics according to linear theory match very well up to $kh=5$, whereas the dispersion relation pertaining to the Boussinesq-like model is accurate up to $kh=8$. These results are a significant step forwards compared to the common Boussinesq-like models.

Formulation of a numerical method for integrating Boussinesq-like equations

In order to integrate Boussinesq-like equations by Keller's Box method, it is necessary that the third-order Boussinesq-like equations are transformed in a set of first-order partial differential equations by means of introduction of new variables. Since the Box method is an implicit scheme all equations have to be solved simultaneously every time step. The matrix to be solved is a block-diagonal matrix.
This matrix can be reduced to a hepta-diagonal matrix, which is relatively easy to solve with a Thomas algorithm. However, it turns out that it is not possible to solve this matrix using the diagonal elements as usual, but a slightly different procedure should be followed, see Appendix A. This is caused by a poor matrix-condition. The consequence of the different solving technique is that no other Boussinesq-like equations which are reductions of the set considered here, can be solved. Therefore, a slightly different method is considered. Instead of reducing the block matrix to a hepta-diagonal matrix, a diagonal matrix is constructed with a band-width of 17 elements, in which the block-diagonal fits exactly. The condition of the

matrix can be enhanced by changing the sequence of equations and/or variables. The standard Thomas algorithm can be applied, which allows solving other Boussinesq-like equations.
With regard to the specification of boundary conditions it is mentioned that the Box forces the user to specify six boundary conditions, which is in fact equal to the number of boundary conditions demanded by the differential equations. In order to have a stable model it is needed that at both boundaries three variables are specified. The combination ζ, ζx and ζxx at one boundary and u, ux and uxx at the other boundary is most attractive, since no assumptions have to be made for the relation of ζ and the computational velocity u.
Unlike other methods used in Boussinesq-context where often only two boundary conditions have to be specified, the Box method provides full control on the problem, but the boundary conditions should be treated with care.

Verification and validation

By means of numerical experiments both the (numerical) linear dispersion and the (numerical) linear shoaling characteristics are determined. From a comparison between the linear analytical characteristics pertaining to the new Boussinesq-like equations and the numerical characteristics, it is concluded that the numerical model represents the linear characteristics very well. This holds especially for the dispersion characteristics.

In Chapter 3 24 models remained which all have the same optimized linear shoaling characteristics. By subjecting these models to a comparison with measurements it has turned out that best correspondence is obtained by both model 4e and model 4f, which gave identical results. Model 4f is preferred, since model 1f, which has been discussed in detail in Chapter 3 and 4, can be transformed to model 4f by only interchanging α_i and β_i. Subsequently, model 4f has been subjected to a comparison with measurements and DUT2 results for wave conditions A and C.
From these tests it is concluded that in the case of wave condition A, the results are very good, even at the farthest locations X=19 m and X=21 m where DUT2 deviates clearly. In the case of wave condition C, the correspondence with measurements is less good than for wave condition A. However, the performances of model 4f and DUT2 are similar as far as the back of the bar, but from this point model 4f performs better than DUT2. The better performances of model 4f are ascribed to the higher-order dispersion relation of the new Boussinesq-like equations.
Summarizing it is concluded that the higher-order dispersion results in a significant improvement in the correspondence with the measurements of wave condition A and C. With the new Boussinesq-like equations the applicability of Boussinesq modelling for wave propagation over uneven bottoms has been increased.

With regard to Keller's Box method for solving Boussinesq-like equations it is mentioned that it satisfies for several reasons:
- the method is quite fast,
- the method gives full control over the boundary conditions,
- the application of a weakly reflecting boundary gives no complications.

Only when very small mesh-sizes, which are not needed for an accurate solution instability occurs.

6.2 Recommendations

The derivation of the Boussinesq-like equations with higher order dispersion is performed by a kind of *back-door* procedure. First the dispersion relation is formulated and subsequently, the pertaining equations are constructed. Thus, no use is made of a mass- and momentum balance principle. Using balance principles can give more insight in how to specify the boundary conditions.

Although the method used for optimizing the shoaling characteristics give excellent results, this does not mean that no other combinations of γ_i exist, which lead to equivalent linear characteristics but to different (and perhaps better) non-linear shoaling characteristics. To find this out, further investigation is needed.

It is indicated that when at the ζ-boundary the value $kh \not< 1$ the specification of the derivatives is important. When random waves are considered, the specification of the derivatives becomes more important according as the frequency of the wave components increases. In order to determine the derivatives with respect to x, the $\zeta(t)$-record can be transformed into Fourier components. These components can be differentiated with respect to x. The summation of these differentiated components yields the signals for ζx and ζxx. It should be investigated whether this procedure is appropriate for application to random waves.

With regard to the matrix-solver it is mentioned that, although the 17-diagonal solver is quite fast, perhaps more efficient methods exist to solve the actual block-diagonal matrix.

During convergence investigation it has turned out that the possibility of mesh refinement is limited. Especially when Δx is refined instabilities occur. It should be investigated what really causes this phenomenon.

7 Acknowlegdements

The research presented in this report has been performed as a Master's thesis at the Faculty of Civil Engineering, Hydraulic and Geotechnical Engineering Division, of Delft University of Technology.

I would like to thank my supervisors Prof.dr.ir. J.A. Battjes, Prof.dr.ir. G.S. Stelling at Delft University of Technology and especially Dr.ir. M.W. Dingemans at DELFT HYDRAULICS for the pleasant cooperation and many suggestions.

Yasser Eldeberky at Delft University of Technology has been very helpful; I thank him for many discussions and advices.

References

Beji, S. and Battjes, J.A., 1993. Experimental investigation of wave propagation over a bar. *Coastal Engineering,* **19**, 151-162.

Bosboom, J., 1995. Boussinesq modelling of wave-induced particle velocities. Masters Thesis *Delft Univ. of Technology* and *Delft Hydraulics Report* H 2065.

Cebeci, T. and Smith, A.M.O., 1974. Analysis of turbulent boundary layers. Academic Press, New York, 404 pp.

Dingemans, M.W., 1994a. Comparison of computations with Boussines-like equations. *Delft Hydraulics, Report R728 part2,* 88 pp.

Dingemans, M.W., 1994b. Water wave propagation over uneven bottoms. World Scientific, Singapore, to be published, appr. 780 pp.

Golub, G.H. and Van Loan, C.F., 1983. Matrix computations, North Oxford Academic.

Hill, D.F., 1995. Hamiltonian formulation of water waves; boundary formulations. *Delft Hydraulics Note* H 782, 28 pp.

Keller, H.B., 1970. A new difference scheme for parabolic problems. *Numerical solutions of Partial Differential Equations, II.* Academic Press, New York, pp. 265-293.

Madsen, P.A., Murray, R. and Sørensen, O.R., 1991. A new form of the Boussinesq equations with improved linear dispersion characteristics. *Coastal Engineering* **15(4)**, pp. 371-388.

Madsen, P.A. and Sørensen, O.R., 1991. A new form of the Boussinesq equations with improved linear dispersion characteristics. Part 2: A slowly-varying bathymetry *Coastal Engineering* **18(3/4)**, pp. 183-204.

Nayfeh, A.H., 1981. Introduction to Perturbation Techniques. J. Wiley and Sons, New York, 519 pp.

Otta, A.K. and Dingemans, M.W., 1994. Hamiltonian formulation of water waves. *Delft Hydraulics, Report H 782.*

Peregrine, D.H., 1976. Long waves on a beach. *J. Fluid Mechanics* **27(4)** pp. 815-827.

Petit, H.A.H., 1994. Note on dissipation and dispersion of numerical schemes for hyperbolic problems. *Delft Hydraulics,* Internal note, June 1994.

Schäffer, H.A. and Madsen, P.A., 1994. Further enhancements of Boussinesq-type equations. Submitted to *Coastal Engineering*, 16 pp.

Witting, J.M., 1984. A unified model for the evolution of nonlinear water waves. *J. of Computational Physics* **56(2)** pp. 203-236.

List of symbols

a	=	elevation amplitude	[L]
b	=	velocity amplitude	[LT^{-1}]
CFL	=	Courant number	[-]
c	=	imaginary elevation amplitude	[L]
c	=	phase velocity	[LT^{-1}]
c_g	=	group velocity	[LT^{-1}]
d	=	imaginary velocity amplitude	[LT^{-1}]
E	=	energy per m^2	[MT^{-2}]
g	=	acceleration of gravity	[LT^{-2}]
H	=	wave height	[L]
h	=	water depth	[L]
K_s	=	shoaling coefficient	[-]
k	=	wave number	[L^{-1}]
L	=	wave lenght	[L]
R	=	reflection coefficient	[-]
T	=	wave period	[T]
t	=	time	[T]
u	=	(computational) velocity	[LT^{-1}]
ux	=	first derivative of the (computational) velocity with respect to x	[T^{-1}]
uxx	=	second derivative of the (computational) velocity with respect to x	[$L^{-1}T^{-1}$]
x	=	horizontal coordinate	[L]

α_s	=	shoaling coefficient	[-]
α_s^L	=	exact linear shoaling coefficient	[-]
α_s^B	=	Boussinesq linear shoaling coefficient	[-]
ζ	=	surface elevation	[L]
ζx	=	first derivative of the elevation respect to x	[-]
ζxx	=	second derivative of the elevation with respect to x	[L^{-1}]
ν	=	damping coefficient	[T^{-1}]
ω	=	angular frequency	[T^{-1}]

Appendices

Appendix A Constructing and solving the heptadiagonal matrix

In this appendix an alternative diagonal matrix is formulated. The purpose is to show a different method to solve the linear differential equations. The advantage of this method is that only a heptadiagonal matrix is constructed which demands less memory than the used 17-diagonal matrix. However, it appears that the resulting diagonal matrix is poorly conditioned. Therefore, a slightly different solution technique has to be applied, which is decribed below.

We start with the equation (4.14). For the sake of convenience equation (4.14) is repeated here

$$\begin{bmatrix} Cl_j & Cr_{j+1} \end{bmatrix} \begin{bmatrix} Q_j \\ Q_{j+1} \end{bmatrix} = \begin{bmatrix} r_1 & r_2 & 0 & 0 & 0 & 0 \end{bmatrix}^T \tag{A.1}$$

Sweeping the matrix $\begin{bmatrix} Cl_j & Cr_{j+1} \end{bmatrix}$ in such a way that a heptadiagonal matrix is left, yields

$$\begin{bmatrix} Cl_j & Cr_{j+1} \end{bmatrix} = \begin{bmatrix} c_{11} & c_{12} & c_{13} & c_{14} & c_{15} & c_{16} & c_{17} & 0 & 0 & 0 & 0 & 0 \\ 0 & c_{21} & c_{22} & c_{23} & c_{24} & c_{25} & c_{26} & c_{27} & 0 & 0 & 0 & 0 \\ 0 & 0 & c_{31} & c_{32} & c_{33} & c_{34} & c_{35} & c_{36} & c_{37} & 0 & 0 & 0 \\ 0 & 0 & 0 & c_{41} & c_{42} & c_{43} & c_{44} & c_{45} & c_{46} & c_{47} & 0 & 0 \\ 0 & 0 & 0 & 0 & c_{51} & c_{52} & c_{53} & c_{54} & c_{55} & c_{56} & c_{57} & 0 \\ 0 & 0 & 0 & 0 & 0 & c_{61} & c_{62} & c_{63} & c_{64} & c_{65} & c_{66} & c_{67} \end{bmatrix} \tag{A.2}$$

Notice that the right-hand side of equation (A.1) is swept as well.

A system that encompasses the whole x-domain, reads

$$MQ = R \tag{A.3}$$

where

$$M = \begin{bmatrix} Cl_1 & Cr_2 & & & & & \\ & Cl_2 & Cr_3 & & & & \\ & & \cdot & & & & \\ & & & \cdot & & & \\ & & & & \cdot & & \\ & & & & Cl_{J-2} & Cr_{J-1} & \\ & & & & & Cl_{J-1} & Cr_J \end{bmatrix}$$

$$R = \left[r_1 \;\; r_2 \;\; r_3 \;\; r_4 \;\; r_5 \;\; r_6 \;\; . \;\; . \;\; . r_{6J-4} \;\; r_{6J-3} \;\; r_{6J-2} \;\; r_{6J-1} \;\; r_6 J\right]^T$$

$$Q = \left[Q_0 \;\; Q_1 \;\; . \;\; . \;\; . \;\; Q_{J-1} \;\; Q_J\right]^T$$

Working out the elements Cl_i and Cr_i shows that M is a (6J) x (6J+6) heptadiagonal matrix.

Solving the system of linear equations

As in the case of the 17-diagonal matrix, the first three elements of $\mathbf{Q}_0$ and the last three elements of $\mathbf{Q}_J$ are specified as boundary conditions and are moved together with the corresponding elements in matrix M to the (known) vector **R**. The resulting system now reads **M Q** = **R** where M equals a hepta-diagonal (6J x 6J) matrix and both **Q** and **R** are vectors with lengt (6J). The Thomas algorithm is a very efficient method to solve tridiagonal matrices. Since we are dealing with a heptadiagonal matrix, the Thomas algorithm is extended.

Solving the heptdiagonal matrix with an extended Thomas algorithm

Now, the matrices M and R read

$$M = \begin{bmatrix}
d_1 & e_1 & f_1 & g_1 & & & & & & & \\
c_2 & d_2 & e_2 & f_2 & g_2 & & & & & & \\
b_3 & c_3 & d_3 & e_3 & f_3 & g_3 & & & & & \\
a_4 & b_4 & c_4 & d_4 & e_4 & f_4 & g_4 & & & & \\
 & a_5 & b_5 & c_5 & d_5 & e_5 & f_5 & g_5 & & & \\
 & & & & & \cdot & & & & & \\
 & & & & & & \cdot & & & & \\
 & & & & & & & \cdot & & & \\
 & & & & a_{6J-4} & b_{6J-4} & c_{6J-4} & d_{6J-4} & e_{6J-4} & f_{6J-4} & g_{6J-4} \\
 & & & & & a_{6J-3} & b_{6J-3} & c_{6J-3} & d_{6J-3} & e_{6J-3} & f_{6J-3} \\
 & & & & & & a_{6J-2} & b_{6J-2} & c_{6J-2} & d_{6J-2} & e_{6J-2} \\
 & & & & & & & a_{6J-1} & b_{6J-1} & c_{6J-1} & d_{6J-1} \\
 & & & & & & & & a_{6J} & b_{6J} & c_{6J} \\
 & & & & & & & & & & d_{6J}
\end{bmatrix}, \quad R = \begin{bmatrix} r_1 \\ r_2 \\ r_3 \\ r_4 \\ r_5 \\ \cdot \\ \cdot \\ r_{6J-4} \\ r_{6J-3} \\ r_{6J-2} \\ r_{6J-1} \\ r_J \end{bmatrix} \tag{A.4}$$

To solve the matrix M, the matrix is swept three times from top to bottom and three times from bottom to top. The first sweep makes the elements a_i equal to zero by

$$row_i = row_i - \frac{a_i}{b_{i-1}} row_{i-1} \quad , \quad r_i = r_i - \frac{a_i}{b_{i-1}} r_{i-1} \quad , \quad i = 4,5,6,\ldots,6J \tag{A.5}$$

The second sweep makes the elements b_i equal to zero by

$$row_i = row_i - \frac{b_i}{c_{i-1}} row_{i-1} \quad , \quad r_i = r_i - \frac{b_i}{b_{i-1}} r_{i-1} \quad , \quad i = 3,4,5,\ldots,6J \tag{A.6}$$

The third sweep makes the elements c_i equal to zero by

$$row_i = row_i - \frac{c_i}{d_{i-1}} row_{i-1} \quad , \quad r_i = r_i - \frac{c_i}{d_{i-1}} r_{i-1} \quad , \quad i = 2,3,4,\ldots,6J \tag{A.7}$$

We continue the procedure with three sweeps in opposite direction. The fourth sweep makes the elements g_i equal to zero by

$$row_i = row_i - \frac{g_i}{f_{i+1}} row_{i+1} \quad , \quad r_i = r_i - \frac{g_i}{f_{i+1}} r_{i+1} \quad , \quad i = (6J-3),(6J-4),\ldots,1 \tag{A.8}$$

The fifth sweep makes the elements f_i equal to zero by

$$row_i = row_i - \frac{f_i}{e_{i+1}} row_{i+1} \;, \quad r_i = r_i - \frac{f_i}{e_{i+1}} r_{i+1} \;, \quad i = (6J-2),(6J-3),\ldots,1 \tag{A.9}$$

And, finally, the sixth sweep makes the elements e_i equal to zero by

$$row_i = row_i - \frac{e_i}{d_{i+1}} row_{i+1} \;, \quad r_i = r_i - \frac{e_i}{d_{i+1}} r_{i+1} \;, \quad i = (6J-1),(6J-2),\ldots,1 \tag{A.10}$$

The matrix M is reduced to single diagonal matrix and reads

$$M = \begin{bmatrix} d_1 & & & & & & & & & & & \\ & d_2 & & & & & & & & & & \\ & & d_3 & & & & & & & & & \\ & & & d_4 & & & & & & & & \\ & & & & d_5 & & & & & & & \\ & & & & & d_6 & & & & & & \\ & & & & & & \cdot & & & & & \\ & & & & & & & \cdot & & & & \\ & & & & & & & & \cdot & & & \\ & & & & & & & & & d_{6J-4} & & \\ & & & & & & & & & & d_{6J-3} & \\ & & & & & & & & & & & d_{6J-2} \\ & & & & & & & & & & & \\ & & & & & & & & & & & \\ & & & & & & & & & & & \end{bmatrix} \tag{A.11}$$

The matrix Q can easily be calculated by

$$q_i = \frac{r_i}{d_i} \;, \qquad i = 1,2,3,\ldots,6J \tag{A.12}$$

Appendix B The elements Cl_j and Cr_{j+1}

$$Cl_j = \begin{bmatrix} \frac{A_1}{\Delta t}+\frac{ux_{j+\frac{1}{2}}^n}{2} & \frac{A_7}{2}+\frac{z_{j+\frac{1}{2}}^n}{2} & \frac{A_3}{\Delta t} & \frac{A_4}{2}+\frac{zx_{j+\frac{1}{2}}^n}{2} & \frac{A_2}{\Delta t}+\frac{u_{j+\frac{1}{2}}^n}{2} & \frac{A_5}{2}-\frac{A_6}{\Delta x} \\ 0 & \frac{B_4}{\Delta t}+\frac{u_{j+\frac{1}{2}}^n}{2} & \frac{B_2}{2}-\frac{B_3}{\Delta x} & \frac{B_6}{\Delta t}+\frac{ux_{j+\frac{1}{2}}^n}{2} & \frac{B_1}{2} & \frac{B_5}{\Delta t} \\ 0 & -\frac{1}{2} & 0 & -\frac{1}{\Delta x} & 0 & 0 \\ 0 & -\frac{1}{\Delta x} & 0 & 0 & 0 & -\frac{1}{2} \\ -\frac{1}{\Delta x} & 0 & 0 & 0 & -\frac{1}{2} & 0 \\ 0 & 0 & -\frac{1}{2} & 0 & -\frac{1}{\Delta x} & 0 \end{bmatrix}$$

$$Cr_{j+1} = \begin{bmatrix} \frac{A_1}{\Delta t}+\frac{ux_{j+\frac{1}{2}}^n}{2} & \frac{A_7}{2}+\frac{z_{j+\frac{1}{2}}^n}{2} & \frac{A_3}{\Delta t} & \frac{A_4}{2}+\frac{zx_{j+\frac{1}{2}}^n}{2} & \frac{A_2}{\Delta t}+\frac{u_{j+\frac{1}{2}}^n}{2} & \frac{A_5}{2}+\frac{A_6}{\Delta x} \\ 0 & \frac{B_4}{\Delta t}+\frac{u_{j+\frac{1}{2}}^n}{2} & \frac{B_2}{2}+\frac{B_3}{\Delta x} & \frac{B_6}{\Delta t}+\frac{ux_{j+\frac{1}{2}}^n}{2} & \frac{B_1}{2} & \frac{B_5}{\Delta t} \\ 0 & -\frac{1}{2} & 0 & \frac{1}{\Delta x} & 0 & 0 \\ 0 & \frac{1}{\Delta x} & 0 & 0 & 0 & -\frac{1}{2} \\ \frac{1}{\Delta x} & 0 & 0 & 0 & -\frac{1}{2} & 0 \\ 0 & 0 & -\frac{1}{2} & 0 & \frac{1}{\Delta x} & 0 \end{bmatrix}$$

Appendix C Numerical results of models 1f, 2f, 3f and 4f compared with measurements

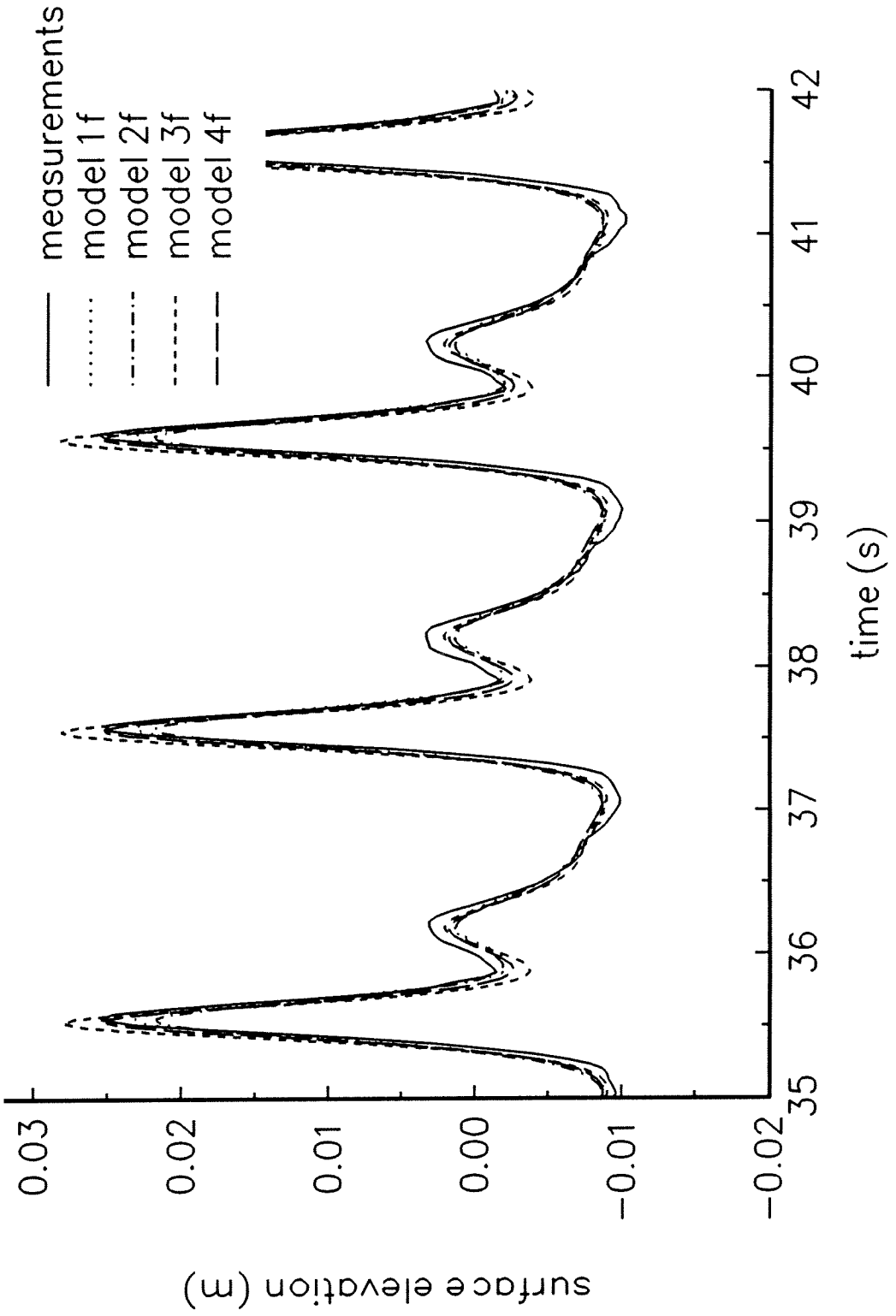

Figure C.1 4 Basic models at X=13.5 m

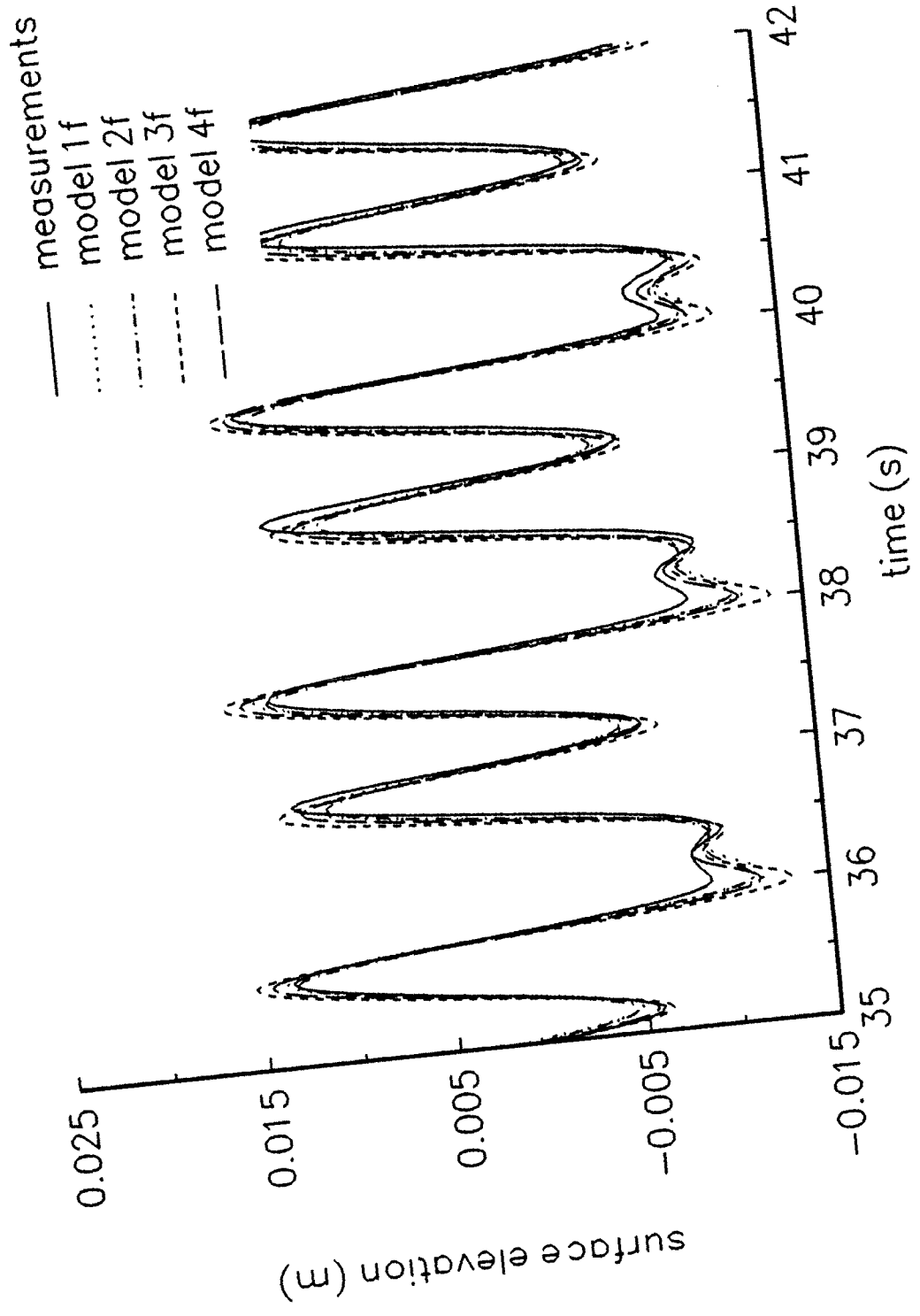

Figure C.2 4 Basic models at X=19.0 m

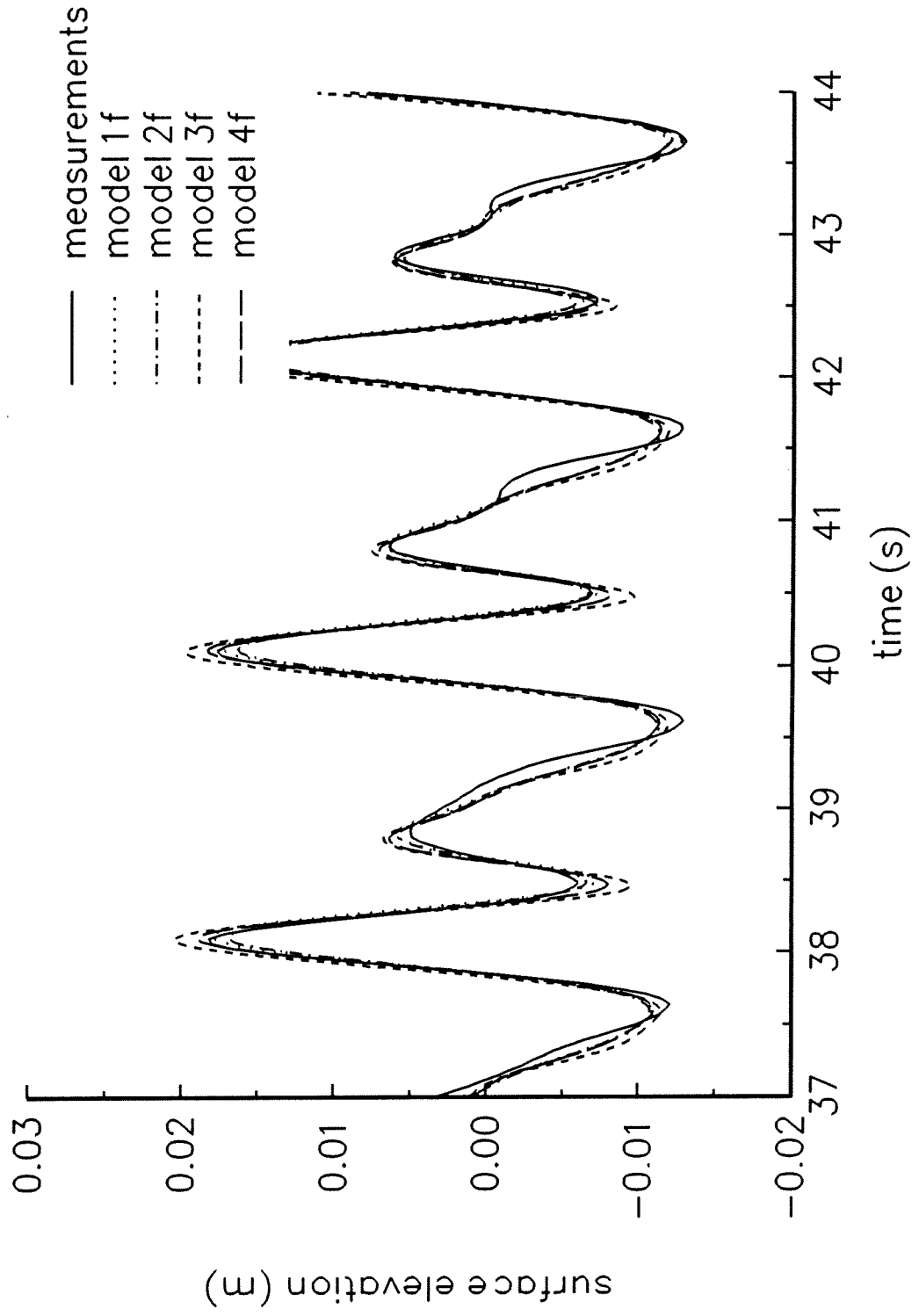

Figure C.3 4 Basic models at X=21.0 m

Appendix D Numerical results of models 4d, 4e and 4f compared with measurements

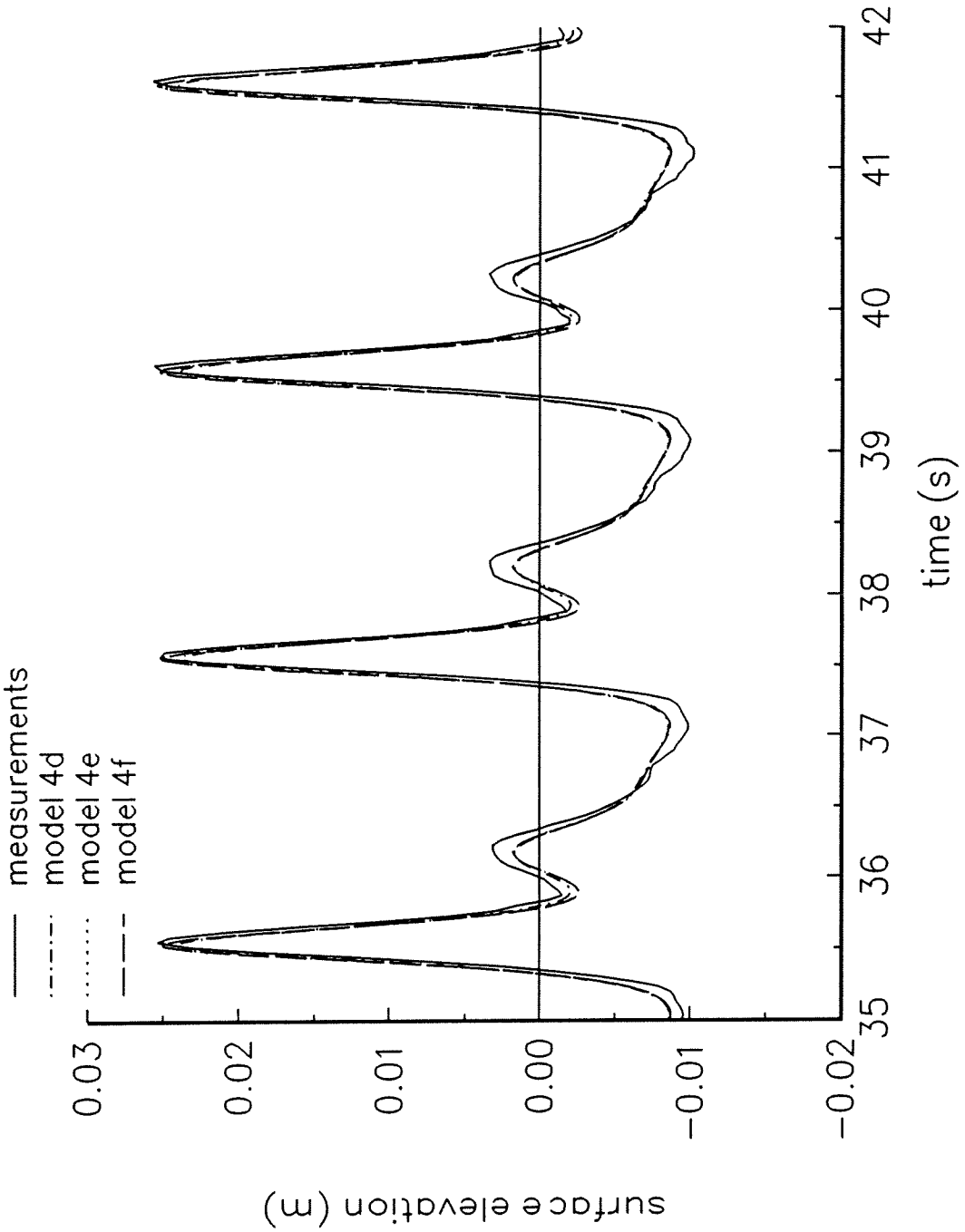

Figure D.1 Variants d,e and f at X=13.5 m

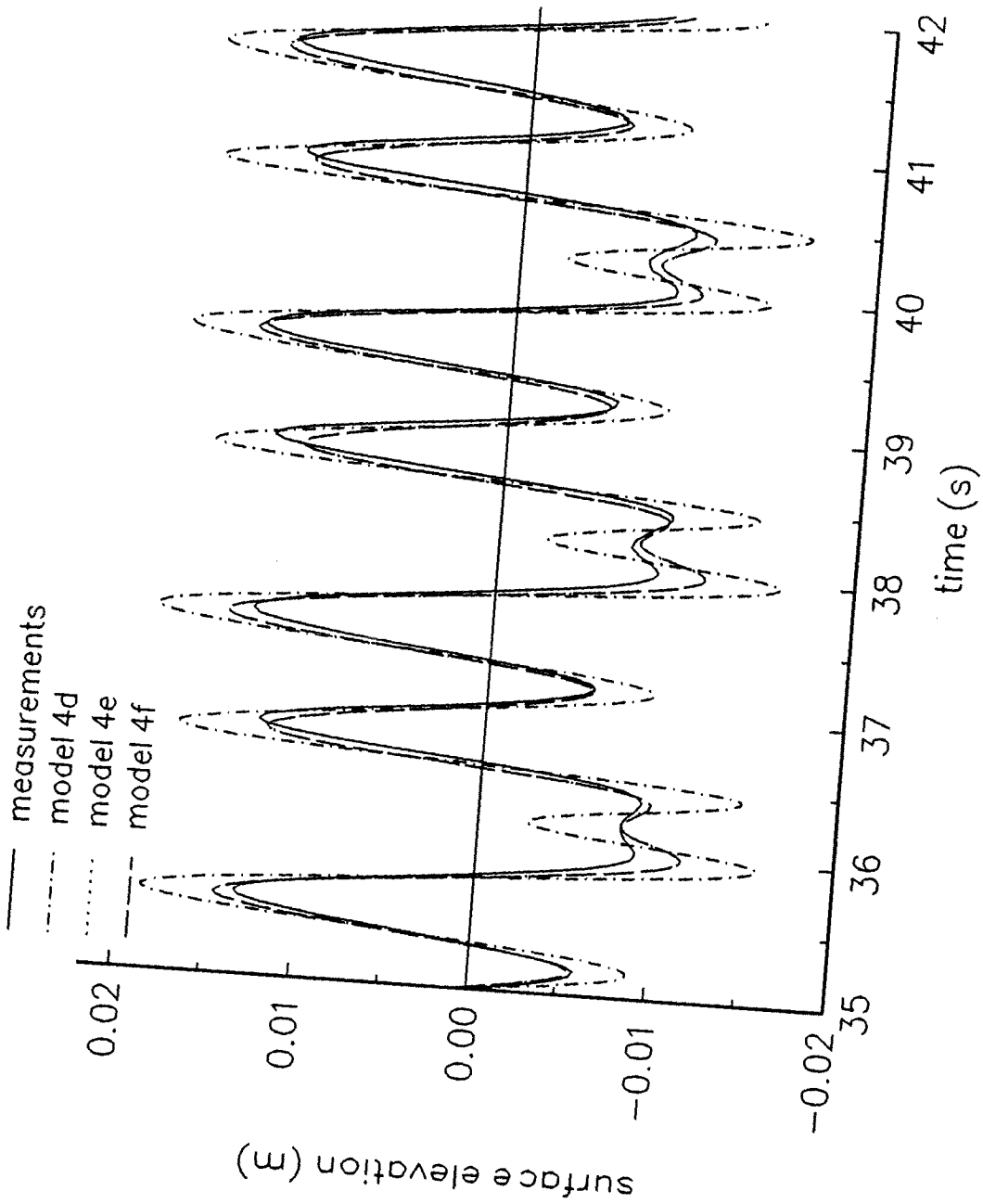

Figure D.2 Variants d,e and f at X=19.0 m

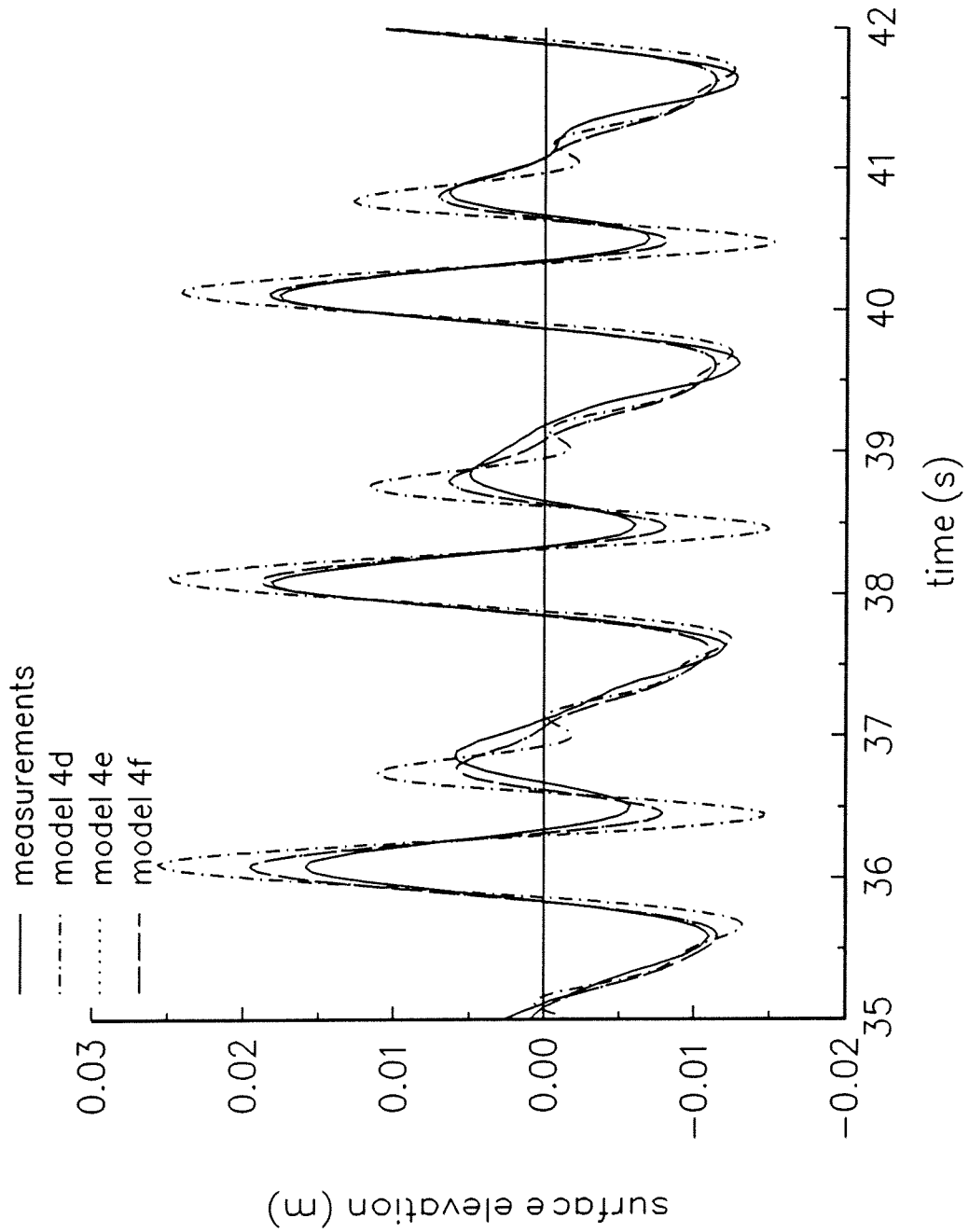

Figure D.3 Variants d, e and f at X=21.0 m

Appendix E Model 4f compared with measurements A at all stations

Normal boundary conditions for ζx and ζxx.

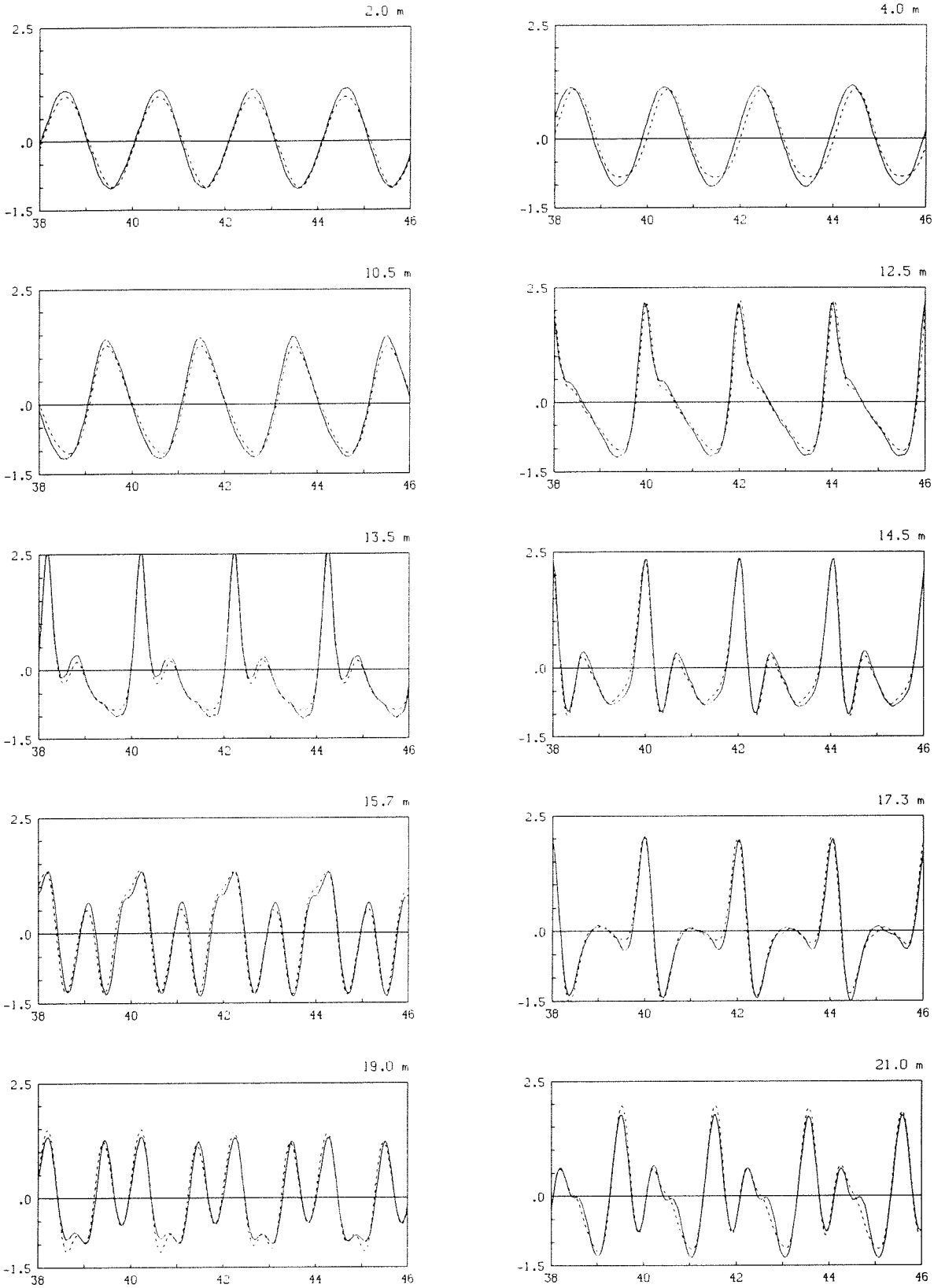

Surface elevation in cm and time in seconds.

Appendix F DUT2 compared with measurements A at all stations

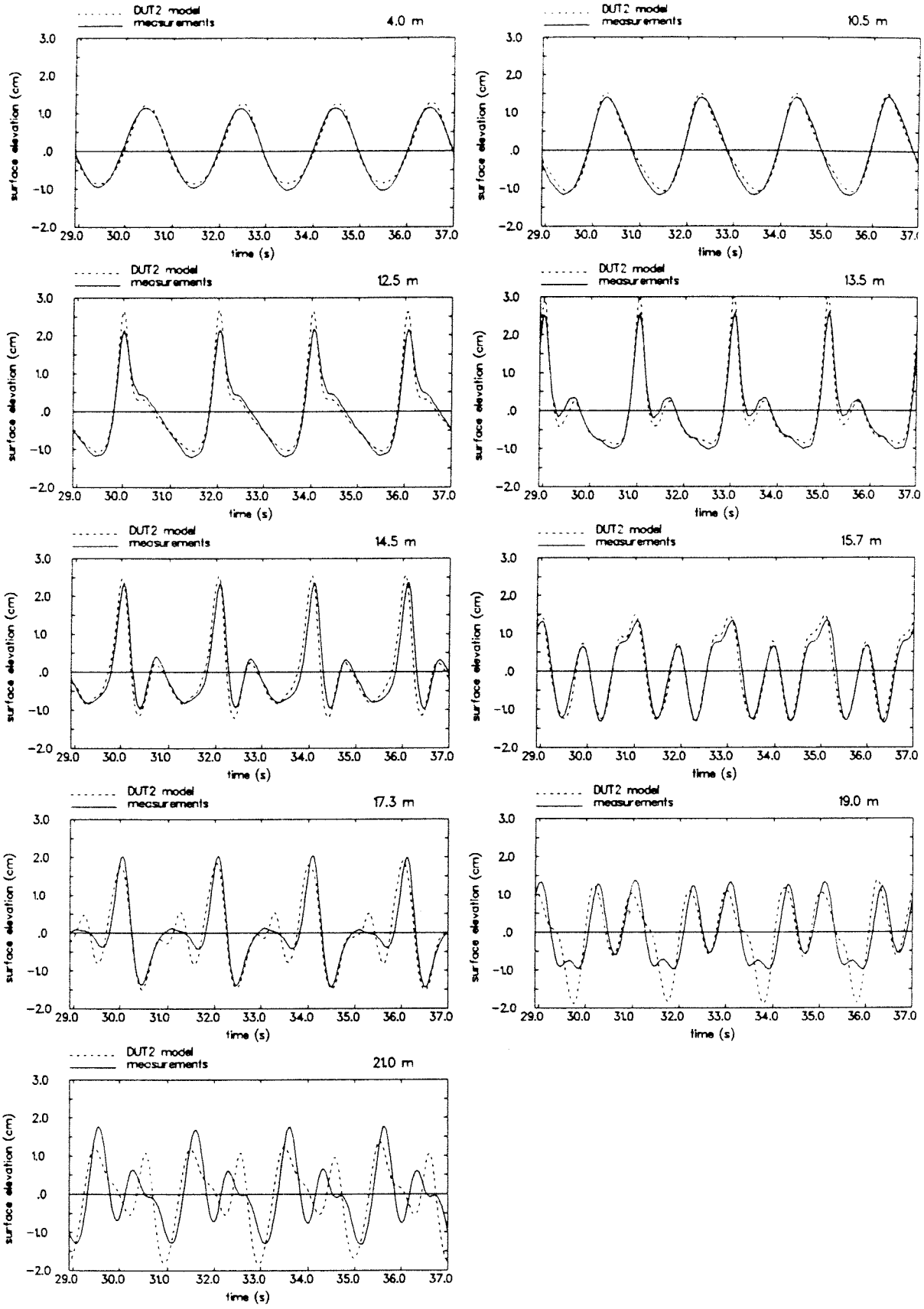

Appendix G Model 4f compared with measurements C at all stations

Normal boundary conditions for ζx and ζxx.

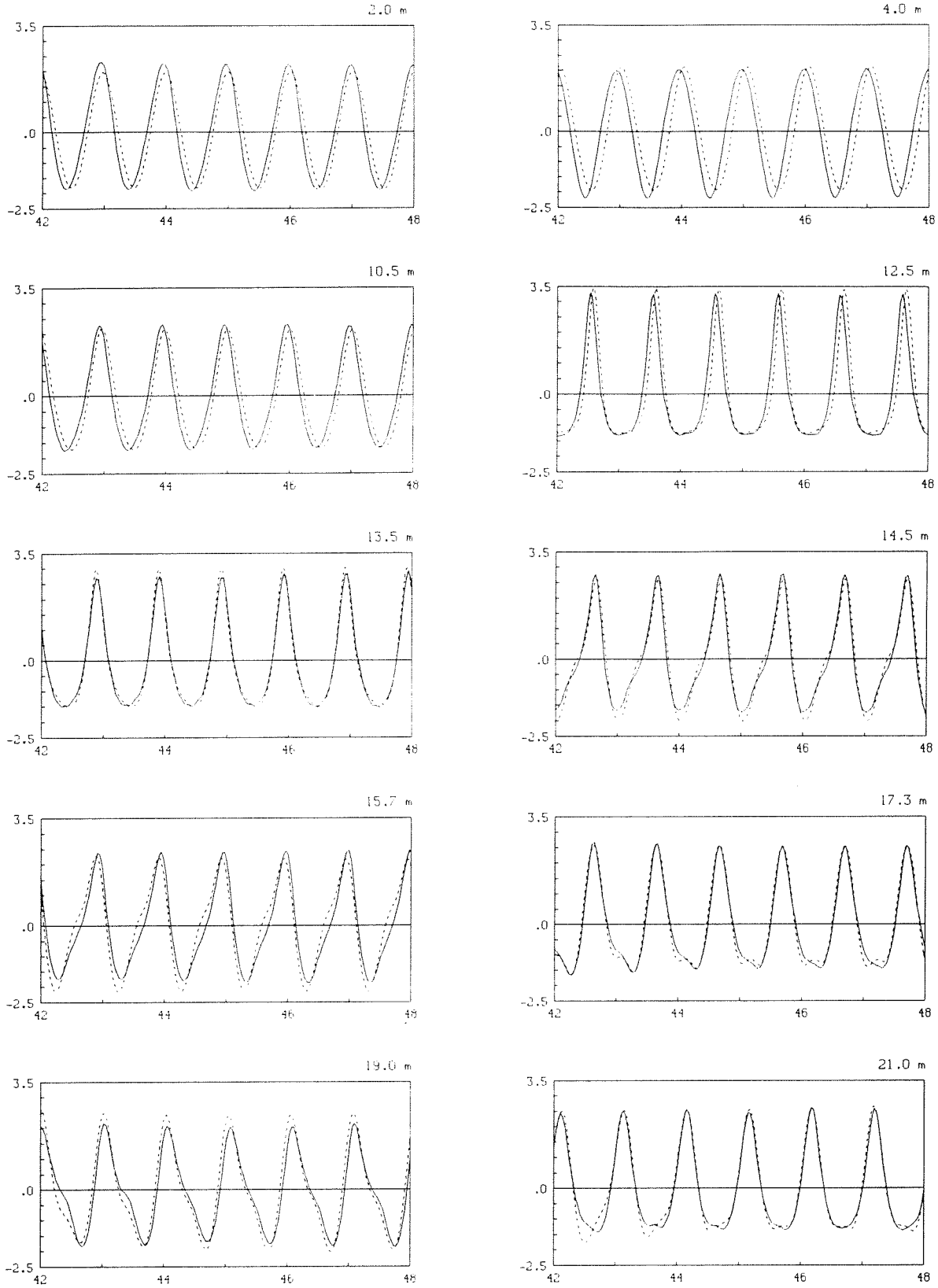

Surface elevation in cm and time in seconds.

Appendix H DUT2 compared with measurements C at all stations

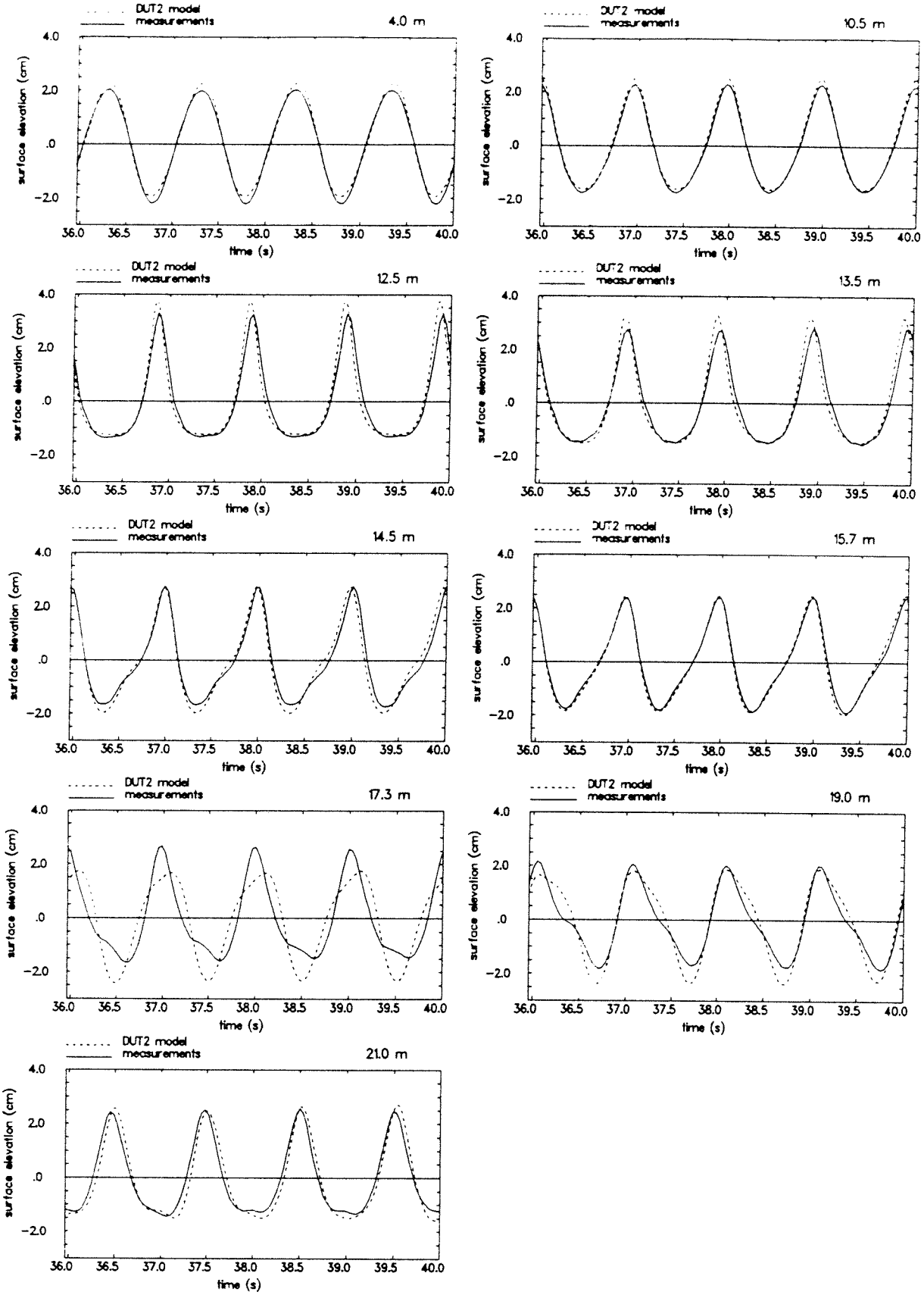

Appendix I Model 4f compared with measurements C at all stations

Simplified boundary conditions for ζx and ζxx.

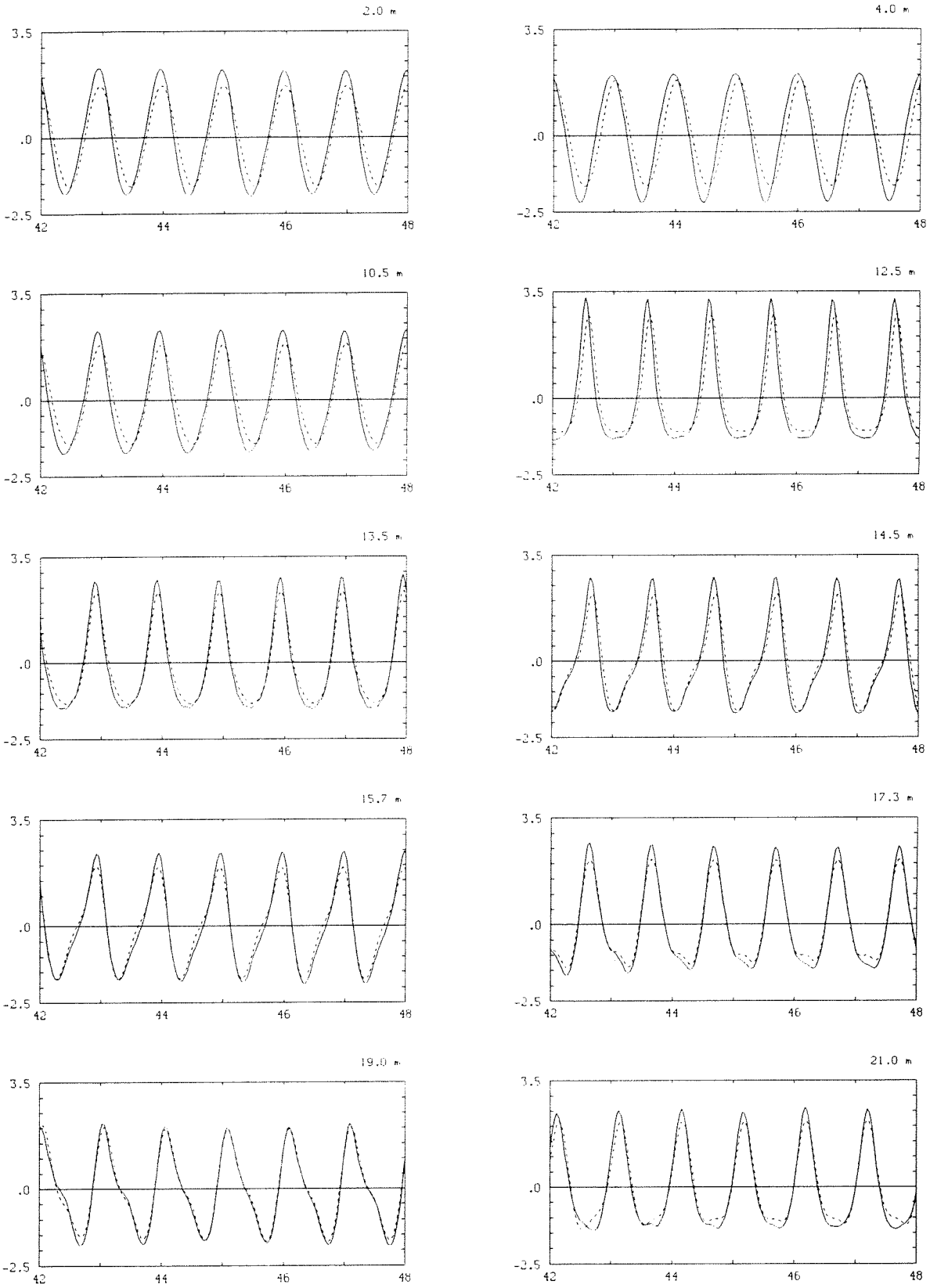

Surface elevation in cm and time in seconds.

Appendix J The optimized shoaling coefficient α_s^B

In this appendix the numerical evaluation of the optimized shoaling coefficient is given. The optimized δ_i have already been substituted. The shoaling coefficient reads

$$\alpha_s^B = \frac{\frac{1}{4}+a_2q^2+a_4q^4+a_6q^6+a_8q^8+a_{10}q^{10}+a_{12}q^{12}+a_{14}q^{14}+a_{16}q^{16}}{\left(1+b_2q^2+b_4q^4+b_6q^6+b_8q^8\right)^2} \qquad \textbf{(J.1)}$$

where

$q = kh$

and

$a_2 = -0.1390$
$a_4 = -0.2490 \cdot 10^{-1}$
$a_6 = 0.4393 \cdot 10^{-3}$
$a_8 = 0.4898 \cdot 10^{-4}$
$a_{10} = -0.3970 \cdot 10^{-5}$
$a_{12} = 0.1356 \cdot 10^{-6}$
$a_{14} = 0.1150 \cdot 10^{-8}$
$a_{16} = -0.1600 \cdot 10^{-9}$

and

$b_2 = 0.2222$
$b_4 = 0.3668 \cdot 10^{-1}$
$b_6 = 0.9406 \cdot 10^{-3}$
$b_8 = 0.1680 \cdot 10^{-4}$